Summer 2016

Prediction of surface roughness in abrasive waterjet cutting of graphite composite using response surface methodology

Prabhakar Bala

Department:

PREDICTION OF SURFACE ROUGHNESS IN ABRASIVE WATERJET CUTTING OF GRAPHITE COMPOSITE USING RESPONSE SURFACE METHODOLOGY

By

PRABHAKAR BALA

A THESIS

Presented to the faculty of the Graduate School of the

MISSOURI UNIVERSITY OF SCIENCE & TECHNOLOGY

In partial Fulfillment of the Requirements for the degree

MASTER OF SCIENCE IN MANUFACTURING ENGINEERING

2016

Approved by

Dr. Grzegorz Galecki, Advisor

Dr. David A. Summers

Dr. Frank Liou

ABSTRACT

In the present work, surface roughness after machining of composite material was the main focus of study. Response surface methodology with Box- Behnken experimental design was applied in predicting the surface roughness (R_a) of abrasive waterjet cut 1-inch-thick graphite/epoxy composite. Second order response equations for R_a were generated with minitab, a statistical software as a function of pressure, traverse speed and isolated abrasive mesh size. Influence of each of these factors on the response were analyzed with 3D response surface plots. Abrasive mesh size was also found be a factor influencing R_a along with traverse speed and pressure. Using 80 HPX Barton garnet in the linear cuts, model equations were generated including abrasive flow rate as a factor. The model equations were well verified with experimental data. As a result, these response equations would be able to predict R_a values within the range of input parameters without actually performing the experiments. Stacking of four ¼" thick composites was done and compared with 1" thick material in terms of R_a. With abrasive size as focus, particle size distribution of Barton garnet was analyzed before and after entering the cutting head. A large fragmentation of the garnet occurred during acceleration in mixing tube and focusing tube. Over 50-60% of the garnet was less than the size of screen #100 mesh size. Pressure has significant influence on abrasive disintegration rather than abrasive flow rate. GMA Australian garnet, Wesjet garnet and Barton garnet were compared for particle size distribution after sieving.

ACKNOWLEDGEMENTS

Foremost, I would like to thank my advisor, Dr. Greg Galecki for his constant support and motivation throughout my research work in master's program and it has been a pleasure working with him. This work would not have been possible without his guidance and patience with me.

I express my sincere gratitude to my thesis committee members, Dr. Frank Liou and Dr. David A. Summers for their co-operation. I would also like to thank Mr. Jeff Heniff for his guidance in waterjet cutting lab at Rock Mechanics and Explosives Research Center and also, Mr. John Tyler for his value input towards my experimental work.

This research was funded by the Center for Aerospace Manufacturing Technologies (CAMT) at Missouri University of Science and Technology, directed by Dr. Ming Leu. The experiments were conducted at Waterjet Laboratory/Rock Mechanics and Explosives Research Center. The support of Dr. James Castle and Mrs. Melissa Johnson from Boeing Company and Dr. Pradeep Nambiath and Mr. Skip Reynolds from KMT Waterjet Systems is greatly appreciated.

I am grateful to Mrs. Kathleen Morris, administrative assistant who has always been cheerful and guided me through necessary paper work. I also thank John Rueschmann, undergraduate student assistant for his help in the shop floor.

I am thankful to my colleagues Mr. Kenneth Bansah and Mr. Kaba Azupuri for their guidance in my thesis writing. Finally, I would like to thank my family, Mr. Madhusudhana Rao, Mrs. Suryavardhini and Jyothsna whose continuous support made this degree possible.

TABLE OF CONTENTS

Page

ABSTRACT …… iii

ACKNOWLEDGEMENTS …….iv

LIST OF ILLUSTRATIONS vii

LIST OF TABLES ……....x

ABBREVATIONS ……..xi

SECTION

1. INTRODUCTION ……1

1.1. BACKGROUND ……...1

1.2. PROBLEM STATEMENT ……....2

1.3. THESIS OUTLINE ……3

2. LITERATURE REVIEW ……4

2.1. ABRASIVE WATERJET CUTTING ……...4

2.2. SURFACE ROUGHNESS CHARACTERIZATION ……...6

2.3. VISUALIZATION OF FLOW OF JET IN THE CUTTING HEAD …..12

2.4. STUDY OF NOZZLE WEAR ……15

2.5. SURFACE ROUGHNESS MEASUREMENTS …….....16

2.6. ABRASIVE FRAGMENTATION ……..17

3. BOX-BEHNKEN RESPONSE SURFACE DESIGN THEORY……20

3.1. RESPONSE SURFACE METHODOLOGY ……..20

3.2. BOX-BEHNKEN EXPERIMENTAL DESIGN……..21

4. EXPERIMENTATION METHODOLOGY ……...26

4.1. INTRODUCTION ……...26

4.2. EXPERIMENTAL SETUP……...26

4.3. SURFACE ROUGHNESS MEASUREMENT ……...29

4.4. ABRASIVE ANALYSIS ……30

4.4.1. Particle Size Distribution of Garnet ……..31

4.4.2. Abrasive Disintegration ……37

4.4.2.1. Disintegration of 80 HPX Barton garnet at different pressures 39

4.4.2.2. Disintegration of 80 HPX Barton garnet at different abrasive flow rates……..41

4.4.3. Comparison of Performance of Barton, Wesjet and GMA Garnet in Terms of R_a ……44

5. MODELING ……...51

5.1. MODEL EQUATIONS ……...51

5.2. RESPONSE SURFACE PLOTS …….....59

5.2.1. Response Surface Plots at an AFR of 1.0 lb/min ……..59

5.2.2. Response Surface Plots at an AFR of 1.5 lb/min ……..63

5.2.3. Response Surface Plots at an AFR of 2.0 lb/min ……..68

5.2.4. Response Surface Plots with 80 HPX Barton Garnet ……...72

5.3. EXPERIMENTATION WITH STYROFOAM BASE ……...79

6. MODEL VERIFICATION ……82

6.1. MODEL VERIFICATION OF 1” THICK COMPOSITE ……...82

6.2. MODEL VERIFICATION WITH STACKING ……..88

7. CONCLUSIONS ……91

8. FUTURE WORK ……....93

APPENDIX …….....94

BIBLIOGRAPHY ……106

VITA ……109

LIST OF ILLUSTRATIONS

Figure Page

1.1. Sectional view of AUTOLINE II cutting head …….....2

2.1. Surface finish at top and bottom surfaces ……..7

3.1. Box-Behnken design for three (3) factors ……22

3.2. Screen shot of response surface design creation in Minitab …….....24

4.1. 5 axis PaR waterjet cutting system coupled with KMT PRO intensifier …….27

4.2. Syntron vibratory electromagnetic abrasive feeder in PaR systems ……28

4.3. Sketch representing the R_a measurement at 3 locations at 3 different levels of cutting depth for 1-inch-thick composite ….……...…..30

4.4. 80 HPX® Barton garnet used for the experiment (Batch number HR 060180) and Microscope observation (60X**)** …….....31

4.5. Particle size distribution of Barton, GMA and Wesjet garnet …….32

4.6. Comparison of experimentally analyzed particle size distribution with the size distribution provided by Barton Mines Corporation ……33

4.7. Particle size distribution of garnet collected using small hopper of PaR systems ……...34

4.8. Particle size distribution of garnet collected using large hopper of PaR systems ……...35

4.9. OMAX waterjet systems gravity controlled abrasive feeder ……...36

4.10. Comparison of particle size distribution of garnet collected using OMAX feeder and PaR systems feeders ...…….....37

4.11. Abrasive capture after jet exit ……38

4.12. Particle size distribution of 80 HPX Barton garnet after passing through cutting head, a) pressure 60 ksi b) pressure 75 ksi and c) pressure 90 ksi ....……40

4.13. Particle size distribution of 80HPX Barton garnet after passing through cutting head, a) AFR 1.0 lb/min b) AFR 1.5 lb/min and c) AFR 2.0 lb/min ……...42

4.14. Microscope observation of a) GMA garnet (60X) b) Wesjet garnet (60X) ……...44

4.15. Comparison of the performance of Barton, Wesjet and GMA garnet with R_a parameter, at different depths of cut, p: 60 ksi and AFR: 1.0 lb/min ……47

4.16. Comparison of the performance of Barton, Wesjet and GMA garnet with R_a parameter, at different depths of cut, p:90 ksi and AFR: 2.0 lb/min ..……...49

5.1. Relation between experimental and predicted values of R_a at 1.0 lb/min AFR a) at a depth of ¼" b) at a depth of ½" c) at a depth of ¾" (eq's 5.1-5.3) 52

5.2. Relation between experimental and predicted values of R_a at 1.5 lb/min AFR a) at a depth of ¼" b) at a depth of ½" c) at a depth of ¾" (eq's 5.4-5.6) 54

5.3. Relation between experimental and predicted values of R_a at 2.0 lb/min AFR a) at a depth of ¼" b) at a depth of ½" c) at a depth of ¾" (eq's 5.7-5.9) 56

5.4. Relation between experimental and predicted values of R_a with 80 HPX Barton garnet a) at a depth of ¼" b) at a depth of ½" c) at a depth of ¾" d) at a depth of 1/8" (eq's 5.10-5.13) …….....58

5.5. Response surface plots showing the effect of variables a) pressure and traverse speed b) pressure and abrasive mesh size c) traverse speed and abrasive mesh size on R_a at a depth of ¼" at an AFR of 1 lb/min ……..59

5.6. Response surface plots showing the effect of variables a) pressure and traverse speed b) pressure and abrasive mesh size c) traverse speed and abrasive mesh size on R_a at a depth of ½" at an AFR of 1 lb/min ……..61

5.7. Response surface plots showing the effect of variables a) pressure and traverse speed b) pressure and abrasive mesh size c) traverse speed and abrasive mesh size on R_a at a depth of ¾" at an AFR of 1 lb/min ……62

5.8. Response surface plots showing the effect of variables a) pressure and traverse speed b) pressure and abrasive mesh size c) traverse speed and abrasive mesh size on R_a at a depth of ¼" at an AFR of 1.5lb/min ...……64

5.9. Response surface plots showing the effect of variables a) pressure and traverse speed b) pressure and abrasive mesh size c) traverse speed and abrasive mesh size on R_a at a depth of ½" at an AFR of 1.5 lb/min ……..…….65

5.10. Response surface plots showing the effect of variables a) pressure and traverse speed b) pressure and abrasive mesh size c) traverse speed and abrasive mesh size on R_a at a depth of¾" at an AFR of 1.5 lb/min ...……...…….....67

5.11. Response surface plots showing the effect of variables a) pressure and traverse speed b) pressure and abrasive mesh size c) traverse speed and abrasive mesh size on R_a at a depth of ¼" at an AFR of 2.0 lb/min …….....68

5.12. Response surface plots showing the effect of variables a) pressure and traverse speed b) pressure and abrasive mesh size c) traverse speed and abrasive mesh size on R_a at a depth of ½" at an AFR of 2.0 lb/min ……..…….…70

5.13. Response surface plots showing the effect of variables a) pressure and traverse speed b) pressure and abrasive mesh size c) traverse speed and abrasive mesh size on R_a at a depth of ¾" at an AFR of 2.0 lb/min ..71

5.14. Response surface plots showing the effect of variables a) pressure and traverse speed b) pressure and abrasive flow rate c) traverse speed and abrasive flow rate on R_a at a depth of ¼" for 80 HPX Barton garnet ..73

5.15. Response surface plots showing the effect of variables a) pressure and traverse speed b) pressure and abrasive flow rate c) traverse speed and abrasive flow rate on R_a at a depth of ½" for 80 HPX Barton garnet 75

5.16. Response surface plots showing the effect of variables a) pressure and traverse speed b) pressure and abrasive flow rate c) traverse speed and abrasive flow rate on R_a at a depth of ¾" for 80 HPX Barton garnet 76

5.17. Response surface plots showing the effect of variables a) pressure and traverse speed b) pressure and abrasive flow rate c) traverse speed and abrasive flow rate on R_a at a depth of 1/8" for 80 HPX Barton garnet 78

5.18. Relation between experimental and predicted values of R_a at a depth of 1/8" with 80HPX Barton garnet (eq 5.14) ..80

5.19. Response surface plots showing the effects of various parameters a) pressure and traverse speed b) pressure and abrasive flow rate c) traverse speed and abrasive flow rate on R_a for 80 HPX Barton garnet with styrofoam base 80

6.1. Model verification at an AFR of 1 lb/min (eq's 5.1-5.3) 82

6.2. Model verification at an AFR of 1.5 lb/min (eq's 5.4-5.6) 83

6.3. Model verification at an AFR of 2.0 lb/min (eq's 5.7-5.9) 85

6.4. Model verification with 80 HPX Barton garnet (eq's 5.10-5.12) 86

6.5. Model verification at a depth of 1/8" from top surface (eq 5.13) 87

6.6. AWJ cutting of stack of four ¼" thick composites 88

6.7. Fixture of 1" thick composite and stack of four ¼" thick composite for comparison of R_a 89

6.8. Verification of the model at depth of measurement of 1/8" using styrofoam base (eq 5.14) 90

LIST OF TABLES

Table Page

2.1. Standard screen mesh size to particle size conversion ……10

3.1. Treatment combinations for Box-Behnken design for 3 factors ……..23

3.2. Levels of Box-Behnken design for 3 selected factors …….....25

4.1. Properties of graphite/epoxy composite ……...28

4.2. Experimental R_a using WESJET garnet ……..…45

4.3. Experimental R_a using BARTON garnet ……....45

4.4. Experimental R_a using GMA garnet ……....46

ABBREVATIONS

AFR	Abrasive Flow Rate
AWJ	Abrasive Waterjet
BWI	Bond Work Index
CCD	Central Composite Design
CFRP	Carbon Fiber Reinforced Plastic
CNC	Computer Numerical Control
GEP	Genetic Expression Programming
GFRP	Glass Fiber Reinforced Plastic
IDR	Initial Damage Region
KMT	Karolin Machine Tool (Swiss)
MMC	Metal Matrix Composite
PCD	Poly Crystalline Diamond
PVC	Polyvinyl Chloride
R_a	Average Surface Roughness Parameter
RCR	Rough Cutting Region
RMS	Root Mean Square
RSM	Response Surface Methodology
R_z	Average Peak to Valley Height- Roughness Parameter
Rsq	R squared
SiC	Silicon Carbide
SCR	Smooth Cutting Region
SEM	Scanning Electron Microscopy
HV	Vickers Hardness

1. INTRODUCTION

1.1. BACKGROUND

Waterjetting is a process in which power is generated by a pump pushing a given volume of water through a high pressure feedline thus; providing a high energy flow. This energized flow passes through a nozzle from this high pressure feed line, the small diameter orifice at the end of which creates a high velocity stream directed toward the work piece [Summers, 1995].

In the early stages of waterjet cutting applications, it was primarily used in cutting wood and materials other than ceramics and metals each its own limitations. This was due to low pressure of the water and discontinuities within the waterjet. Later in 1980, for improving the cutting efficiency of waterjets, abrasives were added to the jet stream which was a huge advancement. The high pressure waterjet from the feed line enters the small diameter opening orifice of the nozzle creating a high velocity stream. When the high velocity stream passed into the mixing chamber, there was drop in pressure creating a vacuum. Abrasive was sucked into the mixing chamber due to the venturi effect through a feed pipe from an external storage hopper. The resulting mixture of abrasive, water and air was accelerated to flow through a larger diameter, lengthy focusing tube directed towards the target material. A sectional view of the AUTOLINE II cutting head used in the experimental work was shown in Figure 1.1. Abrasive flows into the cutting head where it is mixed with the waterjet in the mixing chamber. In the process of mixing of abrasive and high velocity waterjet, grain breakage occurs. This is due to the collision of one particle with another in accelerated flow and due to the impact of

particles with the high pressure waterjet stream. Abrasive particle breakage will be analyzed in detail in later sections.

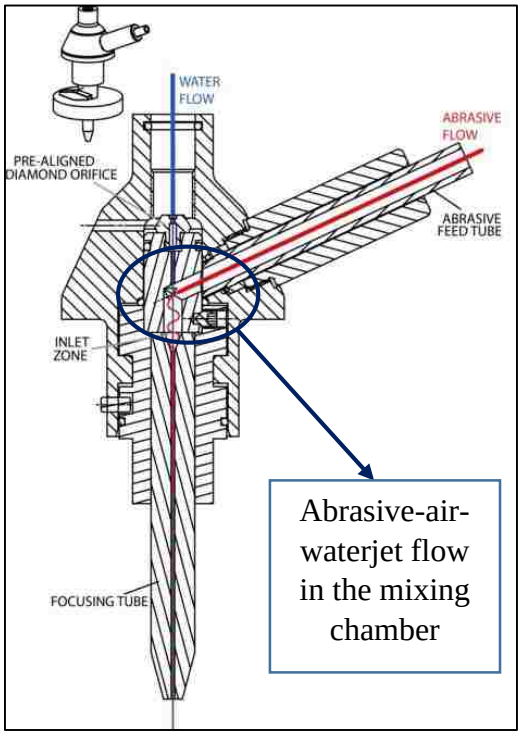

Figure 1.1. Sectional view of AUTOLINE II cutting head
[http://blog.kmt-waterjet.com/category/waterjet-cutting-heads/]

1.2. PROBLEM STATEMENT

As the evolution of abrasive waterjet cutting overcame application limitations, it was used in various industrial applications which now includes cutting materials such as titanium and the composites predominantly used in the aerospace industry [Korat et al, 2014]. With the advantages including no heat affected zone, minimal fixturing, no stress impact and a multiple axis cutting capability, AWJ cutting became one of the most useful, productive and economical machining methods. Surface finish of the cut surface plays a key role in the strength of the material after machining, especially to be noted in composites. This experimental research was mainly focused on, predicting the surface roughness (R_a) as a function of most influential

parameters of abrasive waterjet cutting of composite. For this, a Box-Behnken experimental design was considered for conducting the experiments. Response surface methodology (RSM) was used in analyzing the experimental data and a second order empirical model for R_a was developed. Using this empirical model, it is possible to predict the R_a value to define the desired set of parameters in an experimental range without actually doing the experiment. Predicted values of this model were verified and validated using experimental data. For more and clear understanding of the influence of the parameters, 3D surface plots from RSM were generated using statistical software. Along with this, abrasive disintegration in the cutting head was analyzed with particle size distribution plots so as to check the effect of isolated abrasive size on R_a.

1.3. THESIS OUTLINE

This thesis consists a total of 8 sections which includes an introduction, literature review, Box- Behnken response surface design theory, experimental methodology, modelling and verification of the model, conclusions and future scope of work. The literature review covers recent work in abrasive waterjet cutting from different approaches including flow pattern of the jet in the cutting head, nozzle wear, abrasive disintegration, surface roughness characterization and measurement. The Box-Behnken response surface design theory section provides an introduction of the theory and the reason for adapting this theory in the present experimental design and analysis. Experimental methodology describes the set up for measuring particle size distribution, abrasive disintegration and an analysis of the respective portions. The scope of this experimental work was defined through modelling and verification of the model using the above mentioned response surface design method. Also, future work in continuation of the current results and analysis was defined.

2. LITERATURE REVIEW

2.1. ABRASIVE WATERJET CUTTING

Abrasive waterjet (AWJ) technology is being used extensively in cutting a wide range of material from automotive and aerospace use to medical and in the food industries. The AWJ is not limited to cutting but finds its use in surface treatment, cleaning, coating removal, drilling and milling applications with a significant advantage of no heat damage in the cutting zone and minimal force compared to other conventional machining methods [Folkes, 2009].

Krajcarz [2014] discussed the relative advantages of waterjet cutting with laser and plasma cutting. Waterjet cutting can cut through any kind of material including titanium, steel, aluminum, glass, ceramics, wood, plastics, composites etc. In this paper, he made an observation in reviewing earlier research, that cutting speed was low for waterjet cutting compared to other cutting techniques resulting in higher operating costs. Akkurt [2009] compared different cutting techniques by studying the surface properties of the cut face on stainless steel materials. The main distinguishable advantage of abrasive waterjet cutting that was observed from his experimental investigation was that there was no thermal deformation of the workpiece in the cutting zone and no change in the properties of the material.

Ease of cutting a material with a good surface finish at low cost creates a machinability index and a group of researchers looked into the machinability of composite materials using an abrasive waterjet. Alberdi et al [2013] carried out experiments on two different carbon fiber reinforced plastic (CFRP) composite materials with F593 hexcel and 8552 hexcel type of ply with two different thicknesses of 6 mm and 12 mm varying jet pressure, abrasive mass flow

rate and standoff distance with feed rate to separation speed ratio of 10 and 50 and found out that the machinability index of composite materials was significantly higher to that of metals indicating that composite materials can be cut significantly faster than metals. The experimental results also revealed that composites with different compositions have different machinability indices.

It was seen that composites could be machined easily with abrasive waterjet and thereafter, the mechanism involved in removal of the material in the machining/ cutting of composites was studied. Arola and Ramulu [1993] seeking to identify material removal mechanism in abrasive waterjet machining conducted their research on commonly used materials in the aerospace industry such as Graphite/Epoxy composite and aluminum. By examining the surface cuts under scanning electron microscopy, they found that the mechanisms of both brittle and ductile material don't change below the initial damage region with cutting depth and failure was observed as a shearing mechanism. However, within the initial damage region, the material removal occurs due to deformation wear caused by abrasives, and influenced by process parameters.

Machining of composites with waterjet technology encountered a problem with fiber pullout and delamination during the process of material removal by fiber deformation and fiber matrix debonding. Srinivasu and Axnite [2014] studied this phenomenon using glass fiber composite material and plain waterjet milling. After studying the surface with micrographs, it was suggested that this fiber damage and delamination in composite materials can be reduced by selecting a suitable set of cutting parameters and by proper clamping of work material with fixtures which eliminates any vibration caused by the high energized jet.

2.2. SURFACE ROUGHNESS CHARACTERIZATION

Abrasive waterjet cutting was able to overcome the problems of fiber pullout, fiber breakage, matrix smearing and delamination encountered which were encountered when machining the composites using conventional methods. Surface roughness was analyzed in abrasive waterjet applications when trimming composites. Hashish [2013] conducted research on the use of AWJ in trimming of CFRP aircraft components over the conventional machining methods. Based on the type and size of the component required, the trimming system selected was either a gantry type or a robotic system with the special attachments required for flexible manufacturing. Based on the experimental work carried on different composite samples with a jet pressure of 400 MPa and an abrasive flow rate of 7.5 g/s using 80 mesh garnet abrasive, while maintaining a nozzle standoff distance at 2.5 mm, it was observed that the kerf width narrows as the cutting speed increases to a level. However, with an increase of cutting speed from 30 mm/s to 70 mm/s, kerf width remains insensitive. Cutting speed had a significant influence on the surface roughness at the bottom surface of the cut rather than at the top surface. The trend of surface roughness with cutting speed at both jet entrance and exit is shown in Figure 2.1.

Abrasive waterjet cutting of composites faced another problem of kerf formation in addition to fiber damage. Typically, kerf width was assumed to be directly related to mixing tube diameter. Kerf characteristics of graphite/epoxy composites in abrasive waterjet machining were examined by Arola and Ramulu [1996] who concluded that inadequate cutting energy was the reason for waviness and striations of the cut surface on the kerf wall. Reduction in standoff distance, higher jet pressures and lower traverse speeds yielded to an extension of the smooth cutting region (SCR) and minimized kerf width taper.

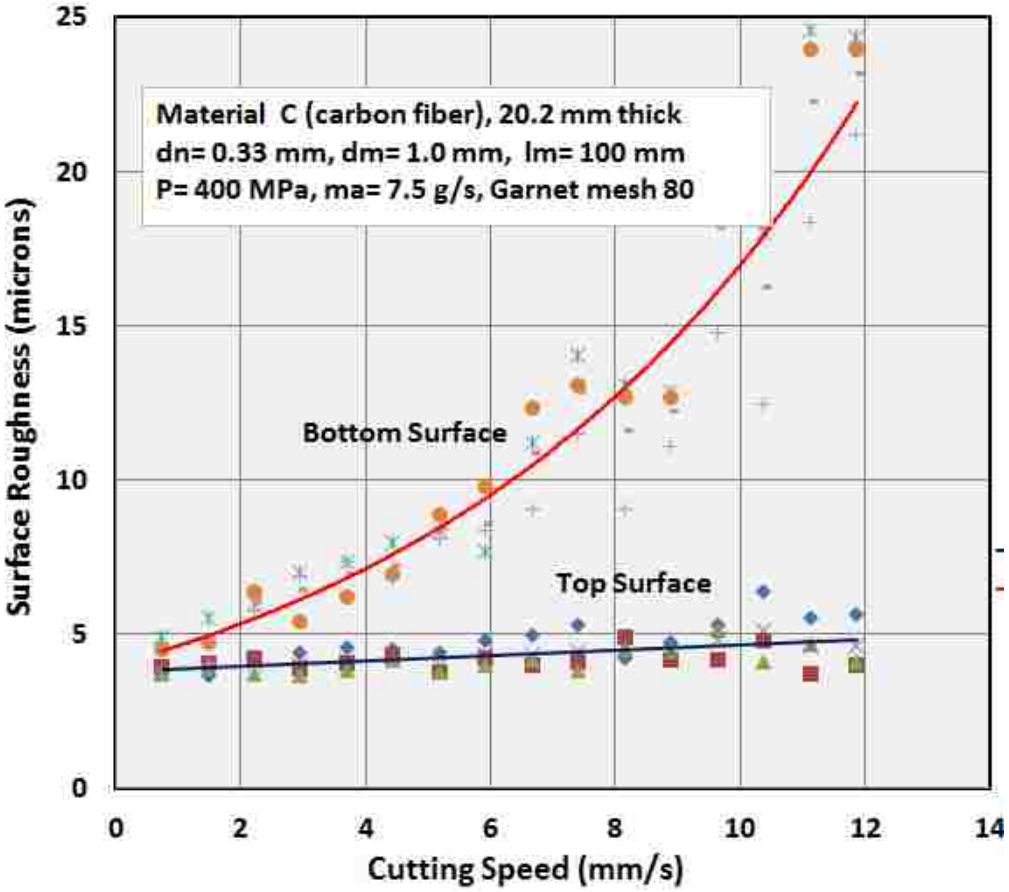

Figure 2.1. Surface finish at the top and bottom surfaces [Hashish, 2013]

Azmir and Ahsan [2009] in their study of fiber glass/epoxy composite laminates used Taguchi's design of experiments and the analysis of variance to characterize the effect of the abrasive waterjet cutting parameters on surface roughness and kerf taper ratio. Experimental results and analysis proved that cutting orientation, pressure and abrasive mass flow rate were insignificant factors on the quality of cut with kerf taper ratio. Abrasive type and waterjet pressure had a significant influence on both surface roughness and kerf taper ratio.

Feed rate was one process parameter in abrasive waterjets that influences the cut surface features. Effect of feed rate on surface roughness in abrasive water jet cutting applications was studied by Akkurt et al [2004] who conducted experiments with different

materials including pure aluminum (Al), Al 6061 alloy, brass-353, AISI 1030 and AISI 304 stainless steel of two thickness 5 mm and 20 mm. Experimental results showed that cutting wear and deformation wear mechanisms were effective in cutting both of the brittle and mild structured materials with AWJ. Reducing the feed rate showed an improvement in surface roughness for same thickness of specimens. Studies also recommended that feed rate makes a significant contribution in cutting thicker AISI stainless steel material by abrasive waterjet stressing the importance of selecting the appropriate feed rate and also revealing that a greater reduction in feed rate for the same thickness of a sample of aluminum based material yields a very small improvement in surface quality.

Different approaches for predicting surface roughness in abrasive waterjet machining were investigated. Surface roughness of 7075 aluminum alloy composites reinforced with Al_2O_3 particles was predicted using genetic expression programming (GEP) in abrasive waterjet cutting [Kok et al, 2011]. Interestingly, the depth of cut was taken as one of the input variables to predict the response on the average and maximum surface roughness of the cut surface. As the depth of cut increases to the thickness of the material, it was observed that surface roughness reached its maximum value gradually. This is mainly due to the jet-material interaction as the cut goes deeper creating the resistance and deflecting the jet upwards. The predicted values of surface roughness using GEP are found to be in good correlation with experimental values.

Abrasive water jet cutting is being used in cutting various materials like borosilicate glass, aluminum, different kind of steels based on their use and real word applications cutting common aerospace materials like titanium. Aich et al [2014] conducted research on abrasive waterjet cutting of borosilicate glass to find the influence of water pressure, abrasive flow rate,

traverse speed and standoff distance on the depth of cut. Three parameters water pressure, traverse speed and abrasive flow rate were found to be significant factors influencing the depth of cut. Particle swarm optimization techniques were used to find the optimal combination of cutting parameters. Brittle fracture and plastic deformation were the material removal mechanisms in cutting borosilicate glass.

Babu and Chetty [2006] experimented with the use of a single mesh size of abrasives in abrasive waterjet machining of aluminum. The experimental work varied waterjet pressure, traverse rate, abrasive flow rate and grain size as process parameters to establish their effect on kerf parameters, depth of cut and surface roughness. Experiments were designed using standard L9 orthogonal array (Taguchi design) to minimize experimentation. Garnet with isolated mesh sizes of 52, 60 and 80 was used for the experimentation. The jet impact angle was kept at 90º, the standoff distance at 3mm and a constant cutting head condition was maintained. Single mesh size abrasives behaved differently to the multi mesh abrasives cas shown by the kerf characteristics of the cut surface. The work was summarized as single mesh size abrasives has significant influence on surface roughness in the upper and middle section of cuts in aluminum.

Mesh sizes are generally expressed in nominal sieve openings for particle size conversion. For example, if the screen size is given as 60 mesh and screens are arranged in order of 50, 60 and 70 mesh, then particles with sizes less than 297 µm and greater than 250 µm will be retained on 60 mesh screen. Selected range of screens for commonly used abrasive sizes were shown in the Table 2.1 with mesh sizes and sieve openings for each mesh.

Table 2.1. Standard screen mesh size to particle size conversion

http://www.sigmaaldrich.com/chemistry/stockroom-reagents/learning-center/technical-library/particle-size-conversion.html

U. S. Mesh	Microns	Inches	Millimeter
40	400	0.0165	0.400
50	297	0.0117	0.297
60	250	0.0098	0.250
70	210	0.0083	0.210
80	177	0.0070	0.177
100	149	0.0059	0.149
120	125	0.0049	0.125
140	105	0.0041	0.105

The type of abrasive used in abrasive waterjet machining plays an important role in defining the characteristics of the cut surface. Khan and Haque [2007] analyzed the performance of various types of abrasives including garnet, aluminum oxide and silicon carbide by varying the cutting parameters of standoff distance, jet pressure and work feed rate examining their influence on the width and taper of cut. Silicon carbide (SiC) abrasives being harder than aluminum oxide and garnet produce the maximum width of cut at the jet exit. It was concluded that the harder the abrasive, the greater the cutting ability.

Srinivas and Babu [2011] studied the influence of garnet and SiC abrasives of 60, 80 and 120 mesh sizes on the depth of penetration into aluminum-silicon carbide metal matrix composites (MMC) in abrasive waterjet cutting. Experimental investigations revealed that 80 mesh size SiC abrasive gave the higher depth of penetration. Material removal mechanisms in these MMCs was found to be by ductile fracture and ploughing of the reinforcement, after careful scanning using an electron microscope.

Physical properties of abrasives including average particle size, density, Bond work index (BWI) and Vickers hardness (VH) was evaluated seeking to optimize abrasive waterjet cutting of ductile material was evaluated [Gent et al, 2012]. The experiments, to identify the maximum cutting depth, were conducted on 12 mm thick 316L stainless steel with different kind of abrasives including polycrystalline minerals, high density glass abrasives and also including GMA 90 (Almandine) garnet which was taken as the standard reference abrasive. The rate of erosion with different properties of the abrasives was evaluated. Increase in either of BWI or HV parameters increases the rate of erosion indicating a correlation between the two properties of the materials. It was also noted that due to higher impact resistance, polycrystalline abrasives result in higher erosion rate compared with their mono crystalline form despite having lower HV. Abrasives with more angularity and sharp edges give the greater erosion capacity. The rate of erosion also depends on the relative difference between the hardness of the target work material and the abrasive particles.

Grit embedment and surface roughness of the cut surface plays a predominant role in the fatigue failure of a component. Grit sticking in abrasive waterjet milling of titanium was studied by conducting experiments varying the parameters traverse speed, jet impingement angle, milling direction and size of abrasive particles [Fowler et al, 2005a]. The experimental data revealed that the jet impingement angle has a significant influence on grit embedment and surface characteristics. At low traverse speeds, forward milling also resulted in high levels of grit embedment. In the continued research, the characteristics of the milled material were also studied and it was concluded that surface waviness decreased with an increase of traverse speed. It was also observed that as the number of passes increased, surface waviness and roughness increased at both high and low traverse speeds of milling [Fowler et al, 2005b].

Valicek et al [2007] proposed a quantitative criterion to study the irregularities of metallic surfaces generated by abrasive waterjet introducing a dimensionless statistical parameter taking into account the importance of surface waviness. The abrasive waterjet cut walls of the test samples of steel material were examined using a contactless optical shadow method where the intensity distribution across the measured surface was scanned using a charge coupled device camera connected to a PC with consequent signal processing. As light distribution spectra are quantified by the surface roughness or waviness, the root mean square (RMS) intensities of the reflected light also quantify the smoothness of the surface. This principle was used in defining the statistical parameter description of the surface waviness. The parameter depends on the material and traverse speed of the jet. According to the proposed criterion, a proper traverse speed could be chosen for the required quality of cut, thereby improving the performance of the abrasive waterjet.

2.3. VISUALIZATION OF FLOW OF JET IN THE CUTTING HEAD

Thery and Osman [1998] conducted a series of experiments to study the flow of the abrasive waterjet, measuring the velocity using a Fabry- Perot interferometer. The effect of changing waterjet pressure, abrasive flow rate (AFR) and the ratio of focusing tube diameter to that of orifice, on the velocity of the abrasive waterjet were observed. With increase in AFR, the velocity of the jet was reduced establishing the result that the mean abrasive waterjet velocity at the focusing tube exit depends on the abrasive flow rates. It was observed that the depth of cut was high when the ratio diameter of the mixing tube to the water orifice was between 3 and 3.5. It was also observed that this optimal ratio depends on the distance between the water orifice and the mixing tube entry which represents the mixing tube length. Keeping this ratio as a constant by maintaining the same cutting head, the jet velocity increases as pump

pressure increased. It was concluded that the velocity of the jet and cutting efficiency depends on the abrasive flow rate, the ratio of the mixing tube and orifice diameter, the length of the mixing chamber and obviously the pressure of the pump.

Abrasive waterjet characteristics were studied using computational fluid dynamics modelling and simulation using the fluent6 flow solver [Liu et al, 2004]. It was shown that the axial velocity of the jet at the center undergoes a rapid decay downstream. It was observed that particle velocity also undergoes a decay downstream smaller than that of the jet and is similar with different sizes of particles. The particle velocities at a given jet cross section were also characterized with a top-hat profile which follows with the downstream evolving from a full developed profile at the inlet.

Osman et al [2004] analyzed the hydrodynamic characteristics of a high speed air water jet flow in an abrasive waterjet mixing tube. Visualization of the waterjet structure at the tube inlet and its downstream outlet results indicated that the flow was annular configured co-current flow at the inlet of the focusing tube and the waterjet occupying the whole part of the tube at another region. It was confirmed that a recirculation region existed after comparing the visualization of air waterjet flow with that of the jet in the absence of air. The pressure distribution experiments revealed that three different flow zones exist along the path of the tube. A negative pressure gradient at the inlet, constant pressure in the middle region and a recompression zone near the tube outlet were observed both with and without suction of air in the jet. At low velocities of 316 m/s and 447 m/s, the ejection of water droplets was observed in the waterjet structure with maximum air suction attributed due to the instability of the jet and the water film formed on the tube wall does not merge with the main waterjet.

Jegaraj and Babu [2005] investigated the effect of variation in orifice and focusing tube diameter on performance and cutting efficiency of abrasive waterjet in terms of the depth of cut, material removal rate, kerf geometry and surface roughness. This experiment was carried out at three pressure levels of 100, 175, 200 MPa, abrasive feed rate of 0.07, 0.11, 0.22 kg/min and three different orifice to focusing nozzle diameter ratios. Traverse speed was maintained at 60mm/min, standoff distance was at 3 mm and impact angle of the jet at 90º with garnet size of 120 mesh. Increase in the orifice diameter has significant influence on depth of cut, material removal rate and cutting efficiency whereas variation in focus tube diameter up to 1.2 mm has a minor effect on these characteristics. Change in the size of orifice and focusing tube has a less influence on kerf width and quality of cut in contrast to kerf taper. It was determined that maintaining the orifice sizes in the range of 0.25-0.3 mm and the focusing nozzle diameter in the range of 0.76-1.2 mm (i.e. a ratio between 3 and 4.5), that the abrasive waterjet can produce quality cuts with maximum cutting efficiency.

The influence of orifice and focusing tube variation on the performance of abrasive waterjets was determined by proposing a soft computing approach which combines the response equations of the empirical model with fuzzy model [Jegaraj and Babu, 2007]. This hybrid strategy was used in creating a suitable set of process parameters to achieve the desired cutting performance. A Taguchi experimental design with L27 orthogonal array with 5 factors (Abrasive flow rate, orifice size, focusing tube size, waterjet pressure and traverse rate) and 3 levels each was adapted for conducting the experiments. The analysis of variance conducted on the experimental data predicted that the most influential parameters on surface roughness were focusing tube bore size, traverse rate and waterjet pressure with a contribution of 21%, 17% and 15% respectively.

Wang [2010] discussed the behavior of the fluid phase and particle phase in both radial and axial directions using a two fluid model in the study of fluid flow of the abrasive waterjet. Particle image velocimetry was used to measure the velocity distribution. The radial velocity distributions of the fluid phase in the pure waterjet and abrasive waterjet looked similar implying that the particle phase has a very minor influence. Even in the axial velocity distribution of the fluid phase, the particle phase influence was not large.

The flow behavior of the jet stream inside the mixing tube was studied regarding velocity distributions downstream. Phase Doppler anemometry was utilized to measure the velocity distributions inside the jet stream. Expansion of the jet stream was observed within a small distance of 3 mm reducing the overall magnitude of the average velocity [Kang et al, 2013]. Morphological features of the cut surface were examined using a scanning electron microscope and an optical profiling instrument proved that the size and shape of the abrasive particles have a significant influence on the surface roughness of the cut surface. Besides this, the stand-off distance also contributes to performance of the jet in terms of the quality of the cut.

2.4. STUDY OF NOZZLE WEAR

Due to the passage of the high pressure jet, nozzle wear occurs generally increasing diameter in an irregular fashion. To prevent nozzle wear in abrasive waterjets, Anand and Katz [2003] introduced a solution using porous lubricated nozzles. The introduced experimental set up formed a thin layer of lubricant on the interior walls of the nozzle by continuous injection of the viscous fluid from a reservoir around the nozzle through porous medium in the structure. The underlying principle for the movement of viscous fluid was the pressure difference

between the high speed flow in the nozzle and the reservoir. This thin film of viscous fluid prevented the abrasive particles from striking the nozzle wall thereby reducing nozzle wear.

The two most critical parameters effecting the nozzle wear are the condition of the waterjet nozzle orifice that creates the jet stream and the alignment of the orifice with the jet. An effort was made to identify nozzle wear in abrasive waterjet machining using the acoustic signals generated by the jet [Kovacevic et al, 1994]. An online monitoring approach (closed loop control system) was developed with the use of a microphone mounted on the cutting head, amplifier and data acquisition system. In this case, acoustic spectra were observed in three different cutting conditions-with only pure water pumped through the nozzle, a mixture of water and abrasive used without material cutting and with cutting. The results from the acoustic spectra showed that the amplitude of spectra increased with increasing nozzle inside diameter in all the three tested cutting conditions. However, the analysis of the acoustic signal produced by a mixture of abrasive and water without cutting was determined as the effective approach in measuring nozzle wear as there would not be any noise factor in the acoustic signal caused by workpiece and jet interaction during workpiece cutting. It was concluded that acoustic signals generated with the use of microphone at nozzle helps in identifying nozzle wear due to changes in nozzle inside diameter.

2.5. SURFACE ROUGHNESS MEASUREMENTS

Miles and Henning [2013] made an effort to elevate the difference between average roughness (R_a) and average peak to valley height (R_z) in the measurement of surface finish of abrasive waterjet cut surfaces. Surface finish measurements were obtained using a Pocket Surf® PS1 profilometer. Since the abrasive waterjet machined surface have some level of striations present, there was argument that surface waviness must be included in the

measurement of overall surface roughness. The recommendation was to use Rz as a measure of surface roughness since it captures the striations present on the machined surface when measured from bottom of the workpiece at the jet exit.

Surface roughness measurement conditions and sources of uncertainty in these measurements were studied using stylus instrument by Vorburger et al [2014] in National Institute of Standards and Technology. Measurement system uncertainty for R_a was analyzed and deduced to be from the uncertainty components of deviation in calibration constants, variation in the measured R_a values due to non-linearity in the instrument transducer and uncertainty in horizontal and vertical resolution of the instrument.

2.6. ABRASIVE FRAGMENTATION

In the process of acceleration of abrasives in the cutting head, the high energized jet comes into act and has its effect on the abrasive breakage in cutting head. Galecki et al [1987] estimated that the energy transfer efficiency is based upon the disintegration of abrasives particles before the exit from the cutting head and the pressure difference created between the water nozzle and the slurry nozzle. Abrasive disintegration of three garnet grit sizes of 425 µm, 250 µm and 150 µm at two different pressures of 138 MPa and 275 MPa were investigated. The ejected slurry was collected in a container directed through a 4.2 m long PVC pipe and dried. After sieving analysis, it was observed that 70 % to 80% of abrasives were disintegrated depending on the garnet grit size flown into the mixing tube. They concluded that the jet energy was lost in the process of acceleration and disintegration of abrasives in the cutting head in the form of heat due to particle to particle collision. This factor has to be considered in finding the effectiveness of the hydro abrasive cutting head design. In the same work, it was also found

out that the cutting capability of a cutting head will depend on the distance between the waterjet orifice exit and the focusing tube entrance.

Similar research was carried out with GMA type of garnet abrasives in studying the particle size distribution after disintegration in the cutting head along with the effect of abrasive flow rate on focusing tube wear by Perec [2011]. A KMT intensifier I50 and 2 axis CNC table with Techni waterjet control system was used in conducting the experiments. Two types of garnet GMA 80 and GMA 120 were analyzed at five abrasive concentrations in the jet using three cutting heads of different orifice and focusing tube diameters ratio. The abrasives were collected in a closed PVC tank catcher with a steel shield in the bottom to avoid penetration. A very significant particle size decrease was observed with the largest fraction of the abrasives being less than 53 μm in size. Difference in the particle size distribution of the two types of garnet was very small after acceleration in the cutting head. Abrasive concentration and focusing tube to orifice diameter ratio had a minor influence in abrasive breakage. Focusing tube wear was similar for the two garnet types and wear was proportional to the mass of abrasives passing.

In concluding this literature review, a lot of research work was observed in the areas of development of abrasive waterjet cutting in various applications, the influence of various parameters on the depth of cut and quality of cut, visualization of AWJ by cutting transparent materials and also in analyzing flow pattern of jet in the cutting head.

Researchers also have carried out experimental work to find the mechanism behind material removal in AWJ cutting using varieties of both ductile and brittle materials. There was some extent of research work focused on nozzle wear.

Commercial calculators are available for predicting the depth of cut at various levels of parameters and in estimation of quality of cut. However, there is no software available for the estimation of exact value of surface roughness of the cut wall. In this research with emphasis on predicting model equation for surface roughness, Box-Behnken experimental design with response surface methodology was adapted. In addition to that, disintegration of abrasives in the cutting head was an area where there was no in depth analysis with experimental work. So, having a focus on the prediction of surface roughness, abrasive fragmentation was studied in depth using 80 HPX Barton garnet.

3. BOX-BEHNKEN RESPONSE SURFACE DESIGN THEORY

3.1. RESPONSE SURFACE METHODOLOGY

Response surface methodology (RSM) was first introduced by G.E.P. Box and K.B. Wilson in 1951. This methodology was used for deriving second order empirical model from experimental data sets and subsequently used for optimization of the response surface that is influenced by various process parameters. These statistical empirical model is only an approximation to reality. Nevertheless, RSM has been used effectively in various applications optimizing products and services [Box and Draper, 1987].

According to Box and Draper, if all variable process parameters are assumed to be measurable, the response surface can be expressed as follows:

$$y = f(x_1, x_2, x_3, \dots\dots\dots, x_k) \tag{3.1}$$

where y is response of the process and x_i are variables of the process named as factors.

The first goal for RSM is to find the optimum response. The second goal is how the response changes in a given direction by adjusting the design variables. It is required to find a suitable approximation defining true functional relationship between the independent variables and response variable. Usually, a second order model is developed in response surface methodology. [NIST/SEMATECH e-Handbook].

$$y = \beta_o + \sum_{i=1}^{k} \beta_i x_i + \sum_{i=1}^{k} \beta_{ii} x_i^2 + \sum_{i=1}^{k-1} \quad \sum_{j=2}^{k} \beta_{ij} x_i x_j + \varepsilon \tag{3.2}$$

Where $x_1, x_2, x_3, \dots\dots\dots, x_k$ are the input variables influencing the response y; β_0, β_{ii} ($i = 1,2,\dots,k$) and β_{ij} ($i = 1,2,\dots,k; j = 1,2,\dots,k$) are unknown coefficients and ε is a random error.

The β coefficients, which should be determined in the second order model are obtained by least squares method.

3.2. BOX- BEHNKEN EXPERIMENTAL DESIGN

Two main response surface designs are the central composite designs (CCD) and the Box- Behnken designs. The choice of experimental design depends upon the number of factors to be investigated and the objective of the experiment. Of the two response surface designs, Box-Behnken design requires a lower number of runs for 3 factors, and was thus chosen for conducting this experiment and also CCD was reputed to require a few extreme levels defined to maintain rotatability which is infeasible.

Box- Behnken design and response surface methodology was successfully applied for modeling of Turkish coals. The variables that were investigated in this model were: ball diameter, grinding time and bond work index [Aslan and Cebeci, 2007].

Box-Behnken design is an independent rotatable quadratic and response surface design which does not include factorial design in it. In this design, treatment combinations include the midpoints of edges of the process and at the center. Compared with full factorial and central composite designs, the Box- Behnken design has a unique advantage of requiring a fewer experiments for a 3 factor design thus providing a time efficient and economical way of obtaining and analyzing the data [NIST/SEMATECH e-Handbook].

Figure 3.1 represents Box-Behnken design for 3 factors showing treatment combinations at the midpoint of each edge and at the center. From geometry of this design, the spheres in the process space were located at midpoints of the edges and at the center such that they are tangential to midpoint of each edge of the space.

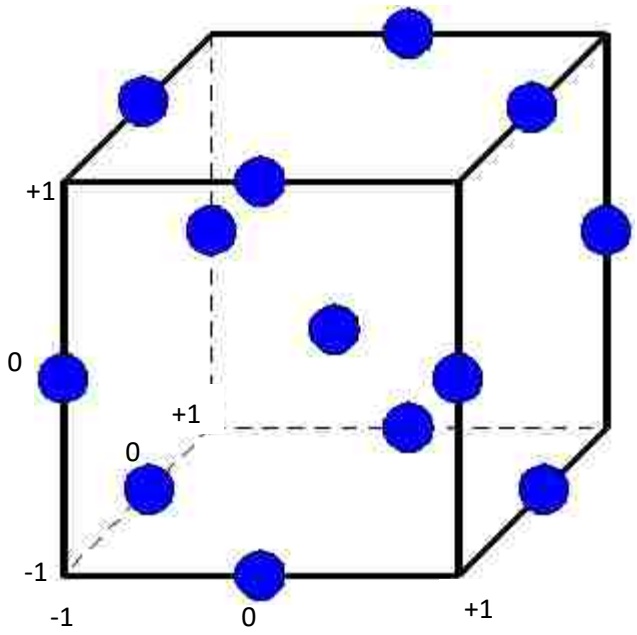

Figure 3.1. Box-Behnken design for three (3) factors
Modified by the author to serve the purpose of explanation of the illustration.
[http://www.itl.nist.gov/div898/handbook/pri/section3/pri3362.htm]

Being a response surface design, this experimental design was identified to have the desirable properties of rotatability- information distribution across the experimental region, fitted values close to observed values and good graphical analysis [Box and Draper, 1987].

Factor settings of Box-Behnken design for three factor each with 3 levels (low, center and high) is represented in Table 3.1. In this, (-1) denotes low level setting of factor, (0) denotes center level of factor and (+1) denotes high level of factor. The treatment combination is the combination of the settings of factors in an experiment trial.

Table 3.1. Treatment combinations for Box-Behnken design for 3 factors

Sequence number	Factor 1	Factor 2	Factor 3
1	-1	-1	0
2	+1	-1	0
3	-1	+1	0
4	+1	+1	0
5	-1	0	-1
6	+1	0	-1
7	-1	0	+1
8	+1	0	+1
9	0	-1	-1
10	0	+1	-1
11	0	-1	+1
12	0	+1	+1
13	0	0	0
14	0	0	0
15	0	0	0

This experimental Box- Behnken design was created using Minitab, a statistical software. The number of experimental runs required for various number of factors for different response surface designs was shown in Figure 3.2. The Box-Behnken design requires 15 experimental runs for 3 factors with 3 levels.

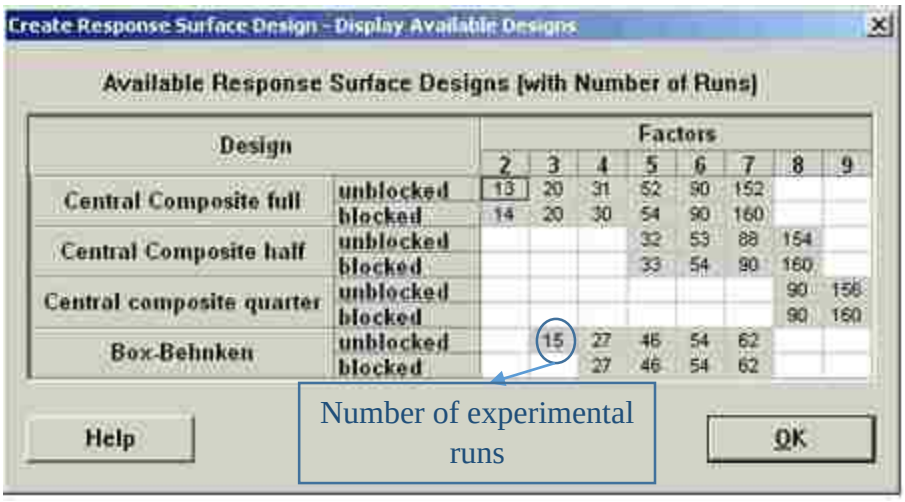

Figure 3.2. Screenshot of response surface design creation in Minitab

The process variables chosen for this experimental design were pressure, traverse speed and abrasive mesh size. Three levels for each factor were taken as per the Box-Behnken response surface experimental design within the interested range of parameters. Standoff distance was kept at a constant value of 1/8 inch for all the experimental runs. A KMT AUTOLINE cutting head configured with a 0.014-inch diameter orifice and an 0.043-inch diameter focusing tube was utilized throughout the experiment. Based on the treatment combination of the design, selected isolated sizes of 80 HPX® grade of BARTON garnet was used as the abrasive and a small hopper above the vibratory magnetic feeder was used to supply the garnet. Abrasive flow rate was taken at three different levels of 1 lb/min, 1.5 lb/min and 2 lb/min. Experiments were conducted according to Box-Behnken design varying the other three process parameters at each abrasive flow rate.

Actual levels of the process parameters (A, B and C) shown in Table 3.2 are calculated and used in the Box-Behnken design. These experimental runs were conducted at three abrasive flow rates with three replications. The replications were done so as to predict the

response in a precise method having great power in detecting the effect of changing levels of parameters.

Table 3.2. Levels of Box-Behnken design for 3 selected factors

Variable	Symbol	Coded variable level		
		Low (-1)	Centre (0)	High (+1)
Water Pressure (ksi)	A	60	75	90
Traverse Speed (in/min)	B	20	40	60
Abrasive Mesh Size	C	50	60	70
Abrasive flow rate (lb/min)	D	1.0	1.5	2.0

Using the same Box-Behnken design, 80 HPX standard Barton garnet directly taken from a 55 lb bag was used in performing a second set of experimental runs with abrasive flow rate (D) as the varying parameter along with water pressure (A) and traverse speed (B).

4. EXPERIMENTATION METHODOLOGY

4.1. INTRODUCTION

In this section, the detailed explanation of the experimental setup, abrasive analysis which includes particle size distribution and abrasive disintegration during acceleration within the cutting head, surface roughness measurement, Box-Behnken experimental design are presented.

4.2. EXPERIMENTAL SETUP

The equipment used for cutting was 5 axis PAR system coupled with 90,000 psi/125 HP intensifier of KMT Pro waterjet systems. Waterjet pressure was set at the required level using the control panel mounted on the KMT intensifier system. Taking into consideration [from the literature review] that an orifice to focusing tube diameter ratio of between 3.5 and 4.5 optimizes the performance of the cutting head, 0.014”/0.043” ratio orifice to focusing tube diameter cutting head was used throughout the experiment. All desired experimental runs for cutting were performed using this equipment set up shown in Figure 4.1.

SurfCAM 5.0 software was used to sketch the pattern with required number of linear cuts and to generate the necessary computer numerical control (CNC) program according to the cutting pattern to be fed into the system. Rapid and cutting feed rate were given as inputs while preparing the CNC program using the software. Here, cutting feed rate refers to the traverse speed which can be changed on the monitor interface of PaR systems as per required.

Abrasive flow rate was controlled by a syntron vibrating electromagnetic feeder attached to the KMT cutting head shown in Figure 4.2. This feeder allows an abrasive flow rate of up to 4.0 lb/min. Though there is suction of the abrasive due to the high pressurized water in cutting head, the flow rate was controlled by this vibratory feeder.

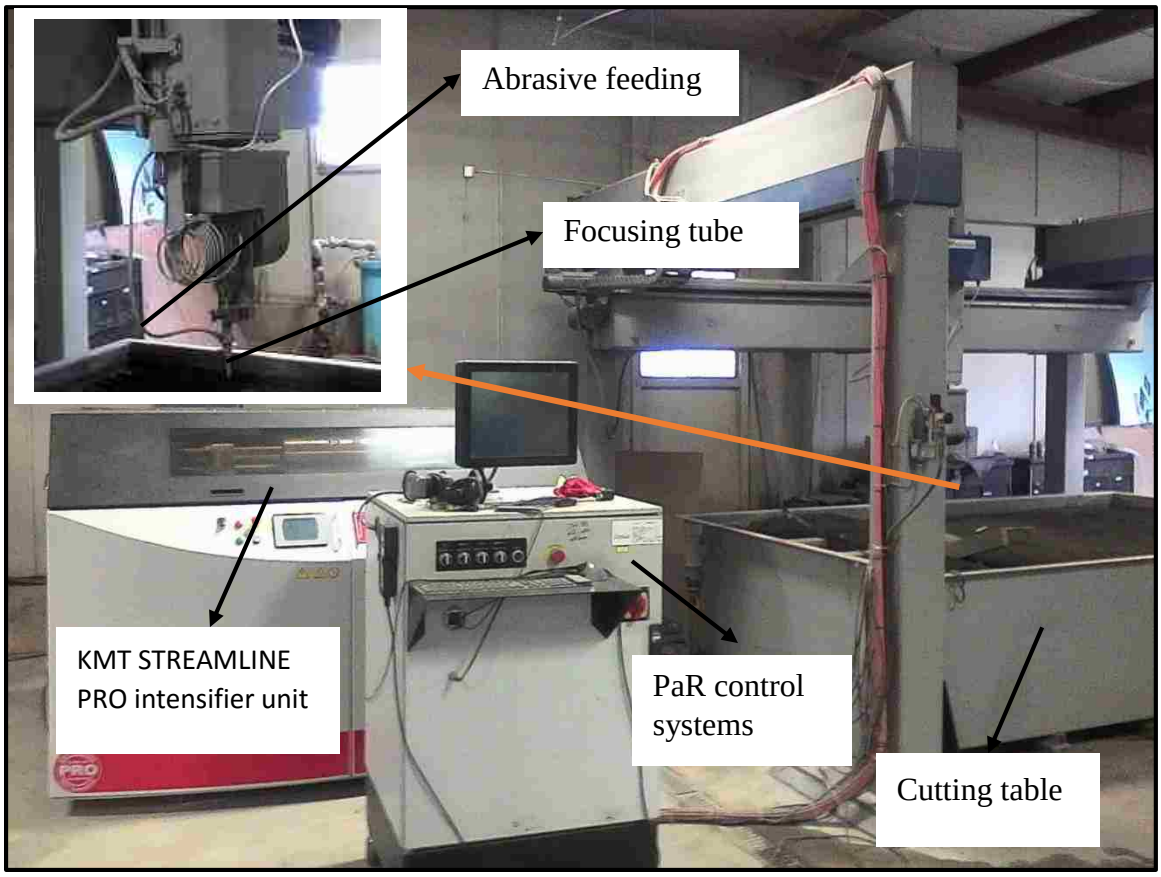

Figure 4.1. 5 axis PAR waterjet cutting system coupled with KMT PRO intensifier

Graphite/Epoxy composite of two thicknesses 1/4 inch and 1 inch was used for this experimental work. The properties of this composite are listed in Table 4.1. This information was provided by the Boeing Company.

Figure 4.2. Syntron vibratory electromagnetic abrasive feeder in PaR systems

Table 4.1. Properties of graphite/epoxy composite

	Property	**Value**
1.	Fiber Orientation	0°, 90°,+/-45°
2.	Fiber Diameter	5-6 microns in a tow of 0.007”
3.	Resin Volume Fraction	0.355 (Nominal)
4.	Lamina Thickness	0.007”
5.	Number of layers in each laminate	33

4.3. SURFACE ROUGHNESS MEASUREMENT

A Mitutoyo surface profilometer, SJ-201was used to measure surface roughness of the cut walls of the linear samples. Average surface roughness (R_a) was measured for assessing the surface quality. This gives a good description of the height variations in a surface. The roughness meter was set at a cutoff length of 0.03”X5 with five sampling lengths for qualitative measurement of R_a and better surface analysis. The surface roughness of the Mitutoyo precision reference specimen used for calibration was 117 µin.

After performing the linear cuts, the cut surface of the linear samples was observed and found out that quality of cut was not uniform throughout the thickness. The surface roughness was measured at three different locations from the top layer of the composite in the jet direction i.e. at the jet entrance, middle of the specimen and at the jet exit shown in Figure 4.3.

Vector waterjet systems of PaR automation was used for the motion control of the 5 axis cutting head. In these experiments, linear movements (x, y and z) of the cutting head were utilized in programming and rotational components of the cutting head were kept constant. For smoothing the axis motion, there was constant acceleration at the beginning of the motion until the desired velocity is reached and constant deceleration at the end of motion until the desired velocity is zero. Along the cut direction, R_a measurement was taken at three locations. In all these measurements, the stylus of the profilometer was oriented in the fiber direction. The mean of these values at each depth was calculated for analysis.

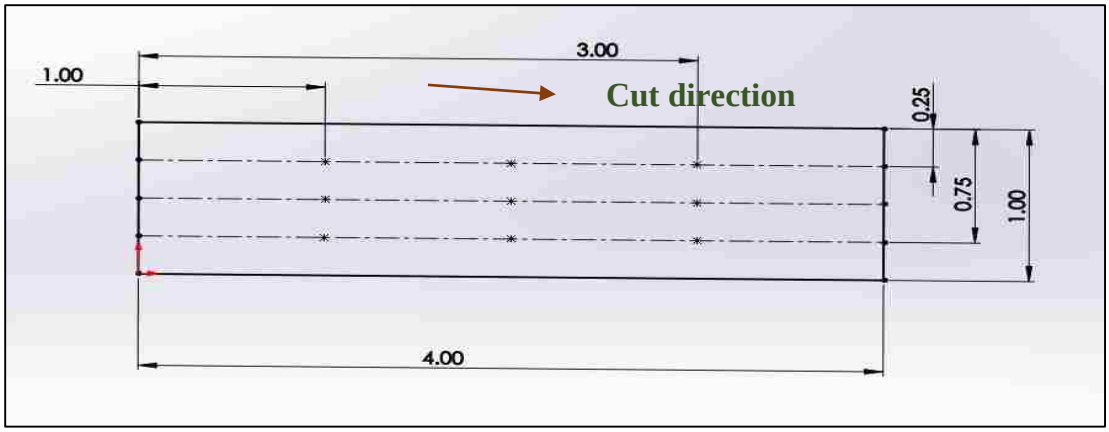

All dimensions are in inches.

Figure 4.3. Sketch representing Ra measurement at 3 locations at 3 different levels of cutting depth for 1-inch-thick composite

4.4. ABRASIVE ANALYSIS

There are various varieties of garnet available in the commercial market today. 80 HPX Barton garnet which was commercially popular and widely used in the industry was chosen for this experimental research. It has the ability to cut wide varieties of materials including all metals, composites, ceramics and stone. It also has a faster cutting speed and greater flexibility which makes industries use it for precision waterjet operations. The 80 HPX® Barton garnet with HR 060180 batch number as identified on side of the bag shown in the Figure 4.4 was used in all the experimental work. This garnet was examined with USB microscope to find the sharp edges and the sizes of the particles were really helpful in faster and precision cutting.

Figure 4.4. 80 HPX® Barton garnet used for the experiment (Batch number HR 060180) and Microscope observation (60X)

4.4.1. Particle Size Distribution of Garnet. A series of experimental runs were conducted on a 55 lb bag of Barton waterjet abrasives to study and analyze the particle size distribution. For this, the aggregate volume was reduced to a testing sample size using a mechanical splitter. A sample splitter for finite aggregate with twelve openings equipped with two receptacles was chosen to serve the purpose of reducing sample size. Taking the reduced sample, sieving was done with mechanical sieve shaker using 40, 50, 60, 70, 80 and 100 US standard 6-inch diameter sieves and sieving was continued for 5 minutes. This sieving period was kept constant for all the samples that are sieved. After sieving, the weight of garnet retained on each mesh screen was recorded.

For the purpose of particle size distribution, three different varieties of abrasives- Barton garnet, GMA Australian garnet and Wesjet garnet of 80 HPX size were analyzed and

results are shown in Figure 4.5. Out of the three types of garnets, Barton garnet was found to have a great percent of small size particles followed by GMA Australian garnet. Wesjet garnet had a higher percent of 50 mesh (large size) particles but the abrasive was not the focus of this study. Garnets of 80 HPX size showed a significant difference in the particle size distribution. However, disintegration analysis was carried out only on 80 HPX Barton garnet due to limited quantities of GMA Australian garnet and Wesjet garnet.

Figure 4.6 represents the particle size distribution determined by mechanical sieving of a 55 lb 80 HPX Barton garnet bag. The particle size distribution is compared with the abrasive particle size distribution provided by Barton, manufacturer of the garnet. This analysis showed a difference between the actual particle size distribution of the garnet and that claimed by the manufacturer.

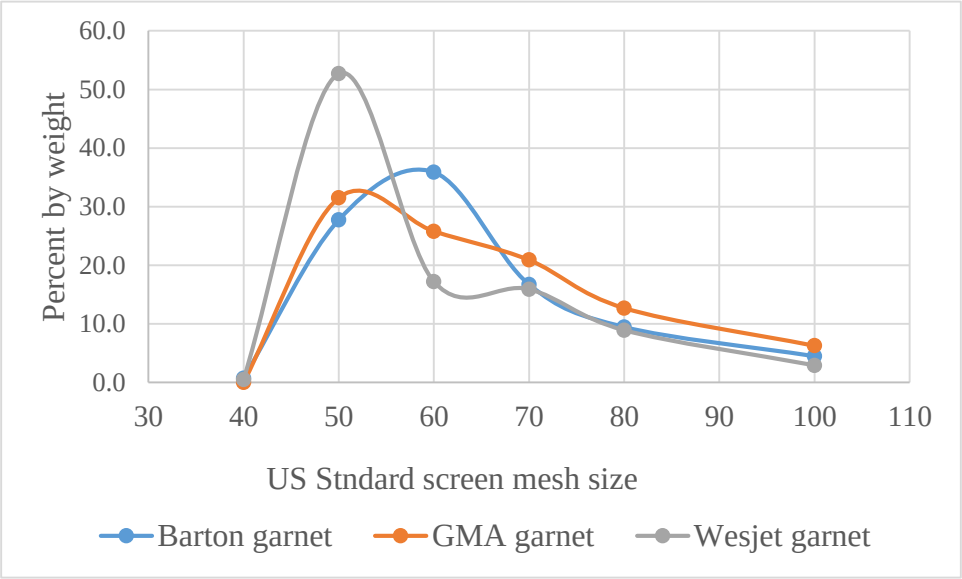

Figure 4.5. Particle size distribution of Barton, GMA and Wesjet garnet.

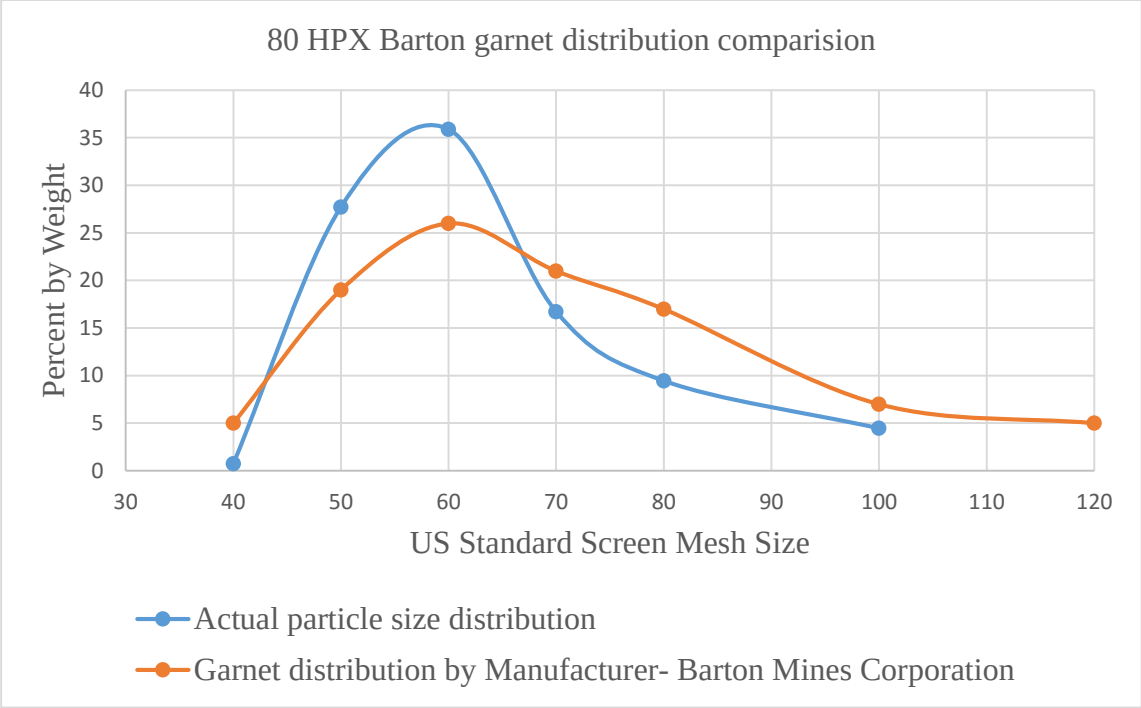

Figure 4.6. Comparison of experimentally analyzed particle size distribution with the size distribution provided by Barton Mines Corporation

Using the PaR systems, a series of experiments was conducted at abrasive flow rates of 1 lb/min, 1.5 lb/min and 2 lb/min. The flow pattern of the abrasive changed when going from the small hopper to using large hopper. So, the experiments were done with small hopper and large hopper separately. All the collected samples of garnet were sieved separately to analyze and compare the particle size distribution at each abrasive flow rate.

Figure 4.7 shows the particle size distribution of the garnet abrasive at abrasive flow rate of 1lb/min, 1.5 lb/min and 2 lb/min. Here, the small hopper was used as the abrasive feeder and the garnet was collected in a container before being introduced into the cutting head at the above mentioned flow rates. There was no significant difference in the particle size distribution of the garnet abrasive at all the three abrasive flow rates.

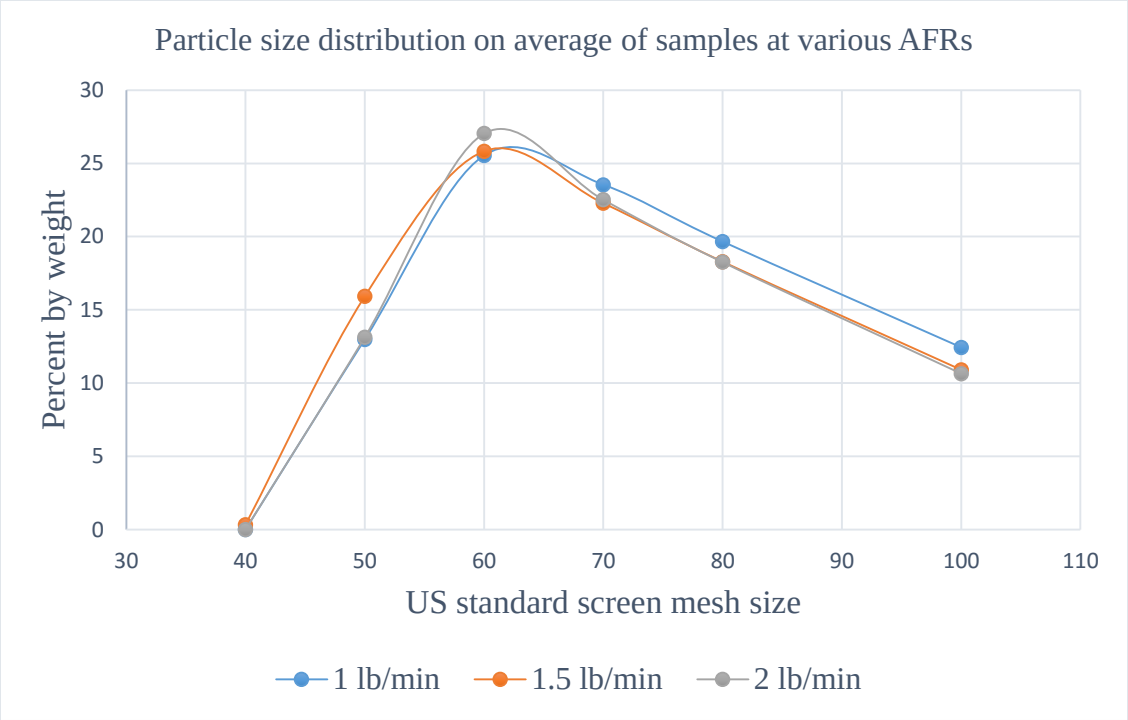

Figure 4.7. Particle size distribution of garnet collected using small hopper of PaR systems

Figure 4.8 shows the particle size distribution of the garnet abrasive at abrasive flow rate of 1lb/min, 1.5 lb/min and 2 lb/min. The large hopper was used as the abrasive feeder and the abrasives flowed through the small hopper before being introduced into the cutting head at the three mentioned flow rates. There was a difference in particle size distribution of garnet but no significant variance was observed from one AFR to another AFR. So, from the experimental observations abrasive flow rate has almost no impact on the particle size distribution of garnet when it did not pass through the cutting head. After analyzing the particle size distribution at different feed rates using different abrasive feeders, there was no significant difference in size distribution from one flow rate to other without actually cutting the workpiece where the abrasive encounters the jet in the mixing tube.

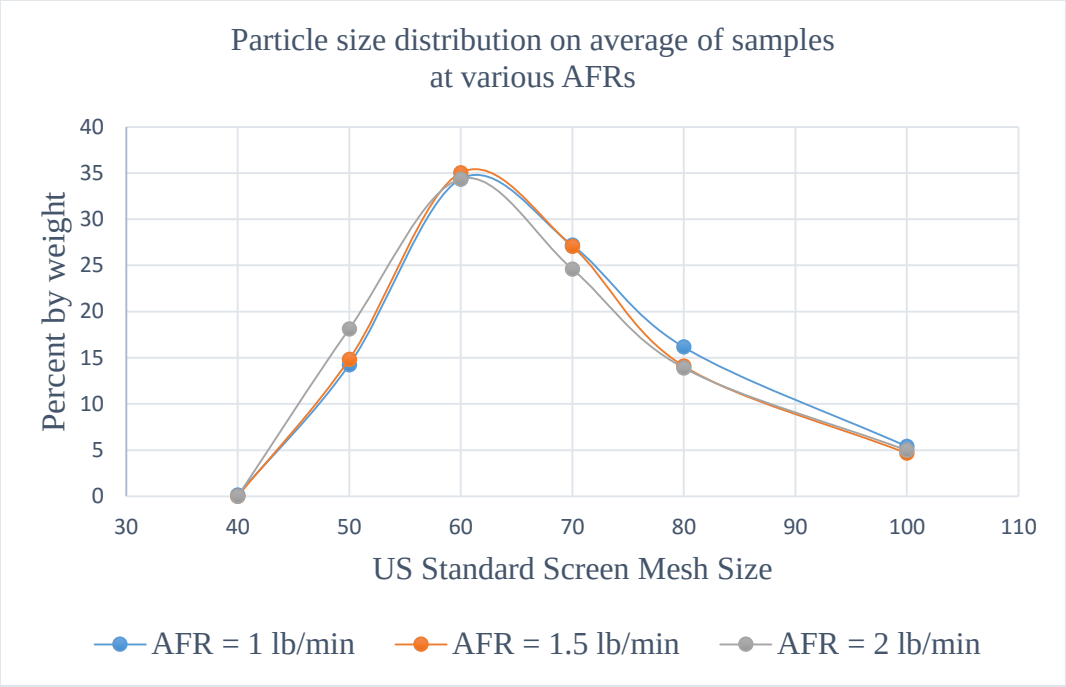

Figure 4.8. Particle size distribution of garnet collected using large hopper of PaR systems

To compare different conditions of abrasive feeding, the experiments were also carried out with an Omax abrasive feeder with 80 HPX Barton garnet [Figure 4.9], in which the abrasive flow rate depends on the opening of the orifice. A sample of garnet was collected for 1 min to find the abrasive flow rate using the test and run on the computer interface. The abrasive flow rate was found to be approximately 0.72 lb/min- the average of 3 repeats, for the condition on production unit used in MST- Waterjet Laboratory. Sieving was performed for each sample following the same procedure mentioned above. Analysis of particle size distribution was performed considering the percent by weight of the sample in each screen mesh.

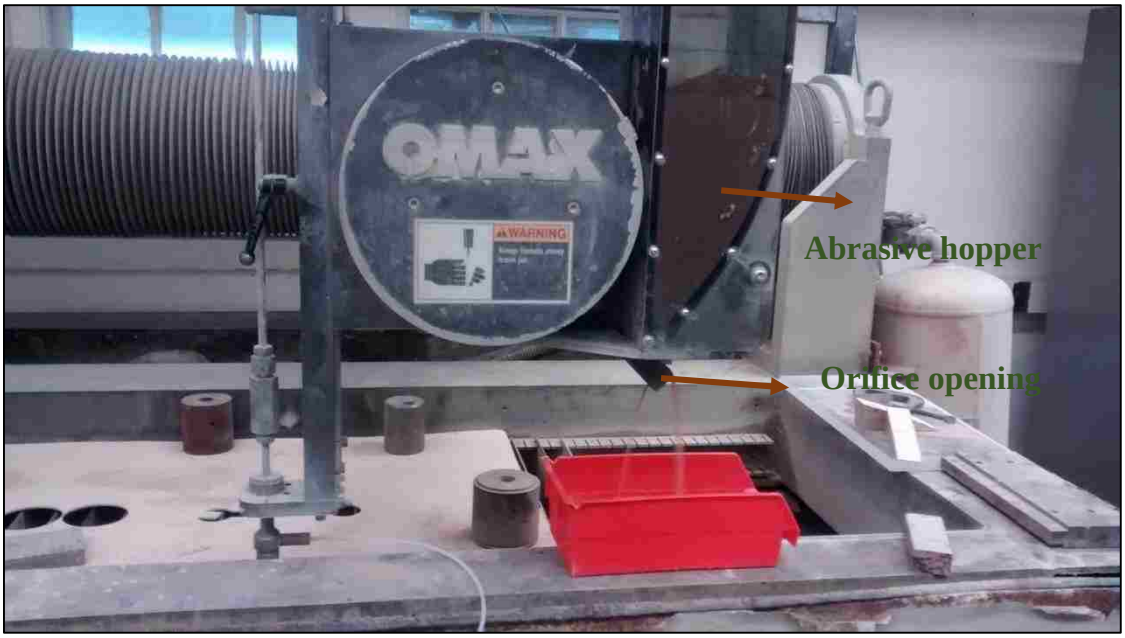

Figure 4.9. OMAX waterjet systems gravity controlled abrasive feeder

The particle size distribution of the garnet when the abrasive was fed through the small hopper, the large hopper of the PaR systems and the OMAX hopper were compared as shown in Figure 4.10. Since there was no significant impact of abrasive feed rate on size distribution, the average percent by weight at all three feed rates is taken and compared to see the impact of feeding type on particle size distribution. The particle size distribution of garnet collected using the small hopper was close to the size distribution provided by Barton, the manufacturer of the garnet. The percentage by weight distribution of abrasive particles delivered using the large hopper of the PaR systems was at 35% on screen #60 whereas the results with the OMAX systems gravity hopper, showed that a greater number of abrasive particles were retained on screen #50 with around 50 percent by weight.

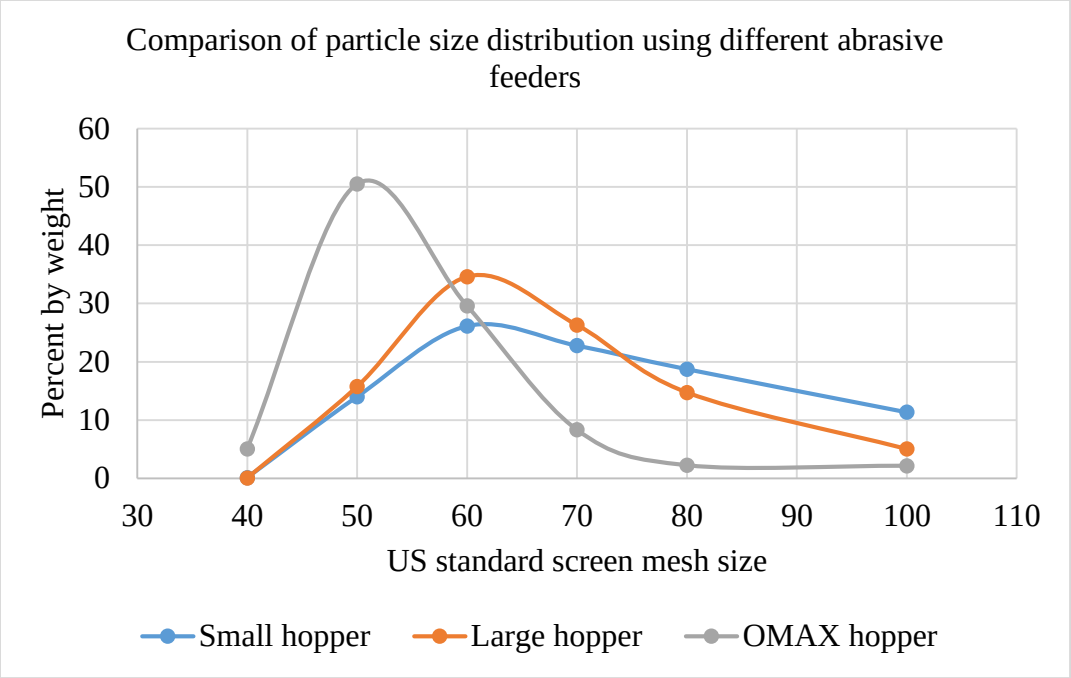

Figure 4.10. Comparison of particle size distribution of garnet collected using OMAX feeder and PaR systems feeders

4.4.2. Abrasive Disintegration. It was shown by Galecki and Mazurkiewicz [1987] that abrasives undergo undesired disintegration during mixing with a jet. Abrasive flows into the mixing chamber drawn in by the venturi effect. Then, the abrasive particles are packed into the focusing tube by the fast moving waterjet. Abrasive particle breakage occurs during the initial impact by waterjet in the mixing chamber and during the further acceleration within the mixing tube. Figure 1.1 helps to illustrate the abrasive path. For the purpose of this study, a cutting head with an orifice diameter of 0.014" and a focusing tube diameter of 0.043" was used. The cutting head was mounted horizontally and was directed into a series of 6" diameter PVC pipes with a length of 30 feet. The abrasive ejected at the exit of the focusing tube was collected in a container placed at the end of the PVC pipe setup as shown in Figure 4.11. Abrasive was collected under a combination of 3 pressure levels and 3 abrasive flow rates. For

accuracy, these experiments were repeated three times. After drying of abrasive slurry, sieving was performed.

Conditions used in the experiment:

- Abrasive type: 80 HPX Barton Garnet.
- Three different pressures: 60 ksi, 75 ksi and 90 ksi.
- Abrasive flow rate: 1 lb/min, 1.5 lb/min and 2 lb/min.

Figure 4.11. Abrasive capture after jet exit

Note: The steam coming out; this is an indicator of energy losses for abrasive acceleration.

4.4.2.1 Disintegration of 80 HPX Barton garnet at different pressures. The effect of abrasive disintegration for different abrasive flow rates at different pressure levels is shown in Figures 4.12a-c. Figure 4.12a show the amount of abrasive that was disintegrated in the cutting head at a jet pressure of 60,000 psi. More than 50% of the recovered garnet collected in the pan placed below the screen #100 indicating that more than half of the sample was smaller than 150 µm. Comparing this with the size distribution of the garnet before disintegration, a very significant decrease in the particle size was observed. Also, it was observed that the abrasive flow rate had no significant impact on the abrasive particle disintegration.

At 75 ksi, the amount of abrasive disintegrated in the cutting head was shown in Figure 4.12b. More than 50% of the collected garnet was found to be smaller than 150 µm. A very significant decrease in the particle size was observed comparing with the size distribution of garnet before disintegration. There was almost no impact of abrasive feed rate on the particle defragmentation.

Figure 4.12c show the amount of abrasive disintegrated in the cutting head at a jet pressure of 90,000 psi. It was evident from the graph that the particle size decreased significantly after disintegration. Roughly 60% of the abrasive particles passed on all the screens and collected in the bottom pan during sieving and this was clearly shown in the graph. Based on the experimental data presented, it can be concluded that effect of abrasive feed rate on the particle breakage is small and is considered as negligible.

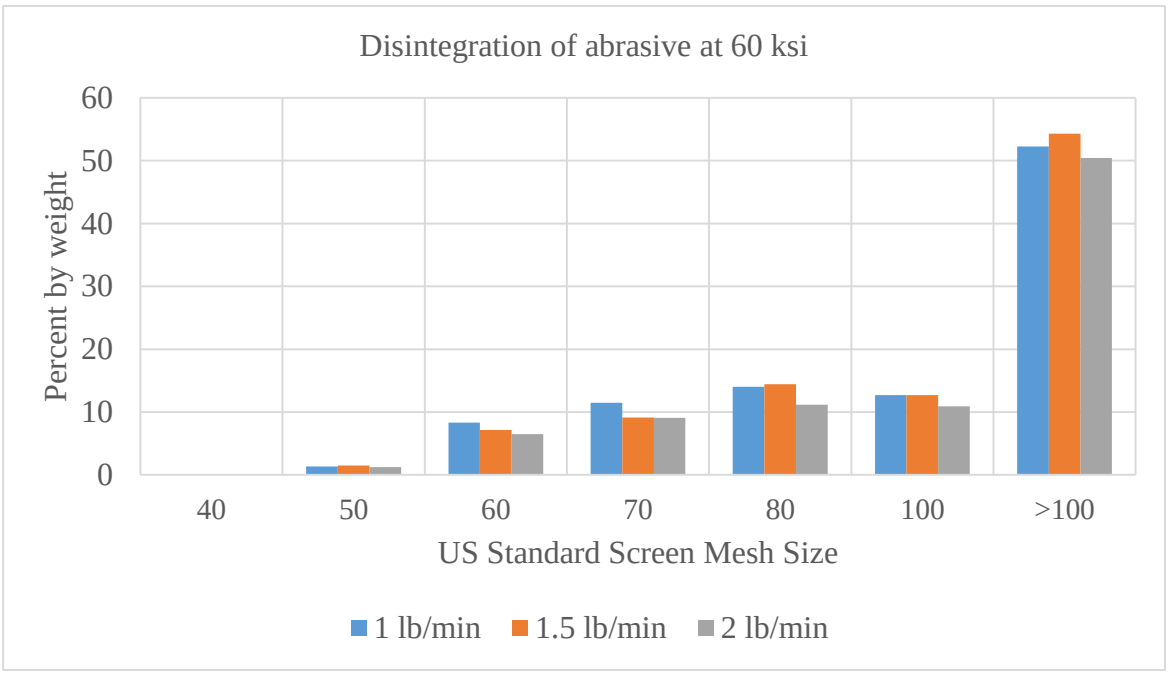

4.12 (a)

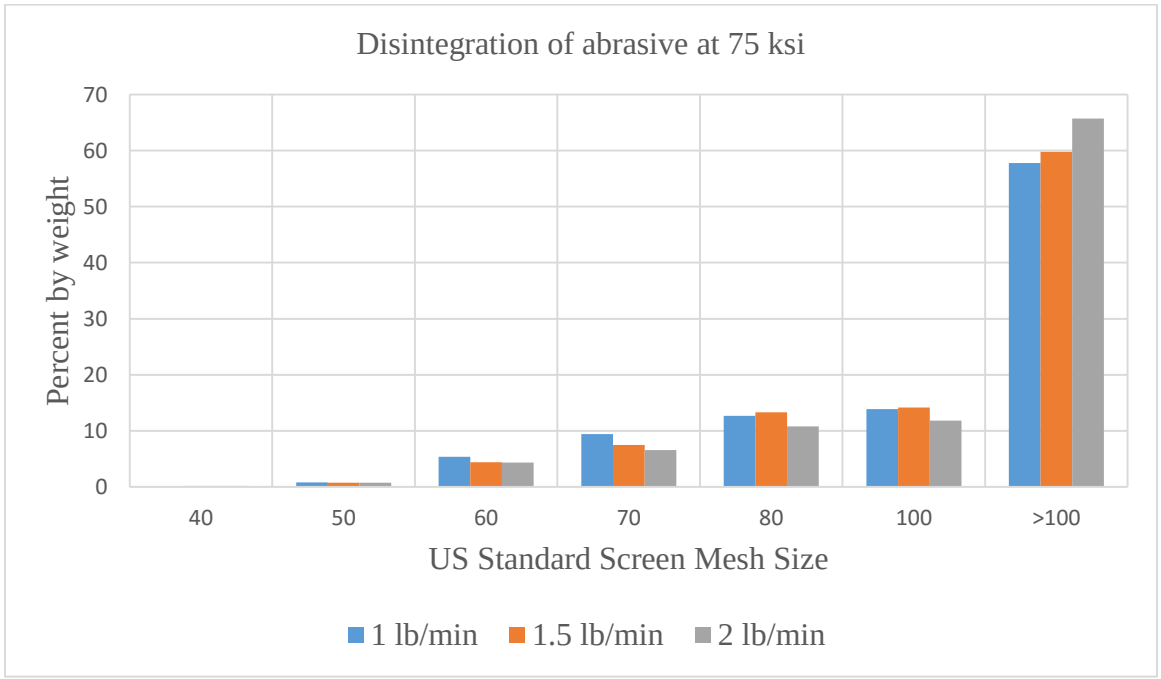

4.12 (b)

Figure 4.12. Particle size distribution of 80 HPX Barton garnet after passing through cutting head, (a) pressure 60 ksi (b) pressure 75 ksi and (c) pressure 90 ksi

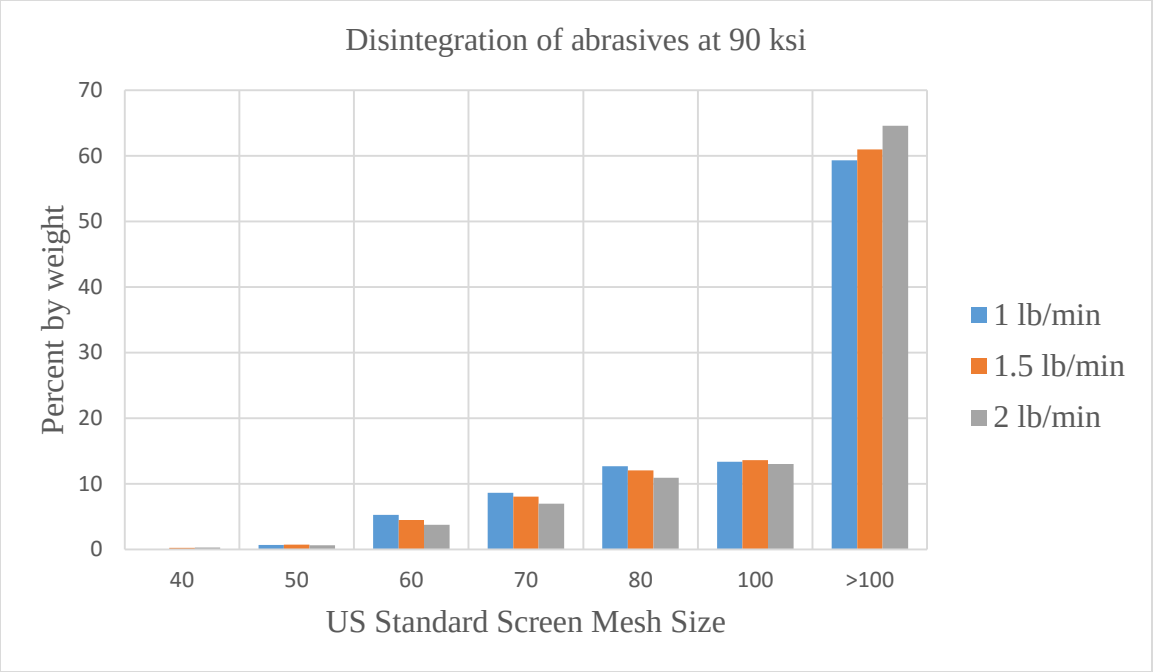

(c)

Figure 4.12. Particle size distribution of 80 HPX Barton garnet after passing through cutting head, (a) pressure 60 ksi (b) pressure 75 ksi and (c) pressure 90 ksi (cont)

4.4.2.2 Disintegration of 80 HPX Barton garnet at different abrasive flow rates. In the Figures 4.13a-c, the effect of pressure on abrasive disintegration is shown. These are the same data as shown in section 4.4.2.1 but rearranged to clearly show how pressure affects abrasive disintegration at different flow rates. Figure 4.13a shows the abrasive disintegrated in the cutting head at an abrasive flow rate of 1 lb/min and three pressures of 60 ksi, 75 ksi and 90 ksi. 50- 60% of the abrasives was smaller than 150 µm. From the original garnet particle size distribution, percent by weight of particles smaller than 150 µm was less than 5%. There was significant decrease in the particle size observed during disintegration. It can be referred from the graph that at an abrasive flow rate of 1 lb/min, the particles look like more disintegrated at 90 ksi pressure rather than at the 60 ksi and 75 ksi pressure levels.

Effect of pressure on the disintegration of abrasives at flow rate of 1.5 lb/min is shown in Figure 4.13b. 50- 60% of the abrasives were smaller than 150 µm and overall, there was significant decrease in the particle size observed during disintegration. Comparing the size distribution before and after the disintegration, not more than 5% of the abrasives were retained on screen #100 or below before disintegration but there was more than 60% of abrasives retained on the pan below all the screens after disintegration. Abrasive disintegration at a flow rate of 2 lb/min is shown in Figure 4.13c. In this case, 60% of the particles accumulated on the bottom pan indicating that pressure has significant influence on the disintegration. At 90 ksi, 60% of the abrasives were smaller than 100 screen size whereas at 60 ksi, 54% were observed to be smaller than 100 screen size after disintegration. This is an indication of increasing percentage of abrasive undergoing disintegration as a function of pressure.

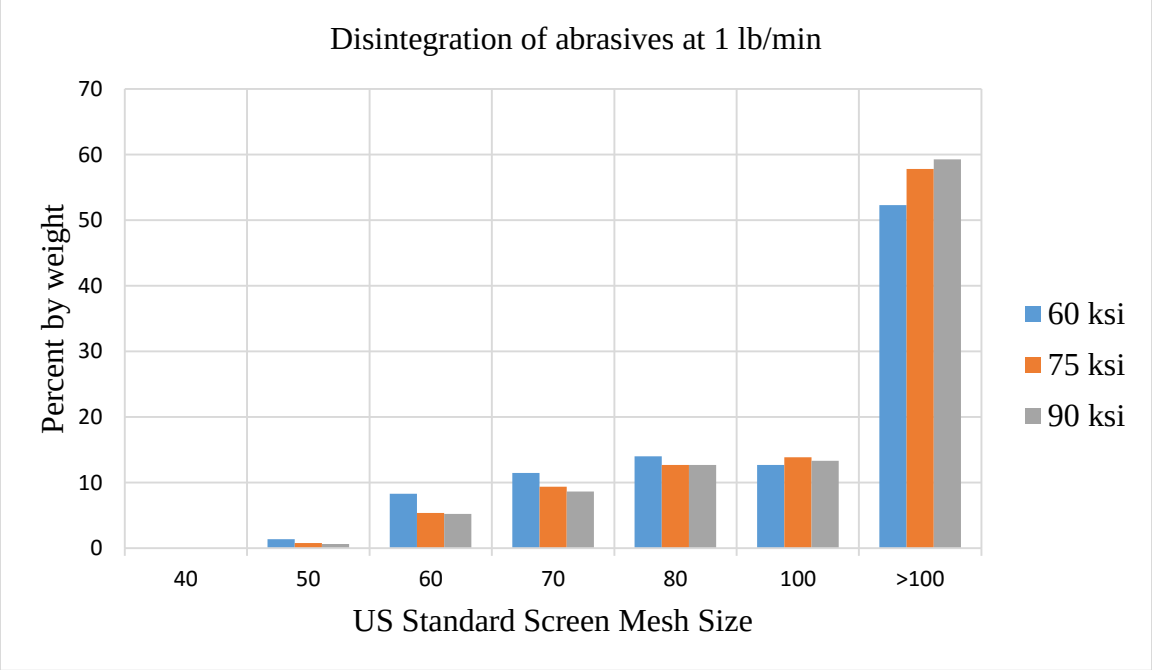

(a)

Figure 4.13. Particle size distribution of 80 HPX Barton garnet after passing through cutting head, (a) AFR 1.0 lb/min (b) AFR 1.5 lb/min and (c) AFR 2.0 lb/min

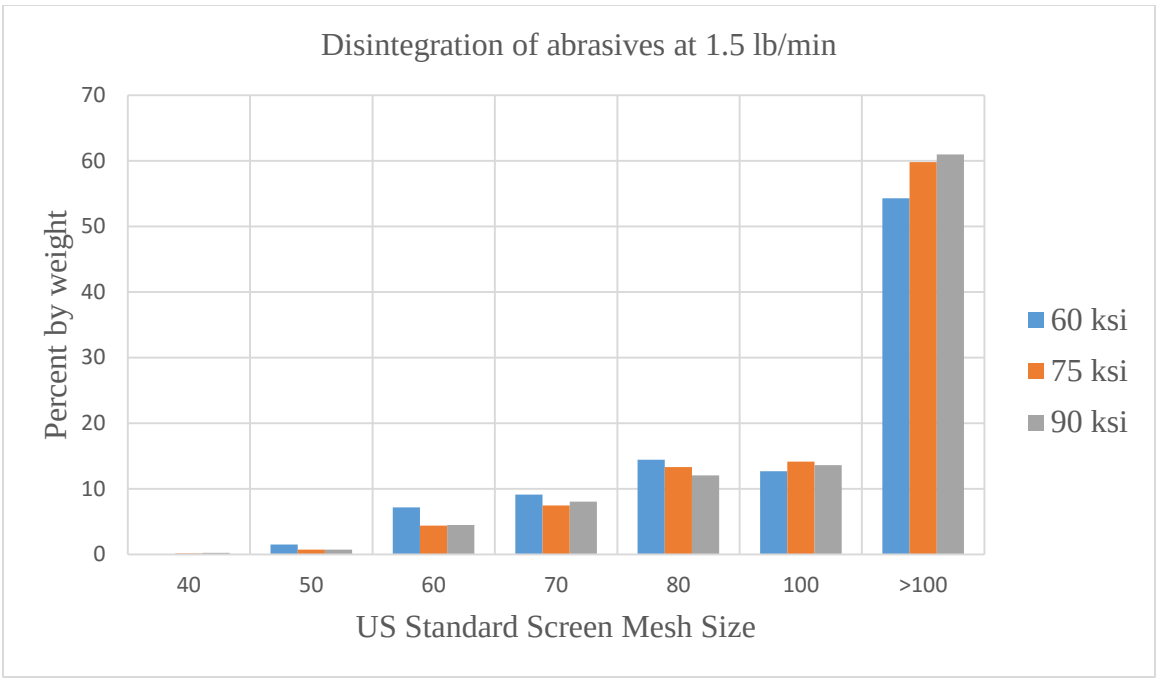

(b)

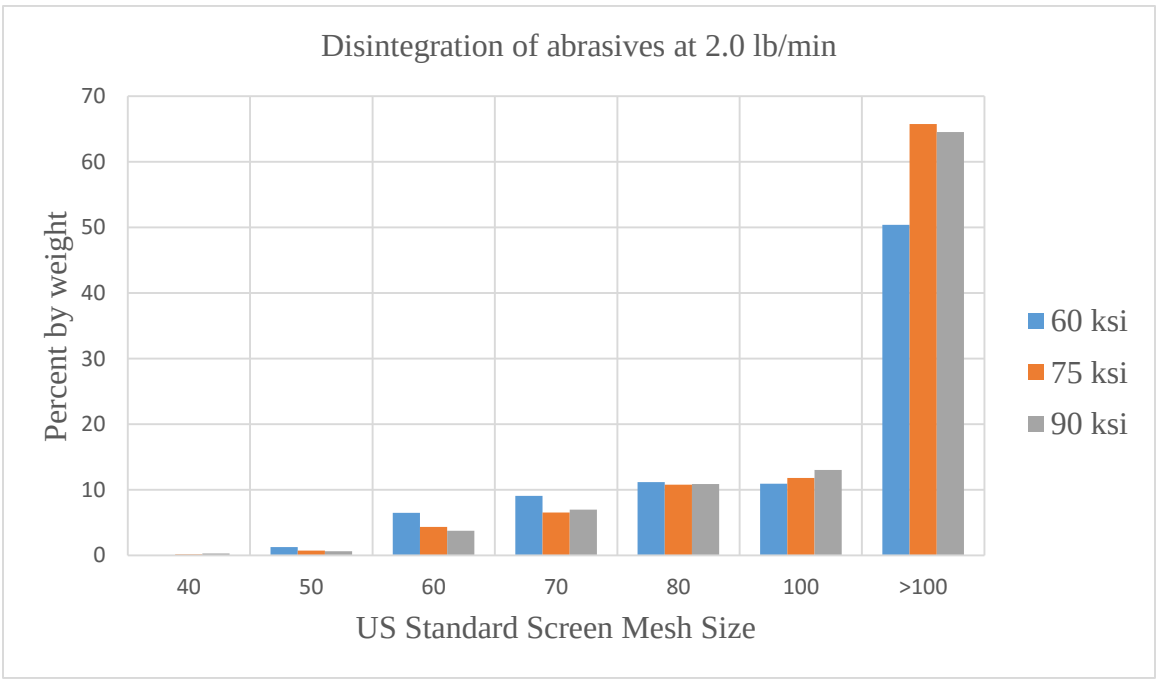

(c)

Figure 4.13. Particle size distribution of 80 HPX Barton garnet after passing through cutting head, (a) AFR 1.0 lb/min (b) AFR 1.5 lb/min and (c) AFR 2.0 lb/min (cont)

4.4.3. Comparison of Performance of the Barton, Wesjet and GMA Garnet in Terms of R_a. Knowing the influence of abrasive flow rate and the effect of pressure on the fragmentation of abrasives, the performance of HPX Barton garnet was compared with the Wesjet and GMA garnet of the same size when cutting composite. Wesjet and GMA garnet were examined under USB microscope to compare the size and shape of the particles as shown in Figure 4.14. The mineral composition was identified based on the color of the component. GMA garnet was found to have more rounded edges compared with Barton and Wesjet garnet. Due to the limited quantity of Wesjet garnet and only for the purpose of comparison, R_a parameter was recorded for cuts made with Barton, Wesjet and GMA garnet. The conditions of the experiment and data are shown in Tables 4.2, 4.3 and 4.4. Graphically, the results are shown in Figure 4.15 and Figure 4.16.

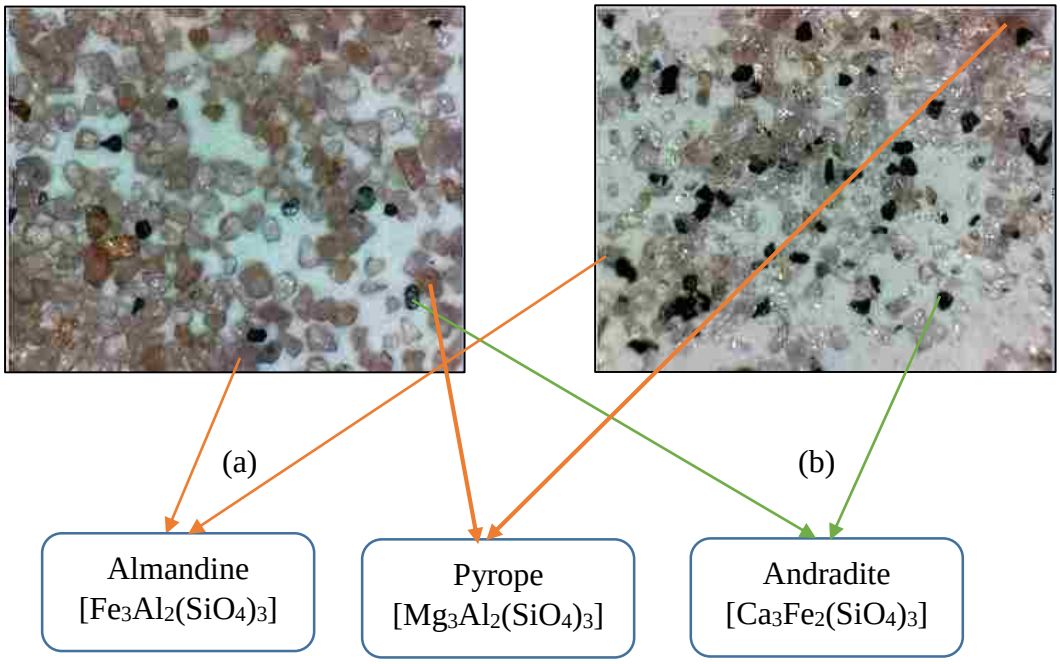

Figure 4.14. Microscope observation of a) GMA garnet (60X) b) Wesjet garnet (60X) [http://geology.com/minerals/garnet.shtml]

Table 4.2. Experimental R_a using WESJET garnet

WESJET garnet			**Surface roughness (R_a) µin**		
Sample number		**Traverse speed (in/min)**	**At depth, d=1/4 in**	**At depth, d=1/2 in**	**At depth, d=3/4 in**
1	Pressure 60 ksi & AFR 1.0 lb/min	20	193.8	227	262.1
2		40	240.4	300.9	528.5
3		60	292.1	425.6	545.1
4	Pressure 90 ksi & AFR 2.0 lb/min	20	153.8	195.5	250.8
5		40	176	259.3	320.4
6		60	187.9	293.2	460.4

Table 4.3. Experimental R_a using BARTON garnet

BARTON garnet			**Surface roughness (R_a) µin**		
Sample number		**Traverse speed (in/min)**	**At depth, d=1/4 in**	**At depth, d=1/2 in**	**At depth, d=3/4 in**
1	Pressure 60 ksi & AFR 1.0 lb/min	20	179.2	215.4	275.7
2		40	225.8	250.4	496.3
3		60	252.1	354	524
4	Pressure 90 ksi & AFR 2.0 lb/min	20	153.8	169.6	214.5
5		40	152.4	234.7	315.6
6		60	234.2	318.3	506.5

Table 4.4. Experimental R_a using GMA garnet

GMA garnet			**Surface roughness (R_a) µin**		
Sample number		**Traverse speed (in/min)**	**At depth, d=1/4 in**	**At depth, d=1/2 in**	**At depth, d=3/4 in**
1	Pressure 60 ksi & AFR 1.0 lb/min	20	170.6	222.3	297.6
2		40	256.1	350.4	429.7
3		60	314.2	523.9	550
4	Pressure 90 ksi & AFR 2.0 lb/min	20	151.1	182	232.1
5		40	165.6	231.1	367.7
6		60	189.1	295.4	432.6

At pressure of 60 ksi and an abrasive flow rate of 1 lb/min, Barton garnet gave lower values of surface roughness compared with the values obtained using the same mesh size of Wesjet and GMA garnet aas shown in Figure 4.15a-c. At a depth of of ¾" from the top surface, GMA garnet produced a rough surface with an R_a value of 550 µin whereas Barton and Wesjet garnet give surfaces with R_a values of 524 µin and 545.1 µin respectively. Barton garnet give a better surface finish when compared with Wesjet and GMA garnet at all depths of measurement of R_a. The same Figure showed that, irrespective of the type of garnet used for cutting composite, surface roughness increased with increase of traverse speed.

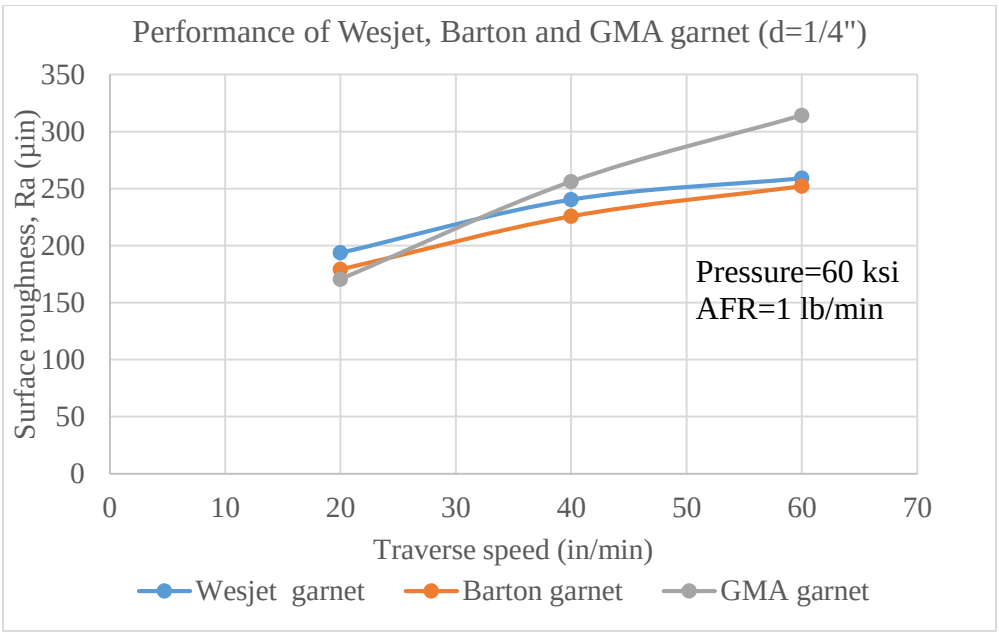

(a)

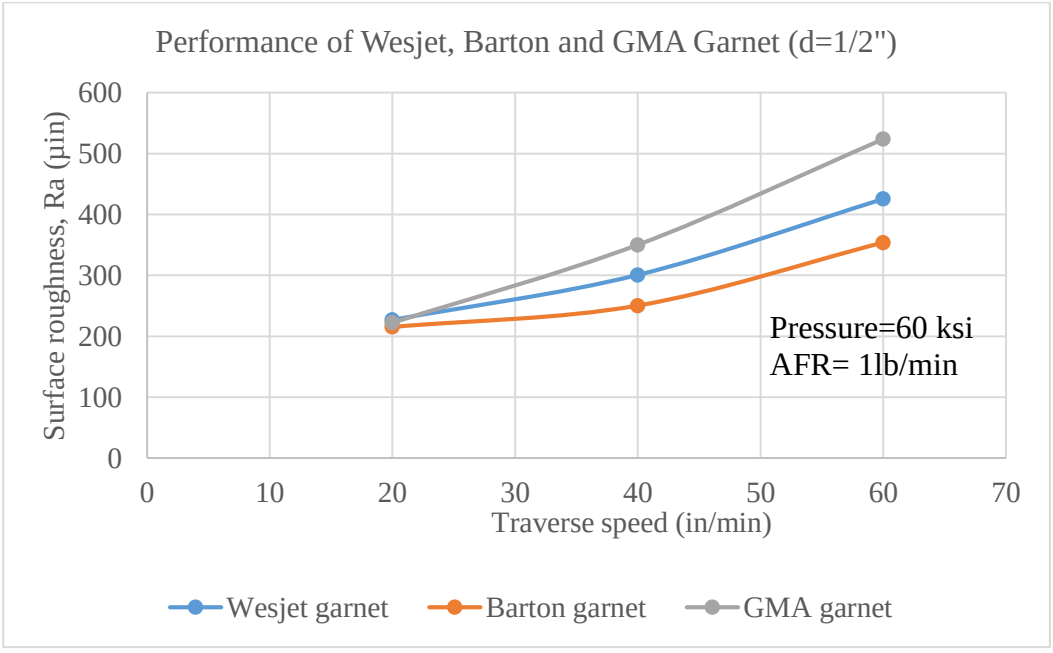

(b)

Figure 4.15. Comparision of the performance of Barton, Wesjet and GMA garnet with R_a parameter at different depths of cut, p: 60 ksi and AFR: 1 lb/min

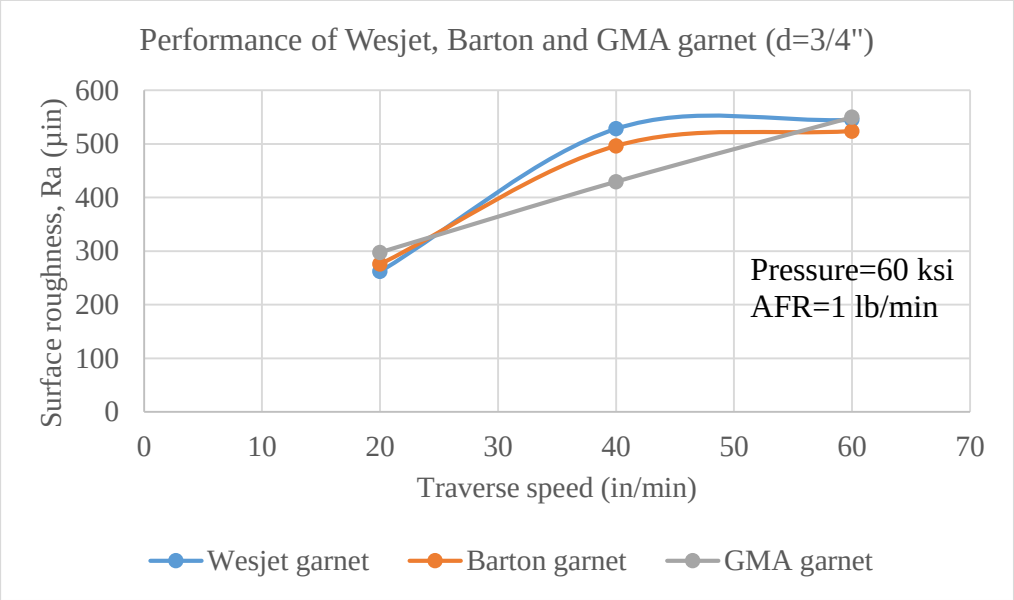

(c)

Figure 4.15. Comparision of the performance of Barton, Wesjet and GMA garnet with R_a parameter at different depths of cut, p: 60 ksi and AFR: 1 lb/min (cont)

From Figure 4.16. a-c, Barton garnet performed better, giving a better surface finish with low values of R_a compared to Wesjet garnet at low traverse speeds, pressure 90 ksi and AFR of 2 lb/min. As the traverse speed increases beyond 45 in/min, Wesjet garnet provided surfaces with a lower surface roughness when compared to Barton garnet. The mean value of R_a was lowest at a pressure of 90 ksi and AFR of 2 lb/min when compared to the mean value of the R_a at a pressure of 60 ksi and AFR of 1 lb/min.

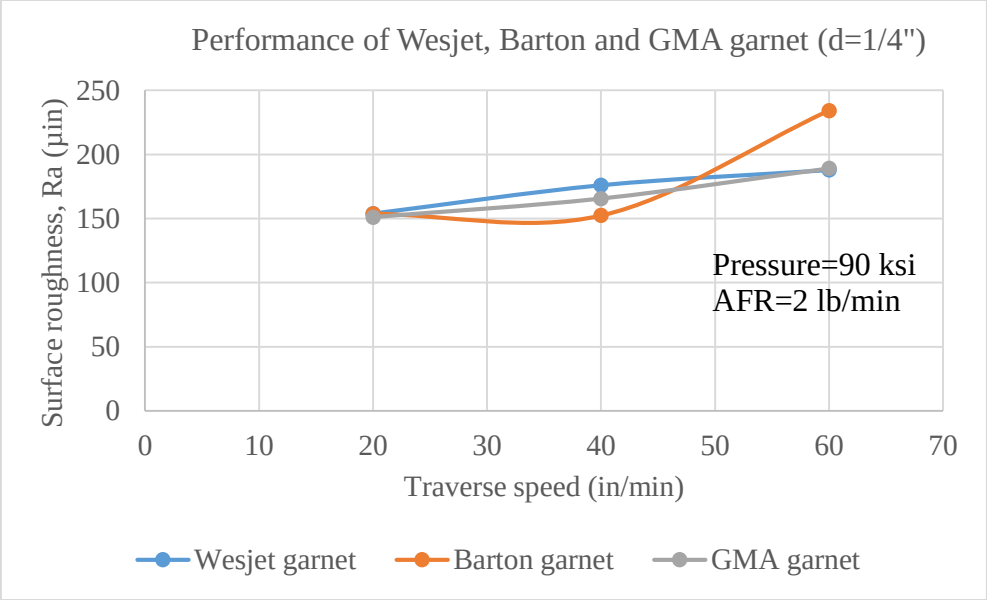

(a)

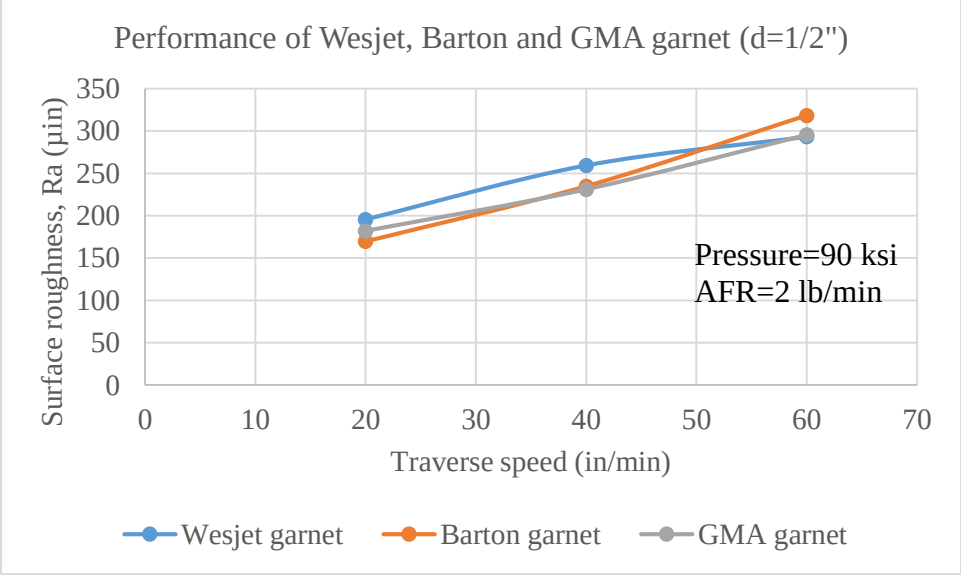

(b)

Figure 4.16. Comparision of the performance of Barton, Wesjet and GMA garnet with R_a parameter at different depths of cut, p: 90 ksi and AFR: 2 lb/min

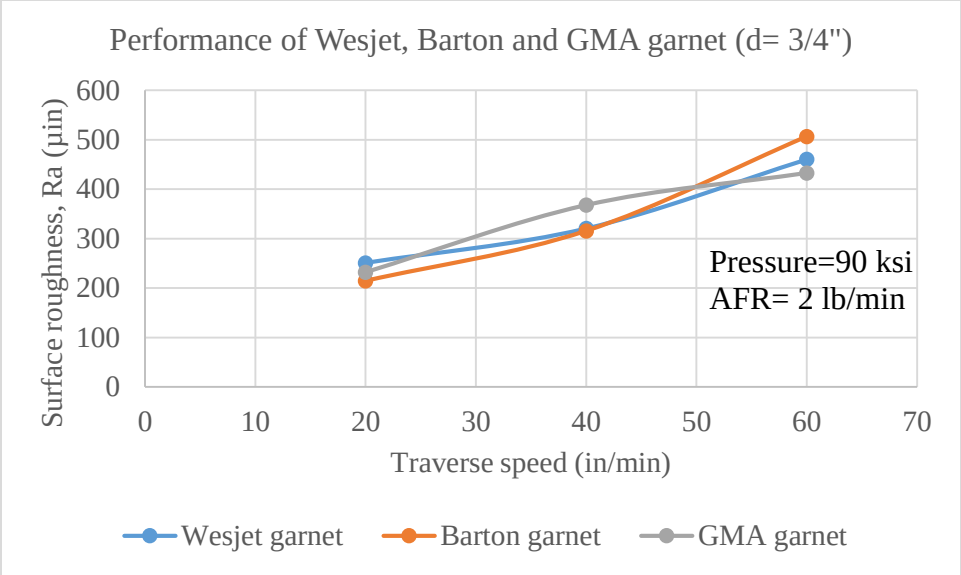

(c)

Figure 4.16. Comparision of the performance of Barton, Wesjet and GMA garnet with R_a parameter at different depths of cut, p: 90 ksi and AFR: 2 lb/min (cont)

In cutting the 1-inch-thick composite material, there was a significant difference in the R_a value at higher depth with different types of abrasives, Barton, Wesjet and GMA garnet. With cutting condition of 60 ksi and 1 lb/min, Barton garnet is giving smoothest surface at depth of ¾" from top surface whereas at cutting conditions of 90 ksi and 2.0 lb/min, GMA garnet is giving smoother surface finish. For the purpose of comparison only, three types of garnet were used in cutting but the experimentation for modeling using Box-Behnken design was done only with 80 HPX Barton garnet variety abrasive. Though some of the measured surface roughness values may match with each other, the model obtained for one type of abrasive cannot be used for prediction of R_a value for other type of abrasive.

5. MODELING

Experimental values of R_a obtained from the Box-Behnken set of experiments were used in developing the predictive model equations. From the experimental data and equation 3.2, second order response functions representing surface roughness (R_a) were expressed as a function of pressure (A), traverse speed (B) and abrasive mesh size (C). At each AFR and each depth of measurement, an empirical model was developed for R_a using the Minitab statistical software. The variables A, B and C represent the water pressure, traverse speed and abrasive mesh size respectively. With the empirical model equations obtained, R_a values at any regime within the interval of our experimental design could be determined.

5.1. MODEL EQUATIONS

As mentioned in section 4.3, surface roughness measurements were recorded at three different depths from the top surface. The model equations describing the relationship between the surface roughness, R_a and the process variables at an AFR of 1 lb/min were as follows:

a) At a depth of ¼" from the top surface of the composite

$$R_a=629+1.333*A-1.29*B-14.71*C-0.0188*A*A-0.01048B*B+0.117*C*C +0.0418*A*B-0.0085*A*C+0.0089*B*C \quad (5.1)$$

b) At a depth of ½" from the top surface of the composite

$$R_a=389+2.81*A+5.36*B-10.6*C-0.0157*A*A-0.0277*B*B+0.1146*C*C+ 0.0149*A*B0.0332*A*C-0.0369*B*C \quad (5.2)$$

c) At a depth of ¾" from the top surface of the composite

$$R_a=2426+14.3*A+1.1*B-93*C-0.112*A*A-0.109*B*B+0.821*C*C+0.163*A*B-0.057*A*C+0.003*B*C \quad (5.3)$$

The relationship between the predicted values of R_a using the empirical model and the actual experimental values of R_a are shown in Figure 5.1 a-c. Experimental and predicted observations were close to each other showing good regression. The predicted values matched with the experimental data points, indicating a good fitness with R^2 value of 0.93 at depth of ¼ inch, R^2 value of 0.93 at depth of ½ inch. So, with the relationships in 5.1 and 5.2, the response (R_a) at any point within the range of the experimental interval could be predicted. At a depth of ¾ inch from the top surface, the predicted values do not match closely with the experimental values of R_a with points scattered in the region (R^2 value of 0.71). Surface roughness (R_a) was high and irregular at this depth and values were not repeatable. The model equation at depth of ¾" is not applicable for generic R_a estimation at other levels of parameters.

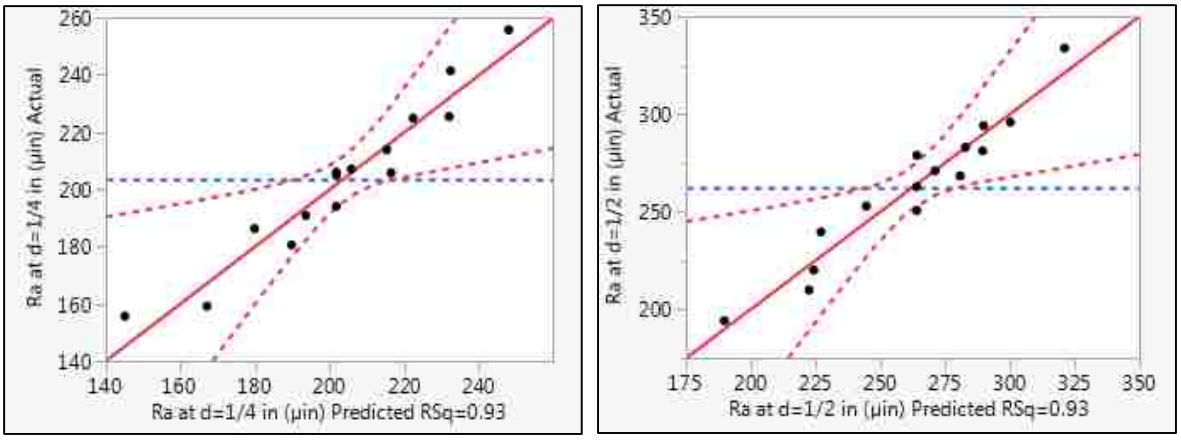

(a) (b)

Figure 5.1. Relation between experimental and predicted values of R_a at 1.0 lb/min AFR a) at a depth of ¼" b) at a depth of ½" c) at a depth of ¾" (eq's 5.1-5.3)

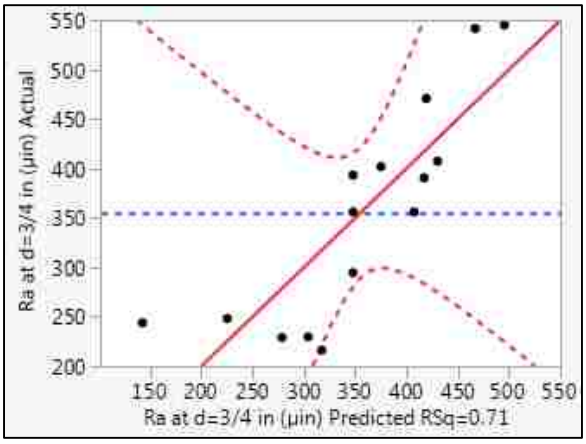

(c)

Figure 5.1. Relation between experimental and predicted values of R_a at 1.0 lb/min AFR a) at a depth of ¼" b) at a depth of ½" c) at a depth of ¾" (eq's 5.1-5.3) (cont)

The relation between the surface roughness, R_a and the process variables of the experimental design at an AFR of 1.5 lb/min at three depths of measurements were as follows:

a) At a depth of ¼" from the top surface of the composite

$$R_a=784-8.14*A+1.34*b-10.12*C+0.0294*A*A-0.0015*B*B+0.0491*C*C +0.0023*A*B+0.0445*A*C+0.0040*B*C \quad (5.4)$$

b) At a depth of ½" from the top surface of the composite

$$R_a= 85-7.14*A+5.49*B+10.3*C+0.0862*A*A-0.0147*B*B-0.03*C*C-0.0286*A*B-0.091*A*C-0.0044*B*C \quad (5.5)$$

c) At a depth of ¾" from the top surface of the composite

$$R_a=427-11.6*A+6.10*B+3.7*C+0.0984*A*A-0.0486*B*B+0.026*C*C+0.0117*A*B-0.083*A*C+0.0399*B*C \quad (5.6)$$

The actual and predicted values of R_a obtained using the model equations (5.4 -5.6) are shown in Figure 5.2 a-c. At an abrasive flow rate of 1.5 lb/min, the relationship between experimental and predicted values of R_a show a good correlation. Predicted values of R_a match the experimental values of R_a indicating a good fitness with R^2 value of 0.97 at depth of ¼", R^2 value of 0.93at depth of ½" and R^2 value of 0.93 at depth of ¾".

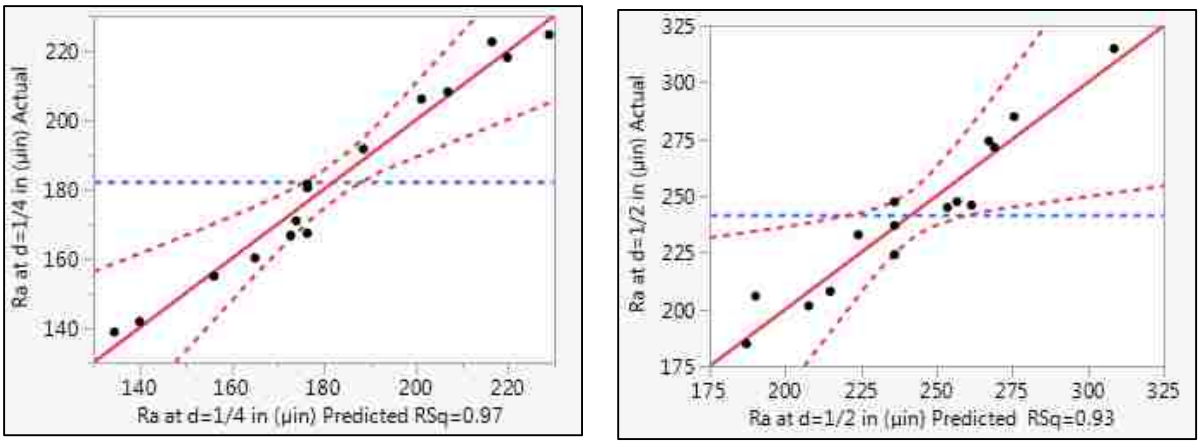

(a) (b)

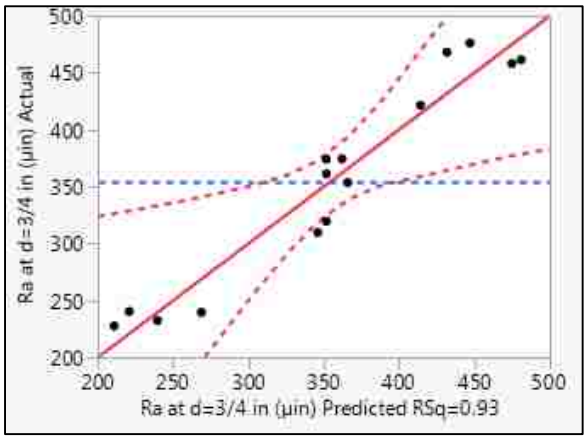

(c)

Figure 5.2. Relation between experimental and predicted values of R_a at 1.5 lb/min AFR a) at a depth of ¼" b) at a depth of ½" c) at a depth of ¾" (eq's 5.4-5.6)

Using the results from the Box-Behnken experimental design at an AFR of 2.0 lb/min, relationship between the surface roughness, R_a and the process variables at different depths of measurements were as follows:

a) At a depth of ¼" from the top surface of the composite

$$R_a=651-8.93*A+1.86*B-5.93*C+0.0325*A*A+0.0139*B*B+0.005*C*C-0.0128*A*B+0.0668*A*C-0.0122*B*C \quad (5.7)$$

b) At a depth of ½" from the top surface of the composite

$$R_a=58-1.15*A+1.84*B+6.53*C+0.0027*A*A-0.0013*B*B-0.0416*C*C+0.0238*A*C0.0157*A*C-0.0316*B*C \quad (5.8)$$

c) At a depth of ¾" from the top surface of the composite

$$R_a=11-6*A-0.4*B+0.63*C-0.067*A*A+0.0643*B*B-0.0014*C*C+0.0515*A*B+0.0071*A*C+0.0071*B*C \quad (5.9)$$

The experimental and predicted values of R_a using the model equations 5.7-5.9 were in good correlation (R^2 value of 0.88 at depth of ¼", R^2 value of 0.93 at depth of ½") with each other as shown in Figure 5.3 a & b. Response for any set of parameters within the interval of our experimental design at an AFR of 2.0 lb/min could be predicted using the relationship shown in Eqs. 5.7 and 5.8. However, at a depth of ¾" from the nozzle exit, R^2 value was 0.69 [Figure5.3 c] indicating that the predicted values of R_a do not well match with experimental values. The reason for this lack of fitness was the inconsistency of measured R_a values at that depth due to jet striations formed on the surface. So, the model equation 5.9 is not applicable for response estimation for the reason of lower R squared value.

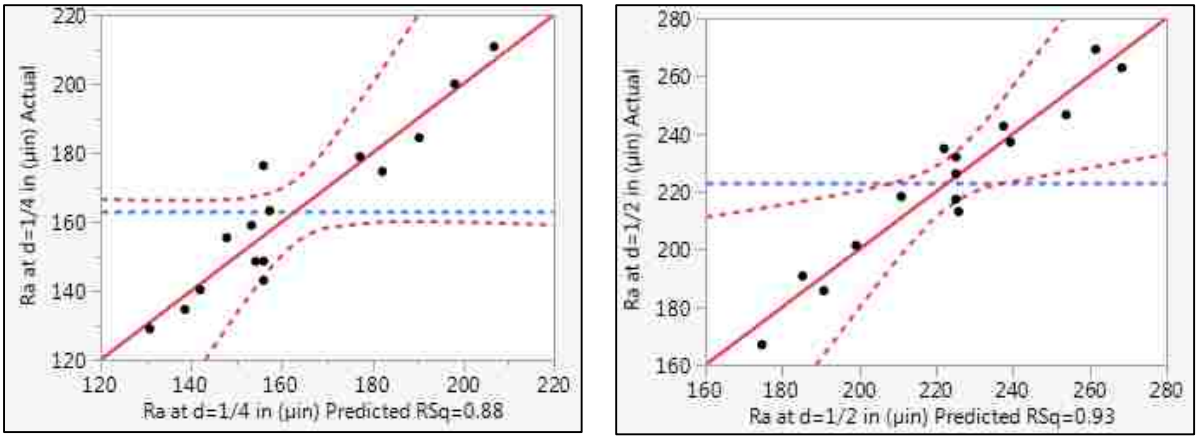

(a) (b)

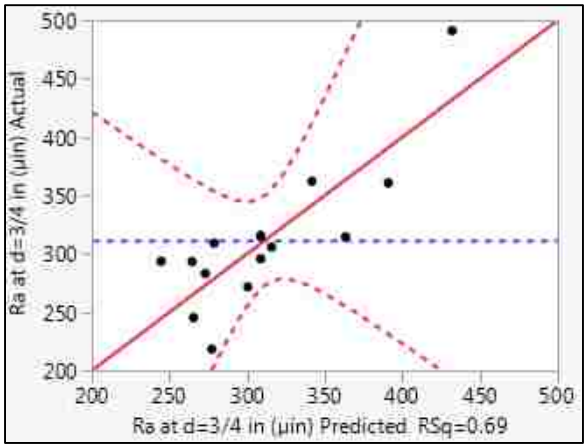

(c)

Figure 5.3. Relation between experimental and predicted values of R_a at 2.0 lb/min AFR a) at a depth of ¼" b) at a depth of ½" c) at a depth of ¾" (eq's 5.7-5.9)

From the experimental results of the Box-Behnken design using standard 80 HPX Barton garnet, the relationships between the surface roughness, R_a and the process variables (pressure, traverse speed and AFR) were as follows:

a) At a depth of ¼" from the top surface of the composite

$$R_a=566-9.98*A+4.92*B-121.2*D+0.0674*A*A+0.0117*B*B+29.8*D*D-0.0355*A*B+0.243*A*D-0.853*B*D \quad (5.10)$$

b) At a depth of ½" from the top surface of the composite

$$R_a=419-5.3*A+4.67*B-94*D+0.0525*A*A+0.0198*B*B+30.1*D*D-0.0640*A*D-0.76*A*D+0.55*B*D \quad (5.11)$$

c) At a depth of ¾" from the top surface of the composite

$$R_a=232-3.8*A+9.22*B+34*D+0.0436*A*A+0.0117*B*B-20.9*D*D-0.0718*A*B-0.57*A*D+0.42*B*B \quad (5.12)$$

d) At a depth of 1/8" from the top surface of the composite

$$R_a= 425.4-5.71*A+2.353*B-100.4*D+0.0259*A*A-0.01392*B*B+5.9*D*D-0.0683*A*B+0.940*A*D-0.180*B*B \quad (5.13)$$

The relationship between the experimental and predicted values of R_a are shown in Figure 5.4 a-d. Predicted values of R_a using the model equations [Eqs 5.10-5.13] match with experimental observations of R_a (R^2 value of 0.98 at depth of ¼", R^2 value of 0.84 at depth of ½", R^2 value of 0.96 at depth of ¾" and R^2 value of 0.95 at depth of 1/8"). The surface roughness, R_a at any point within the interval of the experimental design could be well calculated from equations 5.10-5.13.

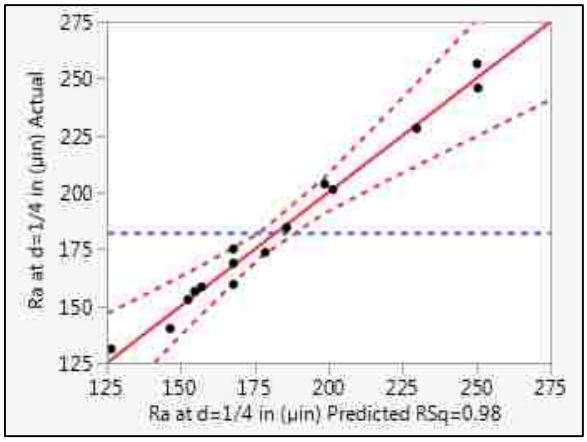

(a)

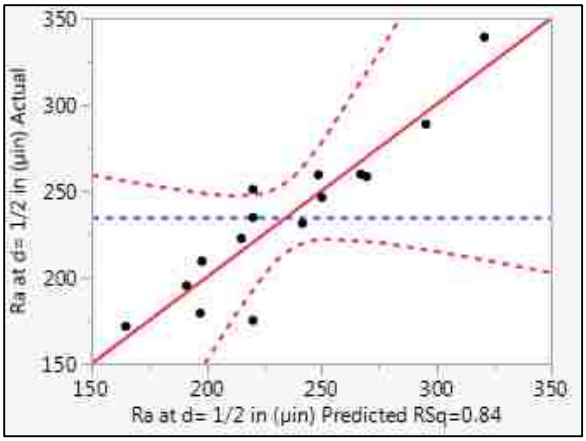

(b)

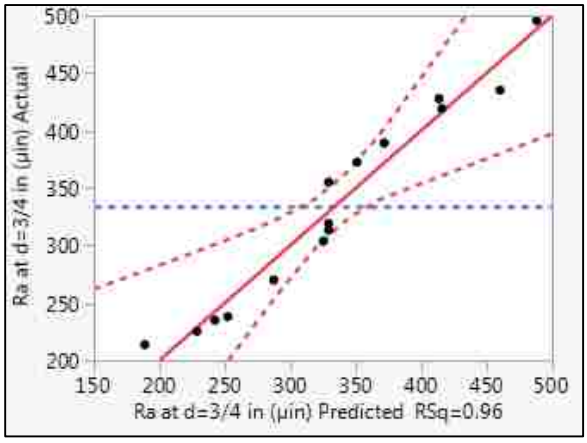

(c)

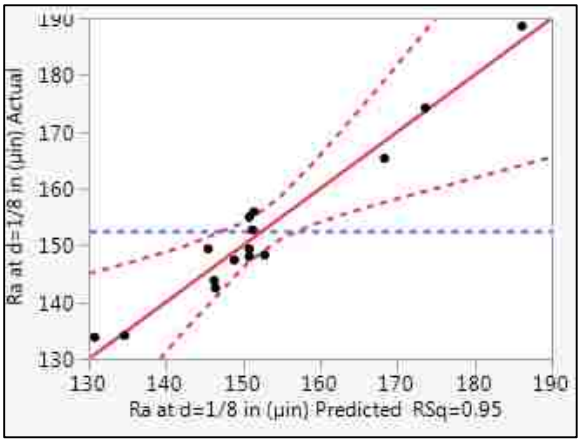

(d)

Figure 5.4. Relation between experimental and predicted values of R_a with 80 HPX Barton garnet a) at a depth of ¼" b) at a depth of ½" c) at a depth of ¾" d) at a depth of 1/8" (eq's 5.10-5.13)

5.2. RESPONSE SURFACE PLOTS

To better understand the effect of the process variables on the surface roughness, 3D response surface plots for the predicted models were generated. This is a unique advantage of using the Box-Behnken response surface experimental design.

5.2.1. Response Surface Plots at an AFR of 1.0 lb/min. Figure 5.5 a-c represent the 3D response surface plots for experimental response, R_a at a depth of ¼" from jet entrance. Figure 5.5a shows the effect of pressure and traverse speed on surface roughness, R_a. This figure shows lower R_a values are found at higher pressure and lower traverse speeds. Figure 5.5b show the effect of pressure and abrasive mesh size on surface roughness, R_a. It indicates that a better surface finish is obtained with lower R_a values at the center of the abrasive mesh size levels. Figure 5.5c show the effect of traverse speed and abrasive mesh size on R_a.

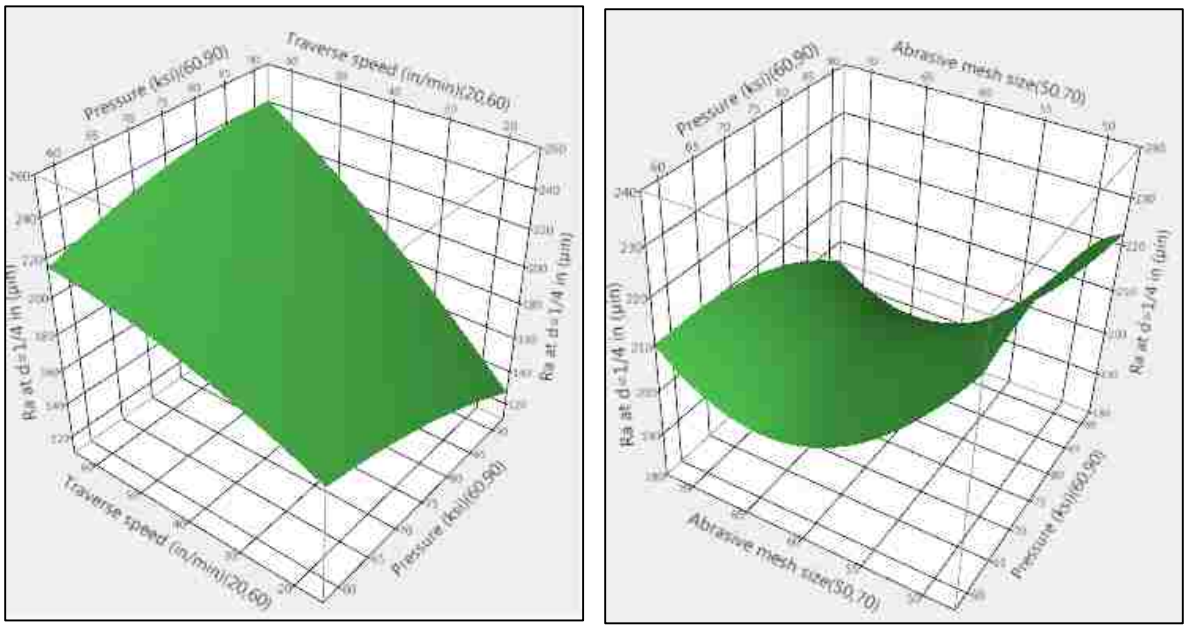

(a) (b)

Figure 5.5. Response surface plots showing the effect of the variables a) pressure and traverse speed b) pressure and abrasive mesh size c) traverse speed and abrasive mesh size on R_a at a depth of ¼" at an AFR of 1 lb/min

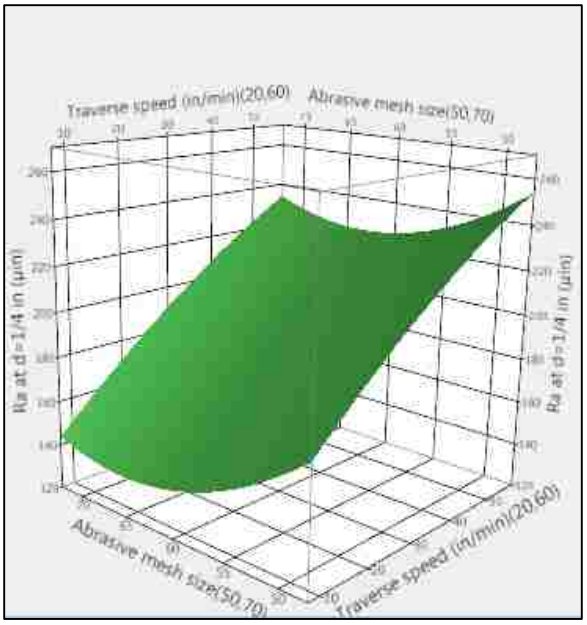

(c)

Figure 5.5. Response surface plots showing the effect of the variables a) pressure and traverse speed b) pressure and abrasive mesh size c) traverse speed and abrasive mesh size on R_a at a depth of ¼" at an AFR of 1 lb/min (cont)

Figure 5.6 a-c shows the 3D response surface plots for the predicted models at a depth of ½" from the jet entrance. Figure 5.6a shows the effect of pressure and traverse speed on R_a. It shows that a lower value of R_a at 170 µin with better surface finish is achieved at high pressure and a low traverse speed. Figure 5.6b shows the effect of pressure and abrasive mesh size on R_a. Figure 5.6c shows the effect of traverse speed and abrasive mesh size on R_a.

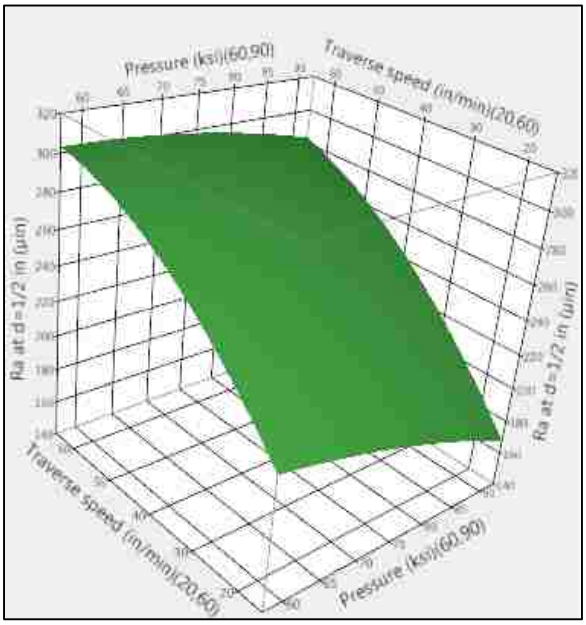

(a)

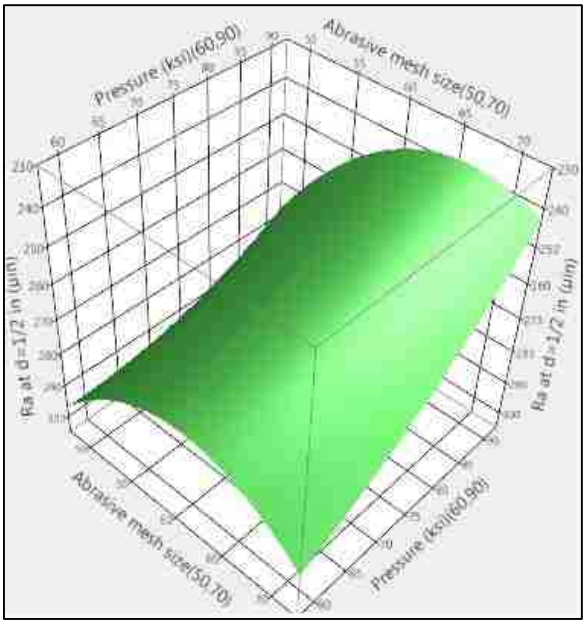

(b)

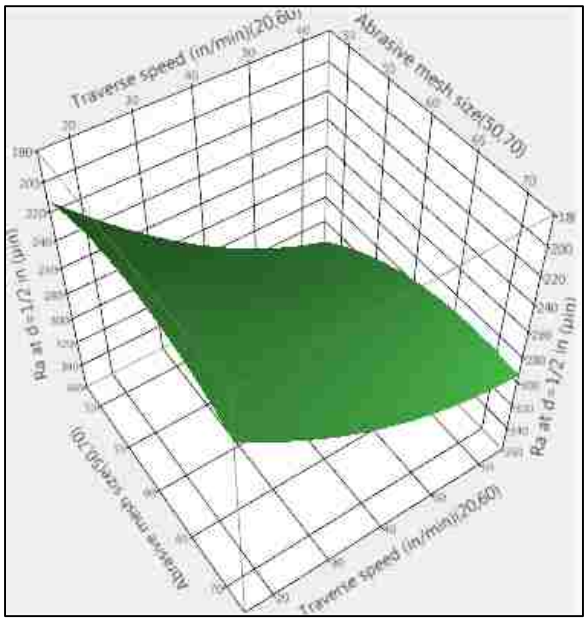

(c)

Figure 5.6. Response surface plots showing the effect of variables a) pressure and traverse speed b) pressure and abrasive mesh size c) traverse speed and abrasive mesh size on R_a at a depth of ½" at an AFR of 1 lb/min

Figure 5.7 a-c give 3D response surface plots for R_a at depth of ¾" from the jet entrance into the composite. Figure 5.7a shows the effect of pressure and traverse speed on surface roughness, R_a. This figure shows low surface roughness (R_a) at high pressure and low traverse speed values. Figure 5.7b shows the effect of pressure and abrasive mesh size on R_a. Better surface finish is achieved with low R_a values at the center of abrasive mesh size range and at high jet pressure. Figure 5.7c shows the effect of traverse speed and abrasive mesh size on surface roughness, R_a. Experimentally, the one distinguishable point for R_a over the different depths of measurement was that there was an increase in surface roughness with distance from the top surface.

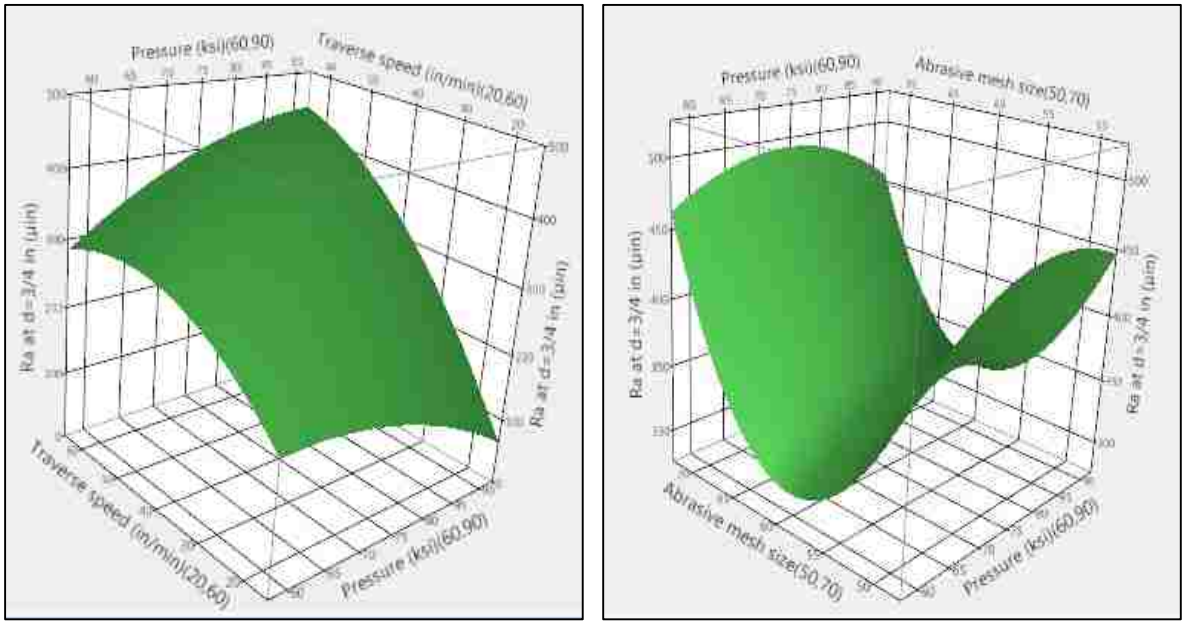

(a) (b)

Figure 5.7. Response surface plots showing the effects of variables a) pressure and traverse speed b) pressure and abrasive mesh size c) traverse speed and abrasive mesh size on R_a at a depth of 3/4" at an AFR of 1 lb/min

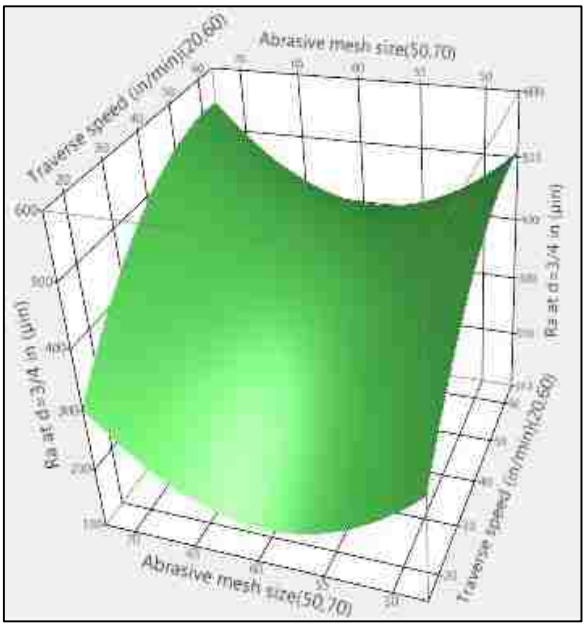

(c)

Figure 5.7. Response surface plots showing the effects of variables a) pressure and traverse speed b) pressure and abrasive mesh size c) traverse speed and abrasive mesh size on R_a at a depth of 3/4" at an AFR of 1 lb/min (cont)

5.2.2. Response Surface Plots at an AFR of 1.5 lb/min. Figure 5.8 a-c shows the 3D response surface plots at a depth of ¼" from the jet entrance at an abrasive flow rate of 1.5 lb/min. Figure 5.8a shows the effect of pressure and traverse speed on surface roughness, R_a. Figure 5.8b shows the effect of pressure and abrasive mesh size on R_a. Figure 5.8c shows the effect of traverse speed and abrasive mesh size on R_a. The effect of parameters change on the response (R_a) was found to have the same trend as in case of an AFR of 1 lb/min. One significant difference identified was quality of cut was better when an AFR of 1.5 lb/min was used over that at the lower abrasive flow rate. The reason that can be implied is that at a greater abrasive flow rate, the flow of abrasive particles deforms the material surface and erodes the material.

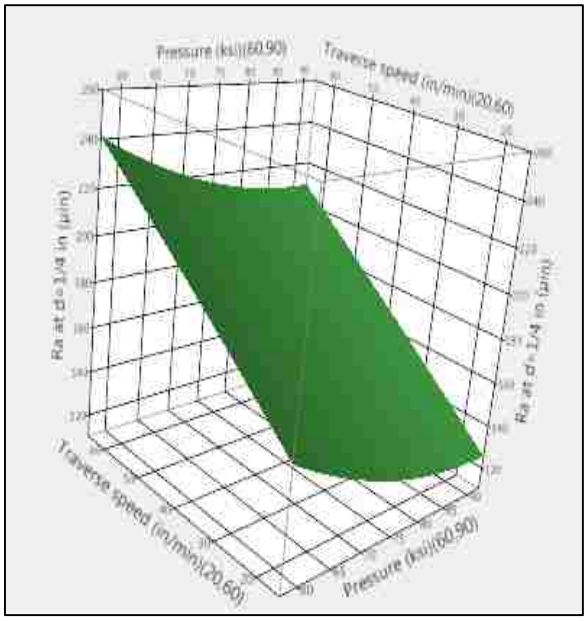

(a)

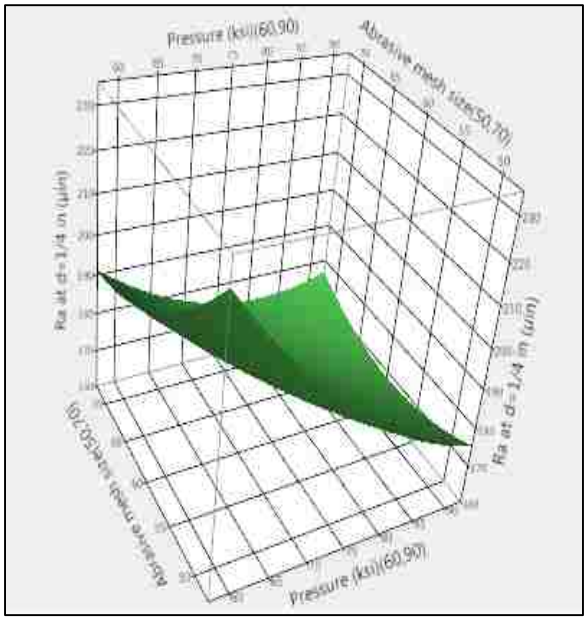

(b)

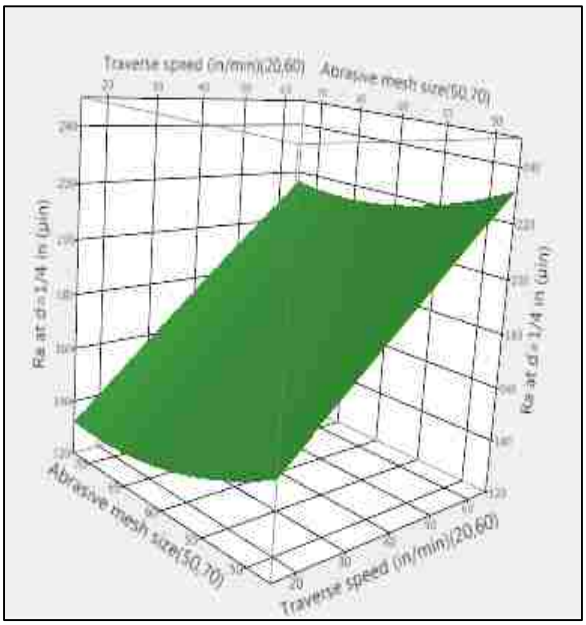

(c)

Figure 5.8. Response surface plots showing the effect of variables a) pressure and traverse speed b) pressure and abrasive mesh size c) traverse speed and abrasive mesh size on R_a at a depth of ¼" at an AFR of 1.5 lb/min

Figure 5.9 a-c shows the 3D response surface plots at a depth of ½" from the jet entrance at an abrasive flow rate of 1.5 lb/min. Figure 5.9a shows the effect of pressure and traverse speed on surface roughness, R_a. This figure shows the lowest roughness value 205 µin was achieved at high pressure and at a low traverse speed. Figure 5.9b shows the effect of pressure and abrasive mesh size on R_a, while Figure 5.9c shows the effect of traverse speed and abrasive mesh size on R_a.

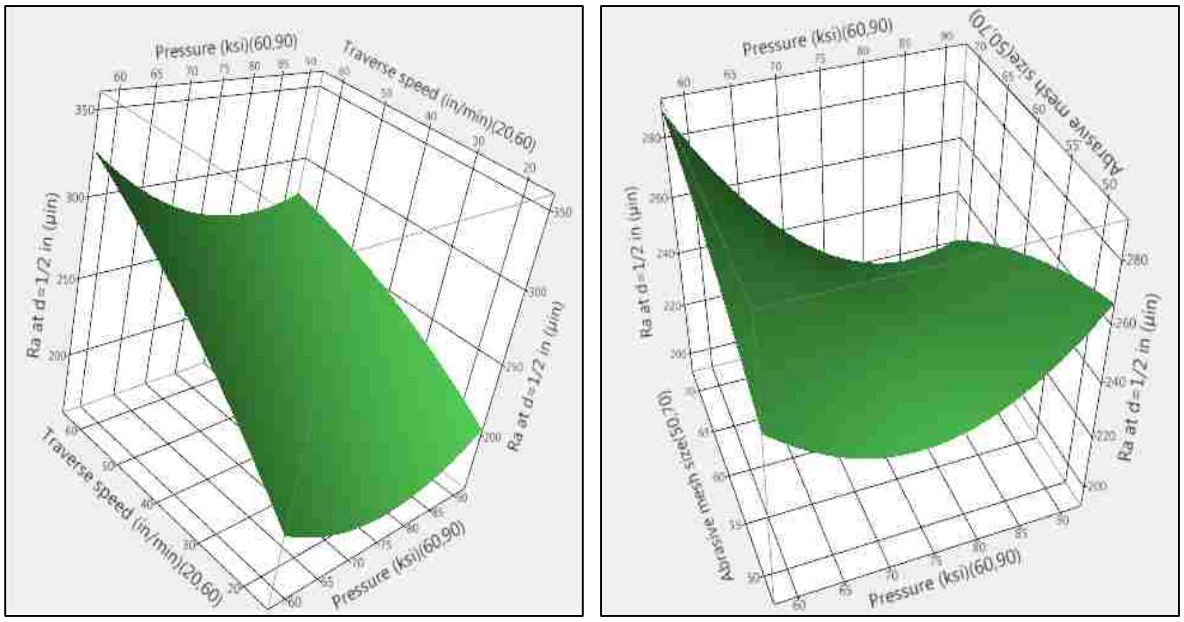

(a) (b)

Figure 5.9. Response surface plots showing the effect of variables a) pressure and traverse speed b) pressure and abrasive mesh size c) traverse speed and abrasive mesh size on R_a at a depth of ½"at an AFR of 1.5 lb/min

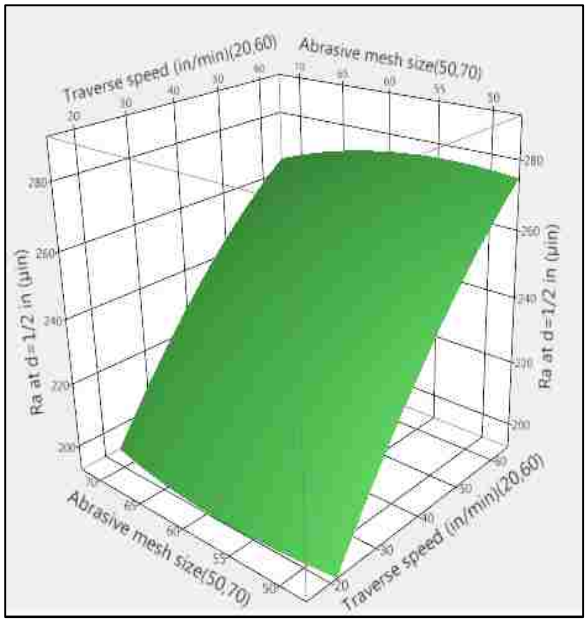

(c)

Figure 5.9. Response surface plots showing the effect of variables a) pressure and traverse speed b) pressure and abrasive mesh size c) traverse speed and abrasive mesh size on R_a at a depth of ½”at an AFR of 1.5 lb/min (cont)

Figure 5.10 a-c shows the 3D response surface plots for R_a at a depth of ¾” from the top surface. Figure 5.10a shows the effect of pressure and traverse speed on surface roughness, R_a. It shows that the best(smallest) surface roughness was generated at high jet pressure and low traverse speed. Figure 5.10b shows the effect of pressure and abrasive mesh size on R_a. Figure 5.10c show the effect of traverse speed and abrasive mesh size on R_a. Higher traverse speed resulted in greater surface roughness irrespective of abrasive mesh size. Mean surface roughness values at a depth of ¾” were found to be higher than those measured at depths of ¼” or ½”.

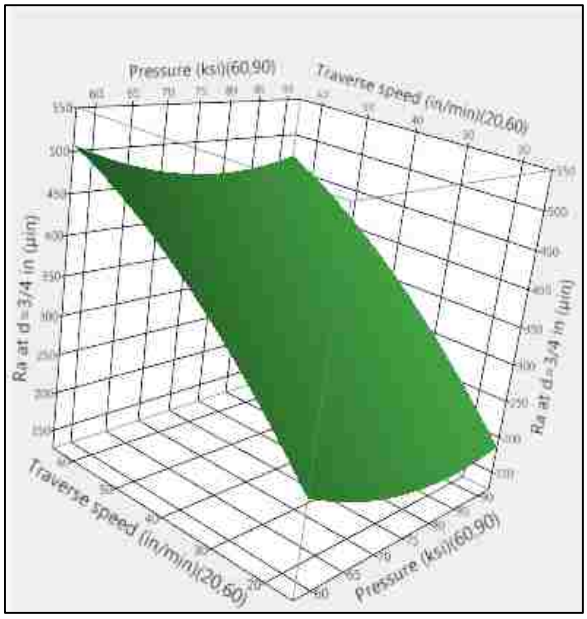

(a)

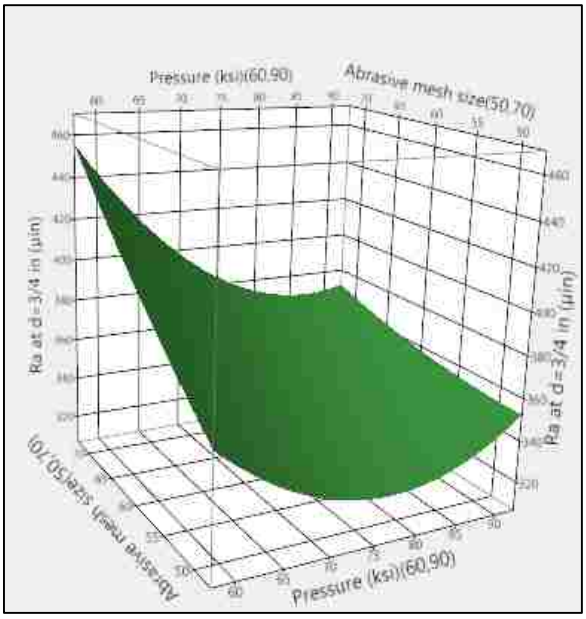

(b)

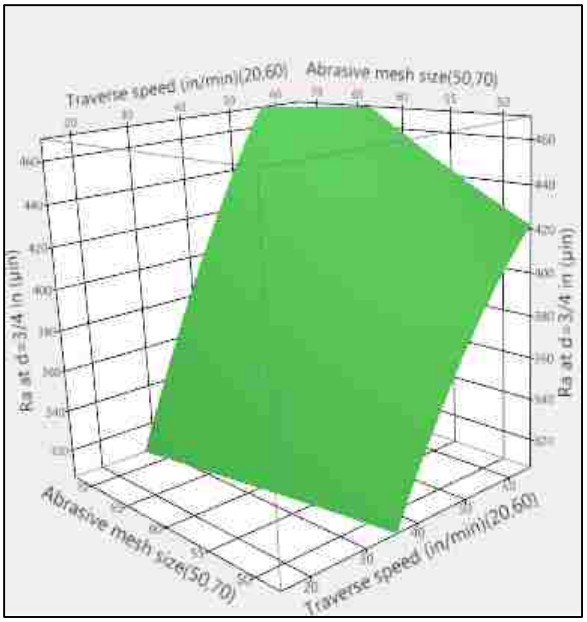

(c)

Figure 5.10. Response surface plots showing the effect of variables a) pressure and traverse speed b) pressure and abrasive mesh size c) traverse speed and abrasive mesh size on R_a at a depth of ¾”at an AFR of 1.5 lb/min

5.2.3. Response Surface Plots at an AFR of 2.0 lb/min. Figure 5.11 a-c shows the 3D response surface plots at a depth of measurement of ¼" and at an abrasive flow rate of 2 lb/min. Figure 5.11a shows the effect of pressure and traverse speed on surface roughness, R_a. These plots shows that high jet pressure and slow traverse speed yields good results for R_a. Figure 5.11b shows the effect of pressure and abrasive mesh size and Figure 5.11c shows the effect of traverse speed and abrasive mesh size. At an abrasive flow rate of 2.0 lb/min and high traverse speed, jet striations were observed on the cut surface of the composite.

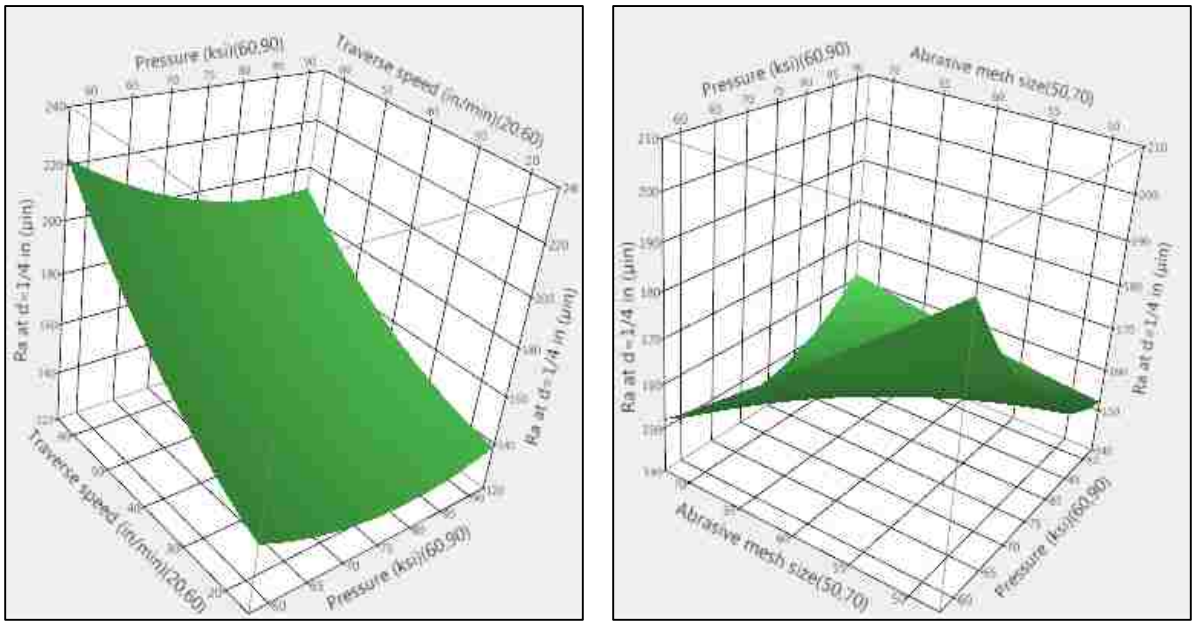

(a) (b)

Figure 5.11. Response surface plots showing the effect of variables a) pressure and traverse speed b) pressure and abrasive mesh size c) traverse speed and abrasive mesh size on R_a at a depth of ¾"at an AFR of 2.0 lb/min

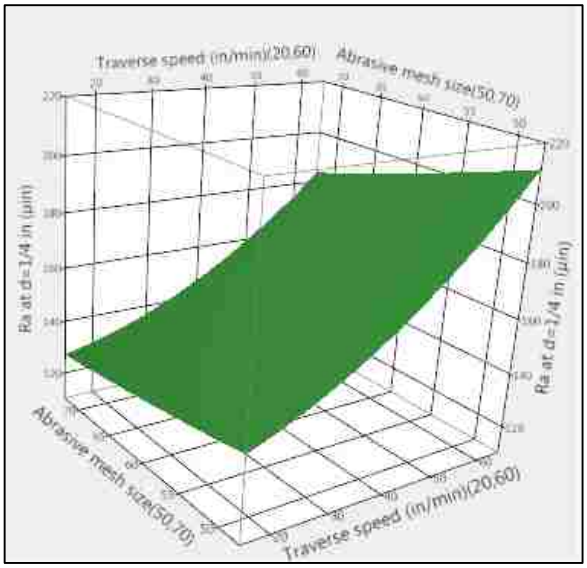

(c)

Figure 5.11. Response surface plots showing the effect of variables a) pressure and traverse speed b) pressure and abrasive mesh size c) traverse speed and abrasive mesh size on R_a at a depth of ¾”at an AFR of 2.0 lb/min (cont)

Figure 5.12 a-c illustrates the 3D response surface plots at a depth of ½” and at an abrasive flow rate of 2 lb/min. Figure 5.12a shows the effect of pressure and traverse speed on surface roughness, R_a. This figure shows that a slow traverse speed and high jet pressure gave the lowest surface roughness, R_a of 160 µin. Figure 5.12b shows the effect of pressure and abrasive mesh size while Figure 5.12c shows the effect of traverse speed and abrasive mesh size on surface roughness.

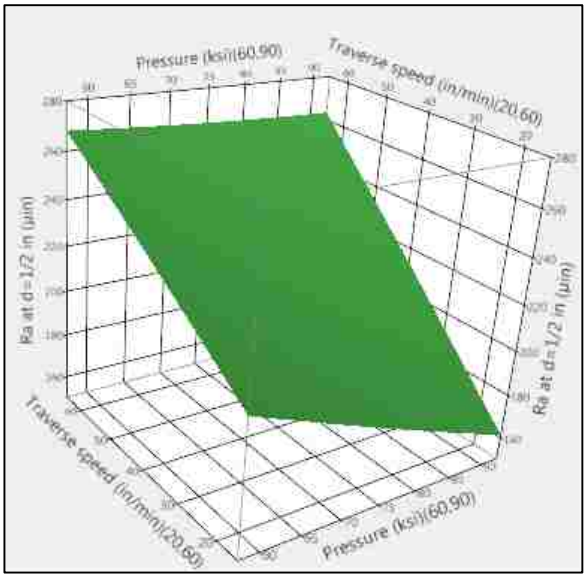

(a)

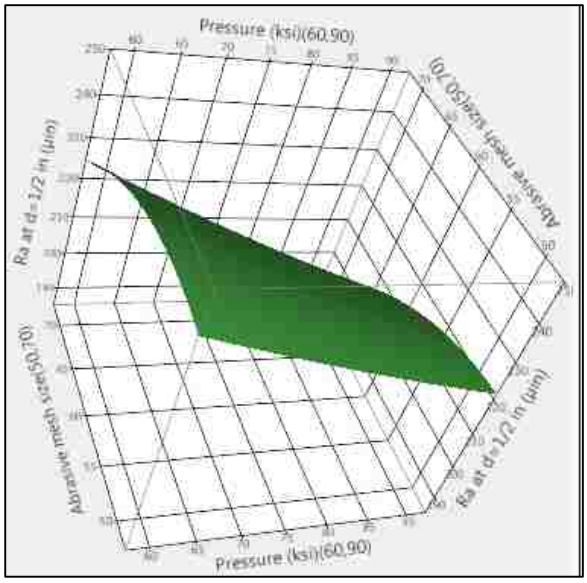

(b)

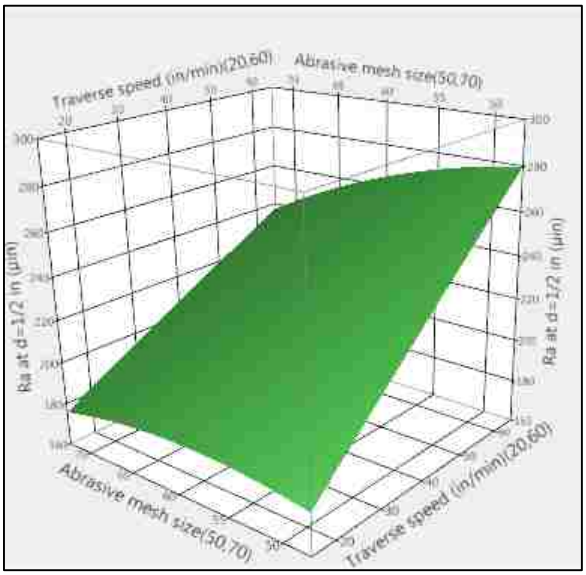

(c)

Figure 5.12. Response surface plots showing the effect of variables a) pressure and traverse speed b) pressure and abrasive mesh size c) traverse speed and abrasive mesh size on R_a at a depth of ½" at an AFR of 2.0 lb/min

Figure 5.13 a-c provides the 3D response surface plots at a depth of measurement of ¾" and at an abrasive flow rate of 2 lb/min. Figure 5.13a shows the effect of pressure and traverse speed on surface roughness, R_a. This figure shows that the lowest value of Ra (~230µin) is found at the highest pressure (90 ksi) and the slowest traverse speed (20 in/min). Figure 5.13b shows the effect of pressure and abrasive mesh size. Figure 5.13c shows the effect of traverse speed and abrasive mesh size on surface roughness. At greater depths, R_a values were found to be higher.

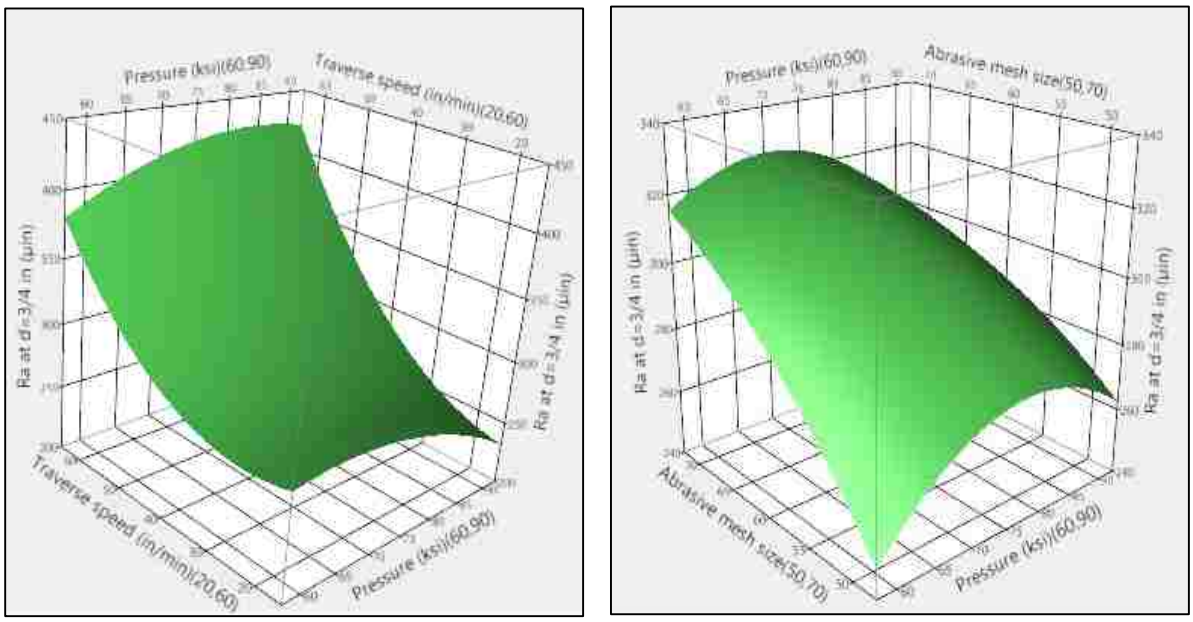

(a) (b)

Figure 5.13. Response surface plots showing the effect of variables a) pressure and traverse speed b) pressure and abrasive mesh size c) traverse speed and abrasive mesh size on R_a at a depth of ¾" at an AFR of 2.0 lb/min

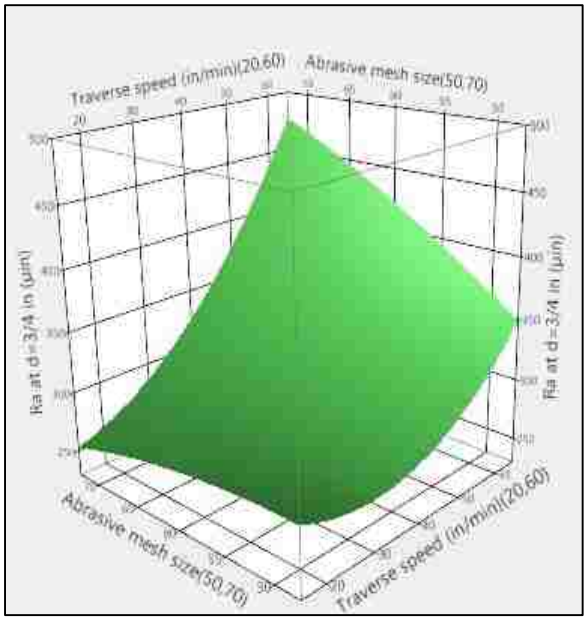

(c)

Figure 5.13. Response surface plots showing the effect of variables a) pressure and traverse speed b) pressure and abrasive mesh size c) traverse speed and abrasive mesh size on R_a at a depth of ¾" at an AFR of 2.0 lb/min (cont)

5.2.4. Response Surface Plots for 80 HPX Standard Barton Garnet. The 3D response surface plots [Figures 5.14, 5.15 and 5.16] generated for R_a with variable parameters pressure, traverse speed and abrasive flow rate based on linear cuts made with 80 HPX Barton garnet for three depths of measurements ¼", ½" and ¾" from the top surface respectively. In industrial applications, thinner composites are often used in abrasive water jet cutting. So, in addition to the three standard depths of measurements, the R_a was also measured at a depth of 1/8" from the top surface of the composite and 3D response surface plots are shown in Figure 5.17.

a) At depth of ¼” from the top surface

Figure 5.14a shows the effect of pressure and traverse speed on surface roughness, R_a. This figure shows that low traverse speed and high pressure give low surface roughness. Figure 5.14b shows the effect of pressure and abrasive flow rate on the response, R_a. It shows that high abrasive flow rate and high pressure give low values of surface roughness (R_a). Figure 5.14c shows the effect of traverse speed and abrasive flow rate on surface roughness. The slow traverse speed of 20 in/min at an abrasive flow rate of 2 lb/min gave the lowest surface roughness of 140 µin.

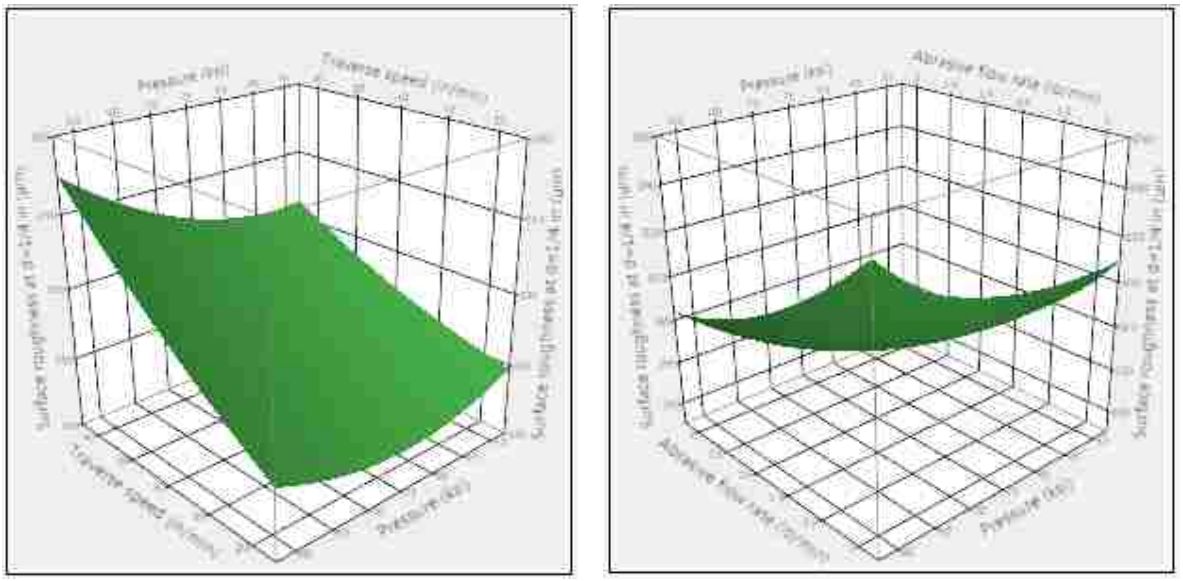

(a) (b)

Figure 5.14. Response surface plots showing the effect of variables a) pressure and traverse speed b) pressure and abrasive flow rate c) traverse speed and abrasive flow rate on R_a at a depth of ¼” for 80 HPX Barton garnet

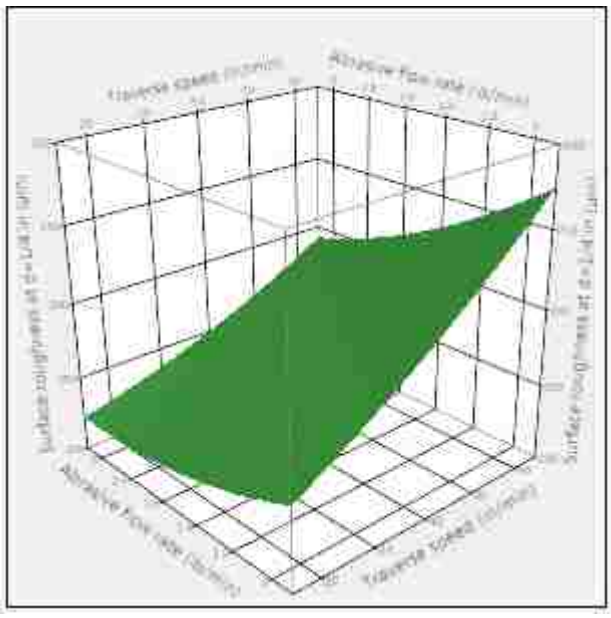

(c)

Figure 5.14. Response surface plots showing the effect of variables a) pressure and traverse speed b) pressure and abrasive flow rate c) traverse speed and abrasive flow rate on R_a at a depth of ¼" for 80 HPX Barton garnet (cont)

b) At a depth of ½" from the top surface

Figure 5.15a shows the effect of pressure and traverse speed on surface roughness, R_a. while Figure 5.15b shows the effect of pressure and abrasive flow rate. It shows that high abrasive flow rate and high jet pressure gave the lowest values of surface roughness (R_a). Figure 5.15c shows the effect of traverse speed and abrasive flow rate on surface roughness. A slow traverse speed of 20 in/min at the high abrasive flow rate of 2 lb/min gave the lowest surface roughness.

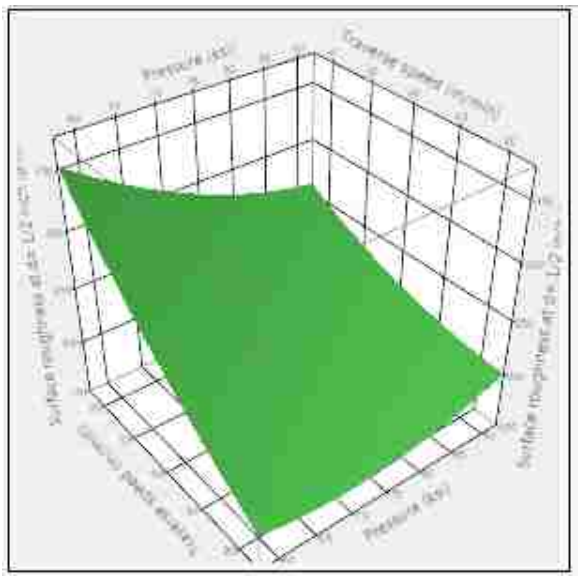

(a)

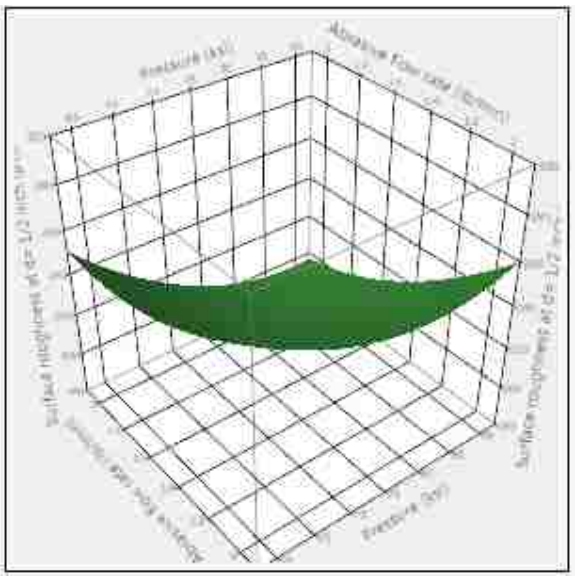

(b)

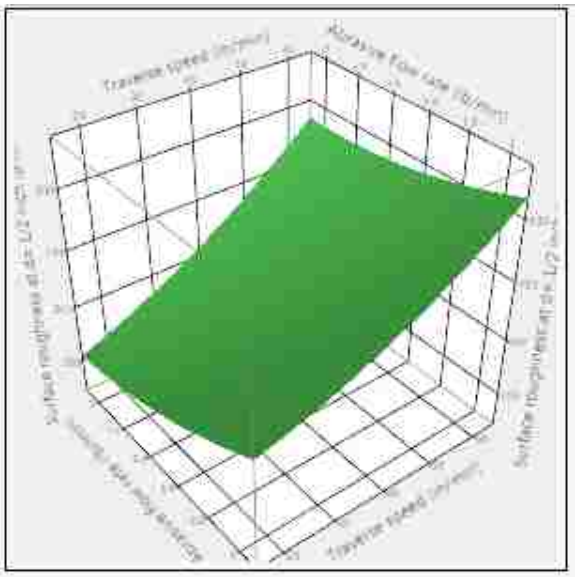

(c)

Figure 5.15. Response surface plots showing the effect of variables a) pressure and traverse speed b) pressure and abrasive flow rate c) traverse speed and abrasive flow rate on R_a at a depth of ½" for 80 HPX Barton garnet

c) At a depth of ¾" from the top surface

Figure 5.16a shows the effect of pressure and traverse speed on surface roughness, R_a while Figure 5.16b shows the effect of pressure and abrasive flow rate. It shows that high abrasive flow rate and high jet pressure gave the lowest values for surface roughness (R_a) ~150 µin. Figure 5.16c shows the effect of traverse speed and abrasive flow rate on surface roughness. The slow traverse speed of 20 in/min at the high abrasive flow rate of 2 lb/min gave the lowest surface roughness.

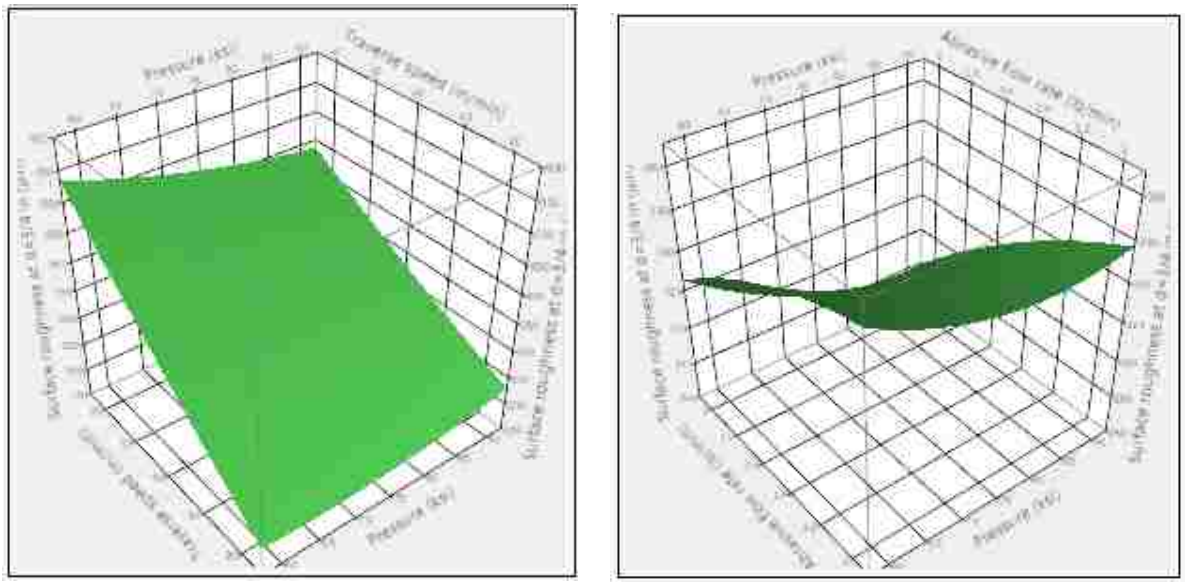

(a) (b)

Figure 5.16. Response surface plots showing the effect of variables a) pressure and traverse speed b) pressure and abrasive flow rate c) traverse speed and abrasive flow rate on R_a at a depth of ¾" for 80 HPX Barton garnet

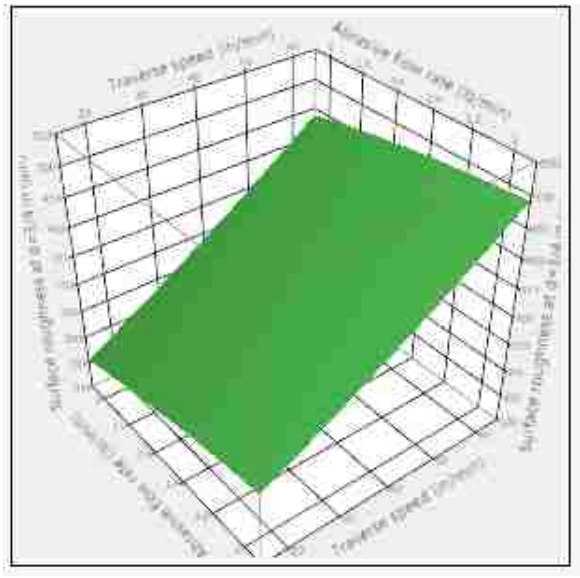

(c)

Figure 5.16. Response surface plots showing the effect of variables a) pressure and traverse speed b) pressure and abrasive flow rate c) traverse speed and abrasive flow rate on R_a at a depth of ¾” for 80 HPX Barton garnet (cont)

d) At a depth of 1/8” from the top surface

Figure 5.17a shows the effect of pressure and traverse speed on surface roughness, R_a while Figure 5.17b shows the effect of pressure and abrasive flow rate. It shows that high abrasive flow rate and high jet pressure gave the lowest values for surface roughness (R_a). Figure 5.17c shows the effect of traverse speed and abrasive flow rate on surface roughness. The slow traverse speed of 20 in/min at the abrasive flow rate of 2 lb/min gave the lowest surface roughness.

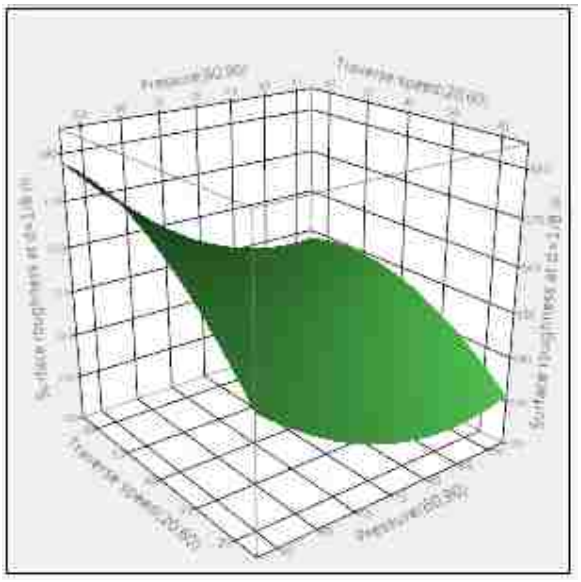

(a)

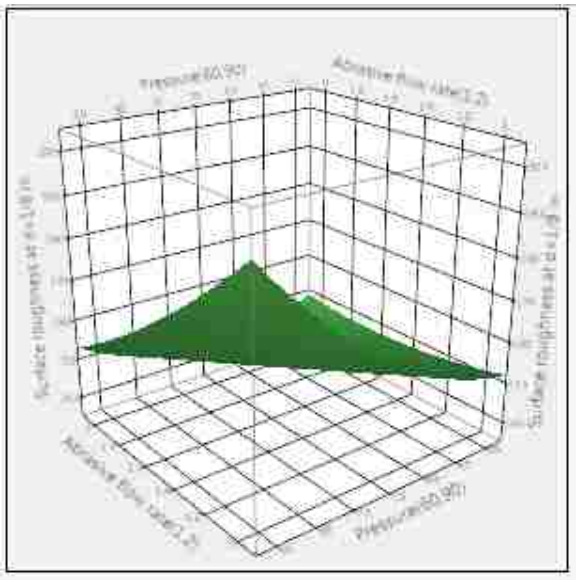

(b)

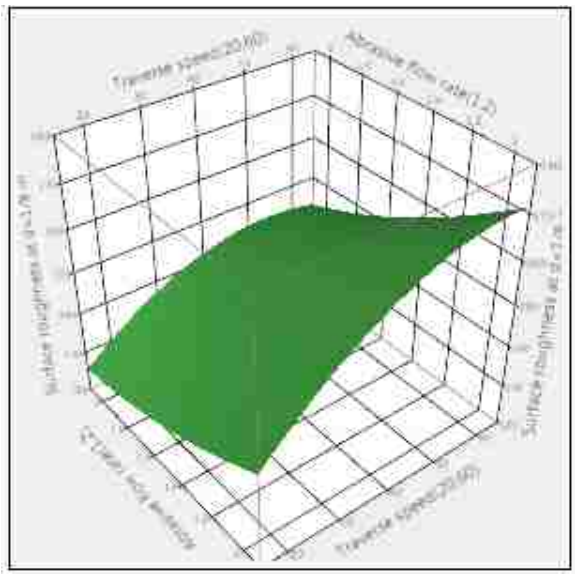

(c)

Figure 5.17. Response surface plots showing the effect of variables a) pressure and traverse speed b) pressure and abrasive flow rate c) traverse speed and abrasive flow rate on R_a at a depth of 1/8” for 80 HPX Barton garnet

5.3. EXPERIMENTATION WITH STYROFOAM BASE

Even though the work material was constrained in all directions by placing supports and by installing a heavy weight on the material to restrain any movement, there were vibrations in the material during cutting with the AWJ. So, a sheet of Styrofoam was introduced as a base on which the work material was placed, to reduce the vibration effect to a minimum where low roughness is an absolute requirement in AWJ cutting parameters.

The Box-Behnken set of experiments were repeated using the standard 80 HPX Barton garnet under these new constraints and with a composite material of 1" thickness. R_a was measured at a depth of 1/8" from the top surface after cutting the material. The relationship between response, R_a and variables [pressure (A), traverse speed (B) and abrasive flow rate (D)] is shown in equation 5.14.

Model equation at a depth of 1/8" from top surface of the composite with styrofoam base

$$R_a = 332-0.47*A+1.35*B-214.7*D-0.0112*A*A+0.0143*B*B+40.3*D*D-0.0117*A*B+1.273*A*D-0.407*B*D \quad (5.14)$$

The relationship between the predicted and experimental value of R_a are shown in Figure 5.18. Predicted values of R_a obtained using equation 5.14 matched observed values of R_a indicating a good fitness (R^2 value of 0.94).

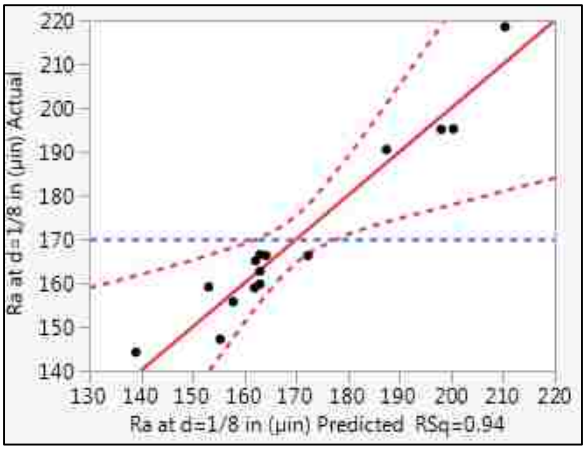

Figure 5.18. Relation between experimental and predicted values of R_a at depth of 1/8" with 80 HPX Barton garnet (eq.5.14)

Figure 5.19 a-c shows the 3D response surface plots for R_a at a depth of measurement of 1/8" for the linear cuts performed after installing a styrofoam base. Figure 5.19a shows the effect of pressure and traverse speed on surface roughness. Figure 5.19b shows the effect of pressure and abrasive flow rate. Figure 5.19c shows the effect of traverse speed and abrasive flow rate on the response, R_a.

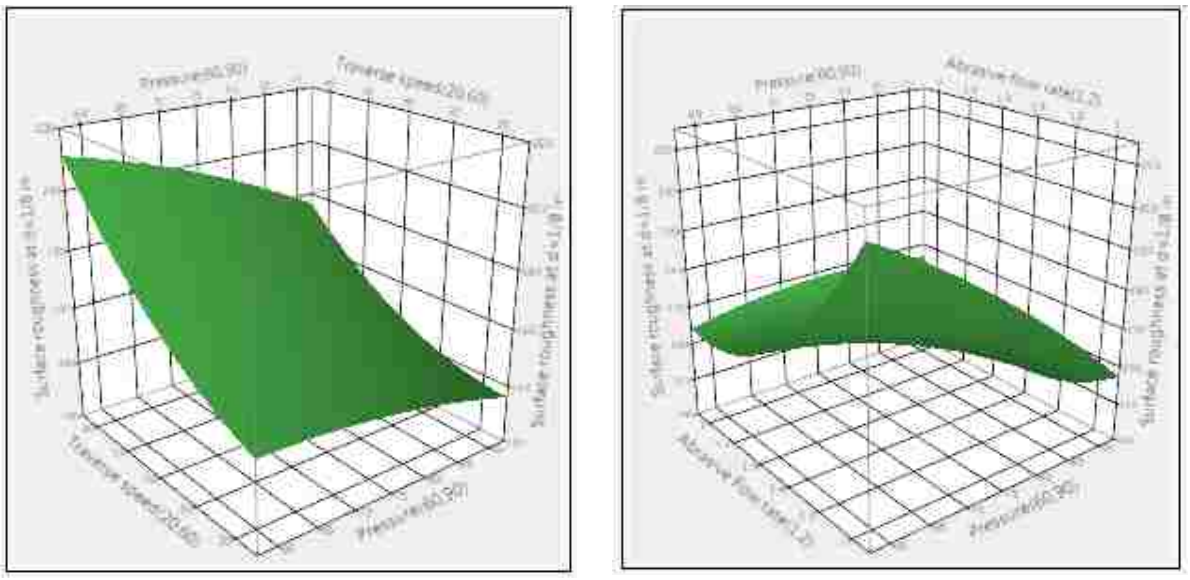

(a) (b)

Figure 5.19. Response surface plots showing the effects of variables a) pressure and traverse speed b) pressure and abrasive flow rate c) traverse speed and abrasive flow rate on R_a for 80 HPX Barton garnet with styrofoam base

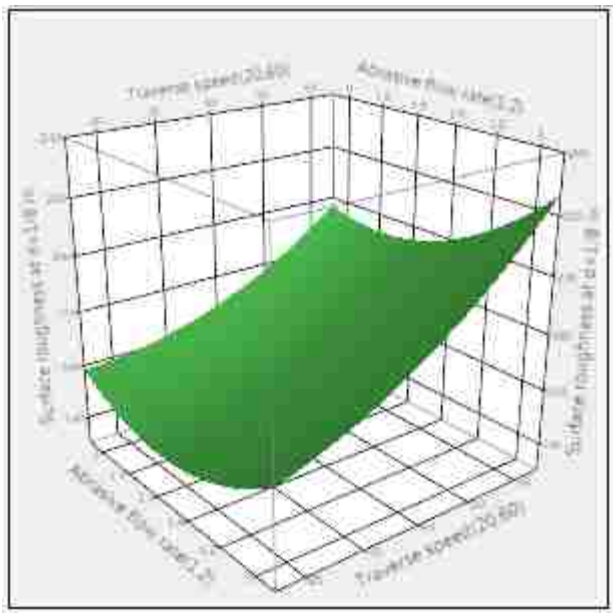

(c)

Figure 5.19. Response surface plots showing the effects of variables a) pressure and traverse speed b) pressure and abrasive flow rate c) traverse speed and abrasive flow rate on R_a for 80 HPX Barton garnet with styrofoam base (cont)

6. MODEL VERIFICATION

Model verification is a vital part of determining if the generated empirical model was able to predict response values close to those found with the experimental values.

6.1. MODEL VERIFICATION FOR 1" THICK COMPOSITE

The model equations each at AFR of 1 lb/min, 1.5 lb/min and 2 lb/min were verified by conducting experiments having parameters within the predicted interval. Model equations generated at each depth of measurement were used in the verification.

For model verification at an AFR of 1 lb/min, the experiments were conducted with parameters (pressure-60 ksi, 70 ksi and 80 ksi; traverse speed-30 in/min, 40 in/min and 50 in/min; abrasive size- 60 mesh) within the range of experimental design with levels different to that of experiments for building the model. The experiments were repeated three times at each AFR. In each repetition, abrasive flow rate was adjusted as close as to the required value. Roughness was measured with stylus of Mitutoyo surface roughness tester. The average R_a (9 measurements) was considered in verifying the model same as the measurements taken for the construction of the model as shown in the data from appendix.

Figure 6.1 shows the verification of model at AFR of 1 lb/min and at different depths of measurement. Experimental values of R_a and predicted values at a depth of ¼"and ½" from top surface of the composite are showing R^2 value of 0.83 and 0.85 respectively which indicates that the second order response model can be used for prediction. But at a depth of ¾" from jet entrance, R^2 value is 0.78 which implies that the model is not good enough to predict the surface roughness. The surface was rougher and more irregular at greater depth of

measurement and this led to inconsistency in the values of Ra and was the reason for the low R-squared values. R^2 value of 0.85 and around is considered as the criteria for verification of the model equations based on closeness of the predicted values to the experimental values.

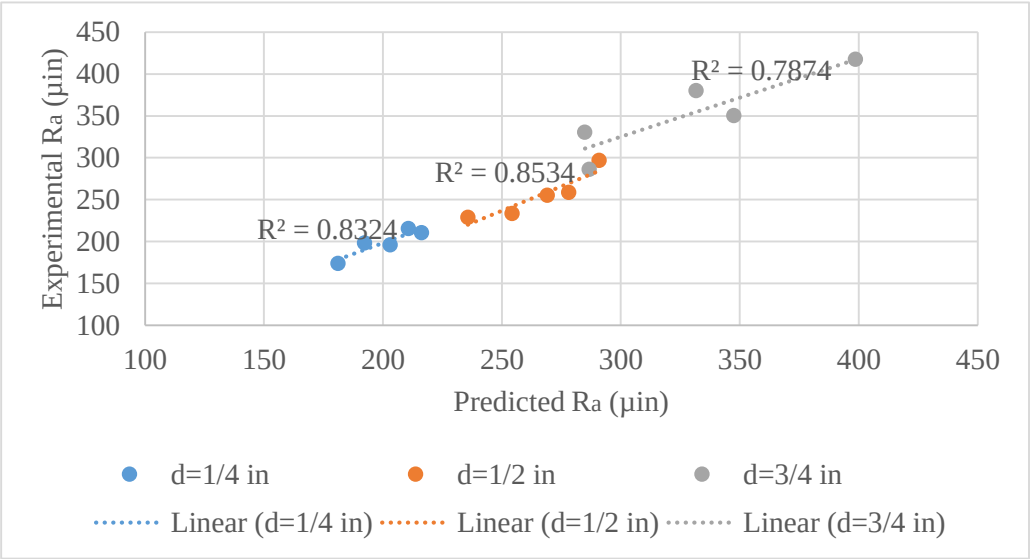

Figure 6.1. Model verification at AFR of 1 lb/min (eq's 5.1-5.3)

Figure 6.2 shows the verification of model at an AFR of 1.5 lb/min and at different depths of measurement of Ra. At a depth of ¼" from the top surface, the R^2 value of 0.84 indicates that experimental values lie close to the predicted values of Ra. Also, at depth of ½" from top surface for the measurement of Ra, an R^2 value of 0.84 was observed. The predicted model can be well applied for estimating roughness values for a given set of parameters within the interval of parameters tested in the experimental design. At a depth of ¾" from the top surface, experimental values of Ra were very close to the predicted values of Ra with an R^2 value of 0.92 indicating that response at any regime in the predicted interval could be predicted without actually performing the cutting.

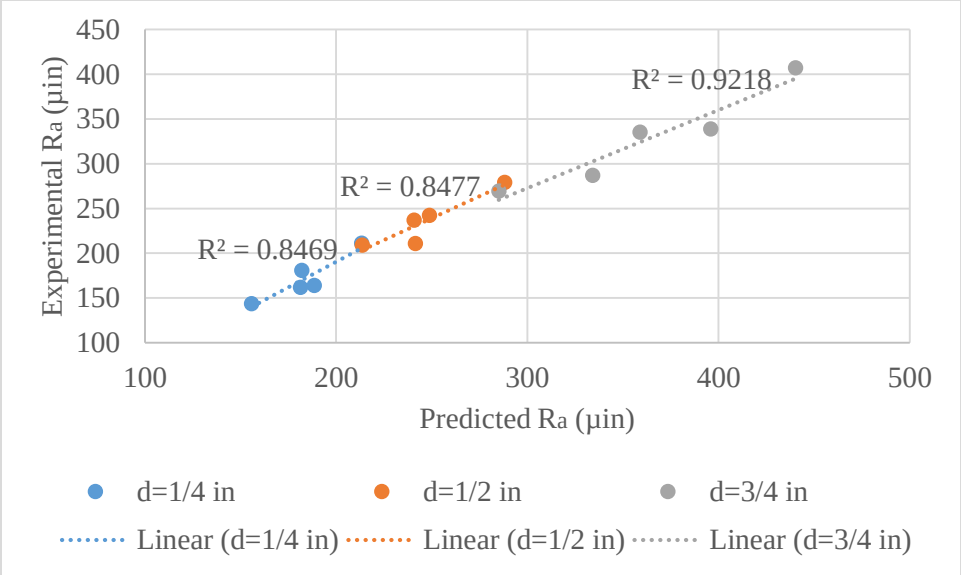

Figure 6.2. Model verification at an AFR of 1.5 lb/min (eq's 5.4-5.6)

Figure 6.3 represent the model verification at an AFR of 2.0 lb/min and at different depths of measurement. An R^2 value of 0.96 and 1 at depth of ¼" and ½" respectively indicate that experimental values of R_a were very close to the predicted values of R_a. Roughness values (R_a) could be calculated at any regime in the interval of experimental design with the predicted second order model equation. At ¾" depth of measurement, R^2 value was 0.68 which makes the model inapplicable for predicting R_a value at that depth based on the criteria of R- squared value of 0.85 for model verification. Low value of R^2 is due to difference in the roughness values in different repetitions of the experiment at the same AFR. This was due to inconsistencies in the surface roughness (R_a) values at depth of ¾" from the top surface of the composite.

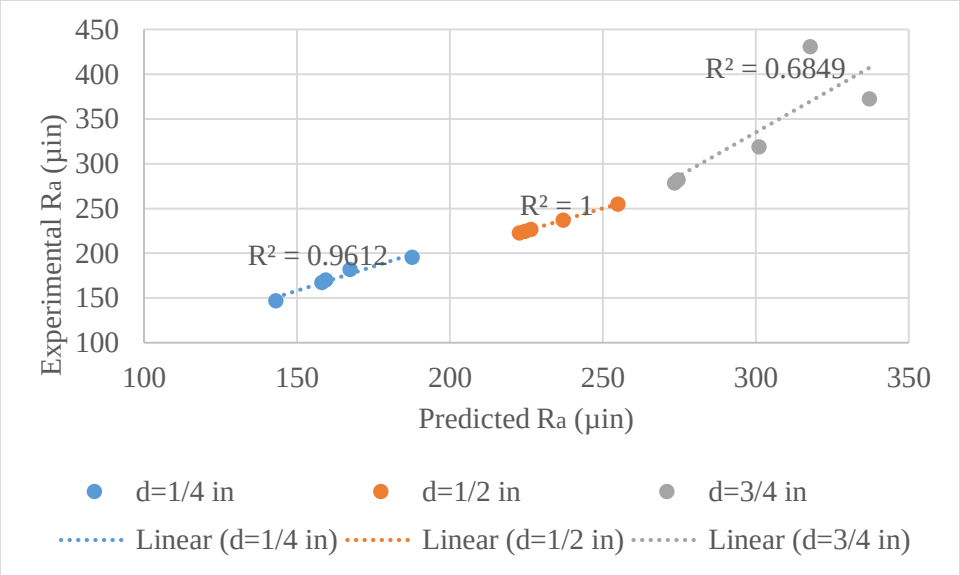

Figure 6.3. Model verification at an AFR of 2.0 lb/min (eq's 5.7-5.9)

For model verification of the second order model for surface roughness R_a, experiments were carried out at different combinations of parameters (pressure-60 ksi, 70 ksi and 80 ksi; traverse speed- 30 in/min, 40 in/min and 50 in/min; abrasive flow rate- 1.5 lb/min) within the experimental design. R_a measurement was taken with the stylus of Mitutoyo surface roughness tester directed along the fiber. The results of the experiment with 80 HPX Barton garnet in model verification is shown in Figure 6.4.

The correlation between the experimental and predicted R_a is determined based on the calculated R-squared value. An R^2 value of 0.91 at a depth of ¼" from the jet entrance indicates that the experimental values of R_a and predicted values of R_a matched. The best combination for lower surface roughness, R_a i.e. better surface finish is found to be at pressure of 80 ksi, traverse speed of 30 in/min and abrasive flow rate of 1.5 lb/min. The same for a given value of R_a, the combination setting of parameters is obtained from 3D response surface plots. The

model equation at the corresponding depth can be applied to predict surface roughness values during AWJ cutting of composite with Barton garnet.

At a depth of measurement of ½" from the top surface of the composite, the R^2 value was 0.73 and the predicted second order model could not calculate the response. An R^2 value of 0.86, at a depth of ¾" from the top surface of the composite meant that second order response, R_a as a function of pressure, traverse speed and abrasive flow rate could be applied in predicting the response at any regime within the interval of experimental design. At this point, there is no explanation in why R^2 value obtained at middle of the composite was low compared to the value at a depth of ¾" from the top surface.

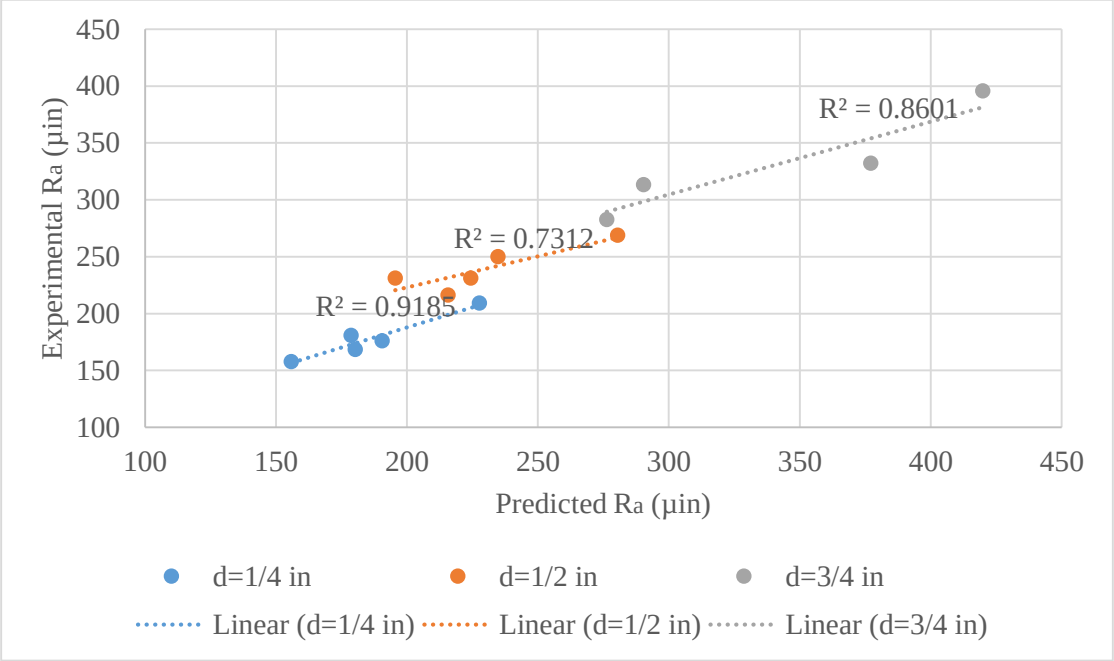

Figure 6.4. Model verification with 80 HPX Barton garnet (eq's 5.10-5.12)

Figure 6.5 represent the model verification at a depth of measurement of 1/8" from the top surface of the composite for both 1" thick and ¼" thick composite. For 1" thick composite,

R^2 was 0.79 indicate experimental values of R_a match with predicted values of R_a. Response at any regime within the interval of experimental design could be calculated with the relationship between surface roughness (R_a) and AWJ cutting parameters. For ¼" thick composite, R^2 value of 0.95 was found out indicating that the predictive model equation generated at a depth of measurement of R_a of 1/8" could be applied for calculating the response in the parameter interval of experimental design.

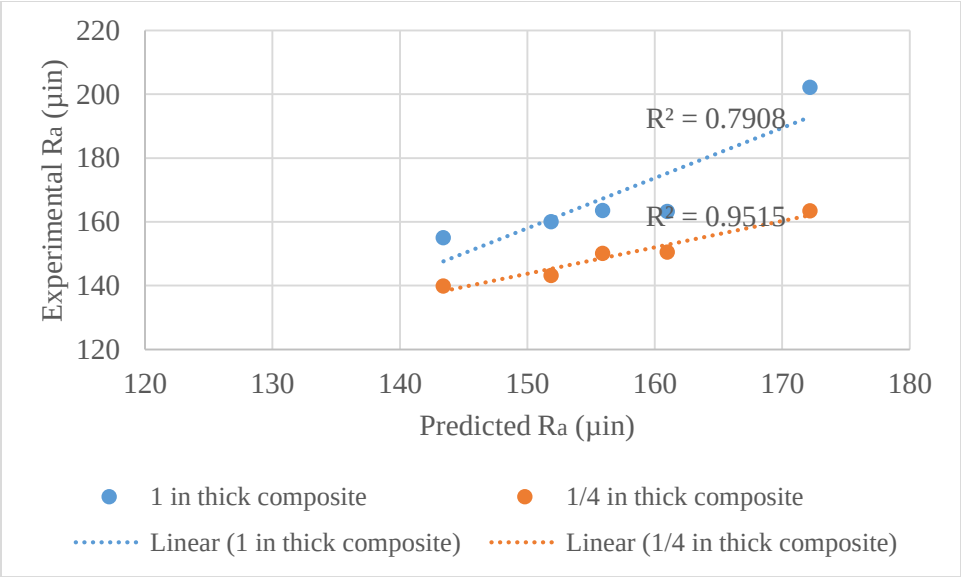

Figure 6.5. Model verification at a depth of 1/8" from top surface (eq 5.13)

R_a values were measured at three points at the same depth as shown in Figure 4.3 of section 4 in the cutting direction and the surface roughness was not the same. The variance in these R_a values was approximately 50-60 µin. This difference in the surface finish was not visible to naked eye but was detected by the surface roughness tester. The possible reason for this variance observed between the measurements is that the stylus of the profilometer lay either on fiber or between the fibers during measurement. This was the reason even for having

correlation value of less than 0.80. Although R_a values measured at one of 3 the points matched with the predicted value of R_a, the average differs from the predicted R_a by few µin.

6.2. MODEL VERIFICATION WITH STACKING

In industries, parts with the same geometry are to be machined in large scale production. Thin composite materials are generally stacked in regular production of various parts. So, a check was made to see if four ¼" thick materials can be joined together to form a single material for cutting such that they can be separated after machining. A stack of 4 quarter inch thick composites form a single 1" thick composite. The piles were stacked such that there was proper alignment. This stacked composite material was loaded on to styrofoam placed on the AWJ cutting table. Clamping was at all corners and weights were placed on top of the material to minimize the effect of vibration. The experimental setup for stacking is shown in Figure 6.6. 1" thick composite material was also clamped together with the styrofoam base. Linear cuts were performed on the stack of composites and 1" thick composite as well shown in Figure 6.7. Surface roughness was measured at a depth of 1/8" from the jet entrance.

Figure 6.6. AWJ cutting of stack of four ¼" thick composites

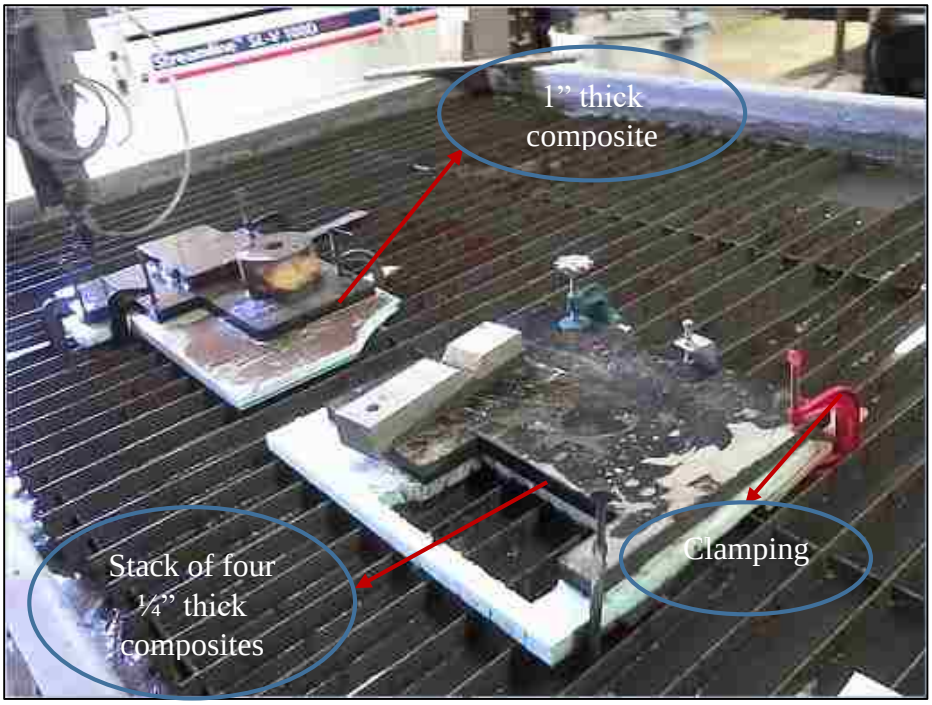

Figure 6.7. Fixture of 1” thick composite and stack of four ¼” thick composite for comparison of R_a

The model equation for surface roughness, R_a derived when using the styrofoam base was verified by AWJ cutting these 1” thick composite and a stack of four ¼” thick composites. Figure 6.8 shows the model verification for R_a at a depth of 1/8” measured from the top surface of the composite. For the 1” thick composite, although experimental and predicted values of R_a were close to each other, the R squared value was 0.77 because some experimental values were above the mean predicted values and some were below the mean predicted values. For the stack of four ¼” thick composites, the experimental values of R_a matched with the predicted values of R_a (R^2 value of 0.85). Surface roughness at any regime within the interval of experimental design could be predicted with the second order model equation.

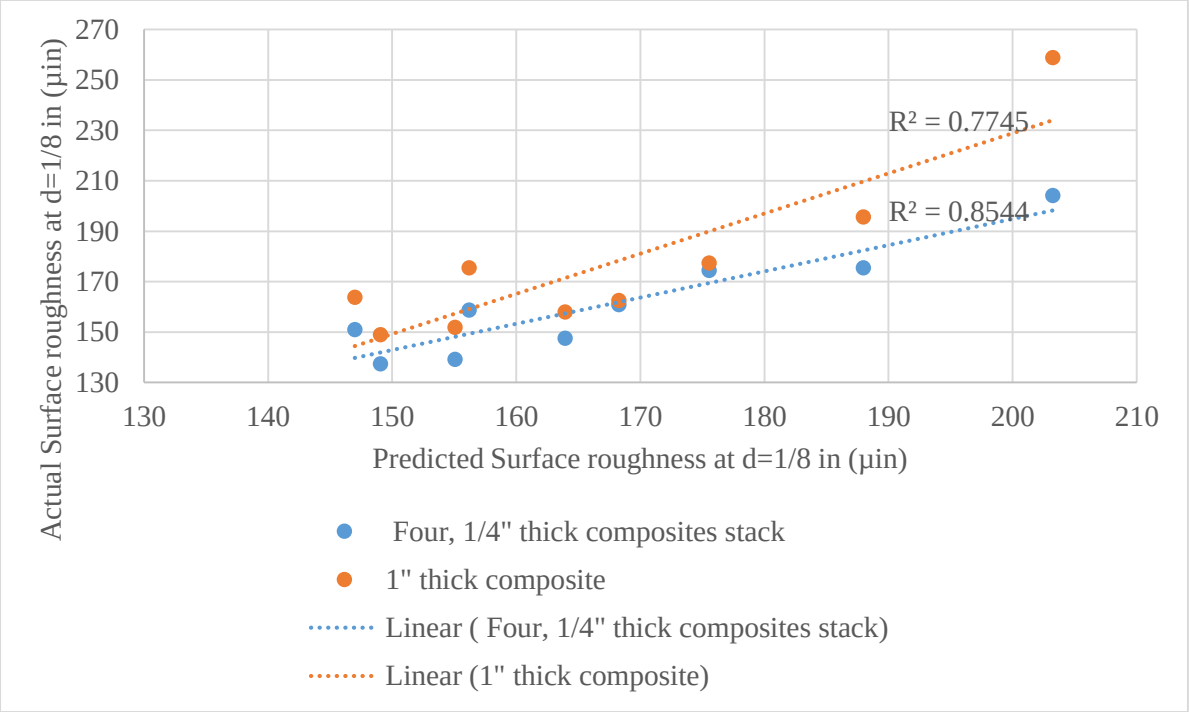

Figure 6.8. Verification of the model at depth of measurement of 1/8” using styrofoam base (eq 5.14)

7. CONCLUSIONS

Every waterjet cutting equipment manufacturer offers calculators for predicting through cutting parameters. However, there is lack of predictive ability for defining the surface roughness parameter, R_a. Surface roughness obtained at different pressure, traverse speed and abrasive flow rate using the Box-Behnken experimental design were used to construct 3D response surface plots for 80 HPX Barton garnet.

Generic behavior of R_a with respect to different process parameters can be summarized as follows:

- Increase of pressure from 60 ksi to 90 ksi resulted in lower values of R_a. In some of the experiments, high pressures combined with high traverse speeds caused vibrations in the workpiece. It was shown that with a proper fixturing, this problem could be reduced. However, this cannot be identified by visual inspection. Accelerometers had to be used to monitor the level of vibration.
- Traverse speed was found to be a much significant factor effecting R_a. With an increase in traverse speed, surface roughness increased. The model of surface roughness will help with the selection of the best traverse speed for a given finish.
- As abrasive mesh size increased from 50 to 70 mesh, lower values of R_a were observed. Abrasive size influences the cutting mechanism. But when cutting was at higher traverse speeds, isolated abrasive size had no significant influence on surface roughness as the experimental results confirmed.
- Surface roughness values decreased by 30% with an increase in abrasive flow rate from 1 lb/min to 2 lb/min.

As a general comment, it can be stated that surface roughness can be modelled using response surface methodology using the Box-Behnken design of experiments. Actual data and predicted values did not show a perfect correlation and this has to be further studied. It was also shown that surface roughness of a stack of composites match with that of a single solid composite.

8. FUTURE WORK

With the increasing use of materials that cannot be processed by conventional manufacturing methods, waterjet technology is securing its strong position on aerospace applications market.

In this research, equations were developed to model surface roughness of 1-inch-thick graphite/epoxy composite and equivalent stack of four ¼" thick composite cuts made under 3 levels of pressure, traverse speed and abrasive flow rate. During experimental work, it was discovered the vibration was a significant factor affecting surface roughness. Vibration was not considered as a variable in these studies. The studies of surface finish have to be continued to better understand the variables and undesired effects influencing the cutting.

Economics of machining with AWJ will focus on optimization of abrasive size, quantity and its distribution, when specific surface finish is required.

APPENDIX

Surface roughness was measured at three different levels from top surface of the composite in the jet direction i.e. at the jet entrance, middle of the specimen and at the jet exit. Along the cut direction, R_a was measured at three different locations on each depth of measurement. The average of these 3 values on each depth of measurement was taken for surface roughness assessment. In all these measurements, stylus was oriented in the fiber direction. Schematic representing surface roughness measurement was shown here.

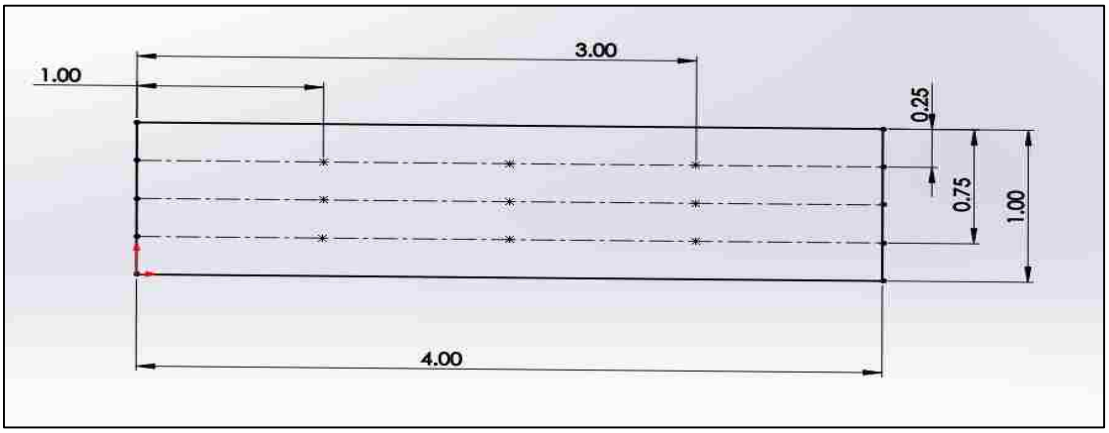

All dimensions are in inches

Surface roughness measurement measured at 3 different depths ¼”, ½”, ¾” and at 3 locations in the cut direction

Experimental values obtained in this research work were put together in Appendix. All the roughness measurements for the samples cut with AWJ in the Box-Behnken experimental design were shown here.

Box Behnken experimental design at AFR of 1 lb/min with R_a measured values

Sample number	Pressure (ksi)	Traverse speed (in/min)	Abrasive mesh size	Surface roughness, R_a (µin)		
				d=1/4 inch	d=1/2 inch	d= 3/4 inch
1	60	20	60	186.3	239.6	248.3
2	90	20	60	155.7	194.1	243.9
3	60	60	60	205.8	295.9	216.4
4	90	60	60	225.4	268.3	407.3
5	60	40	70	207.1	283	470.8
6	90	40	70	190.9	252.9	390.5
7	60	40	50	224.9	281.2	401.9
8	90	40	50	213.8	271	356
9	75	20	70	159.2	209.9	229.8
10	75	60	70	241.4	294.1	545.1
11	75	20	50	180.6	220.1	229
12	75	60	50	255.7	333.8	541.5
13	75	40	60	194.1	250.6	294.7
14	75	40	60	205	278.9	393.3
15	75	40	60	206	262.8	356

Box Behnken experimental design at AFR of 1.5 lb/min with R_a measured values

Sample number	Pressure (ksi)	Traverse speed (in/min)	Abrasive mesh size	Surface roughness, R_a (µin)		
				d=1/4 inch	d=1/2 inch	d= 3/4 inch
1	60	20	60	160.2	207.9	239.6
2	90	20	60	138.8	201.5	240.3
3	60	60	60	224.6	314.9	461.4
4	90	60	60	206	274.2	476.1
5	60	40	70	191.6	284.9	468.1
6	90	40	70	166.7	232.8	353.5
7	60	40	50	222.5	244.9	374.4
8	90	40	50	170.9	247.4	309.7
9	75	20	70	141.8	184.8	232.4
10	75	60	70	208.1	245.9	458
11	75	20	50	154.9	206.8	227.6
12	75	60	50	218	271.4	421.3
13	75	40	60	167.3	224.1	319.7
14	75	40	60	180.4	247.3	374.1
15	75	40	60	181.5	236.9	361.2

Box Behnken experimental design at AFR of 2.0 lb/min with R_a measured values

Sample number	Pressure (ksi)	Traverse speed (in/min)	Abrasive mesh size	Surface roughness, R_a (µin)		
				d=1/4 inch	d=1/2 inch	d= 3/4 inch
1	60	20	60	155.4	218.3	309.1
2	90	20	60	134.6	167	293.5
3	60	60	60	210.8	269.3	314.4
4	90	60	60	174.6	246.6	360.6
5	60	40	70	148.5	213.1	305.7
6	90	40	70	163.2	201.4	271.7
7	60	40	50	184.4	237.2	293.2
8	90	40	50	159	234.9	283.1
9	75	20	70	129	190.8	245.2
10	75	60	70	178.9	242.7	491
11	75	20	50	140.3	185.7	218.3
12	75	60	50	200	262.9	362
13	75	40	60	148.6	217.4	295.7
14	75	40	60	143	226.2	314.7
15	75	40	60	176.3	232	315.7

Box Behnken experimental design using 80 HPX Barton garnet with R_a values

Sample number	Pressure (ksi)	Traverse speed (in/min)	Abrasive flow rate (lb/min)	Surface roughness, R_a (µin)		
				d=1/4 inch	d=1/2 inch	d= 3/4 inch
1	60	20	1.5	152.8	195.3	225.3
2	90	20	1.5	140.1	179.3	235
3	60	60	1.5	256.5	339.1	495.6
4	90	60	1.5	201.2	246.3	419.1
5	60	40	1.0	228.1	258.4	389.2
6	90	40	1.0	203.6	259.4	372.5
7	60	40	2.0	173.6	231.2	303.7
8	90	40	2.0	156.4	209.4	269.9
9	75	20	1.0	158.4	222.6	238.1
10	75	60	1.0	245.8	288.8	435.2
11	75	20	2.0	131.1	171.6	213.7
12	75	60	2.0	184.4	259.8	427.8
13	75	40	1.5	159.5	234.7	319.2
14	75	40	1.5	168.8	175.1	313.4
15	75	40	1.5	175.1	251	355.1

Box Behnken experimental design using 80 HPX Barton garnet with R_a values with and without using styrofoam base

Sample number	Pressure (ksi)	Traverse speed (in/min)	Abrasive flow rate (lb/min)	Surface roughness, R_a (µin) d=1/8 inch	
				w/o styrofoam	styrofoam
1	60	20	1.5	152.7	159.1
2	90	20	1.5	134.1	144.2
3	60	60	1.5	174.2	195.2
4	90	60	1.5	147.4	166.3
5	60	40	1.0	188.6	195.1
6	90	40	1.0	155.9	155.7
7	60	40	2.0	148.3	166.3
8	90	40	2.0	143.8	165.1
9	75	20	1.0	142.5	158.9
10	75	60	1.0	165.3	218.5
11	75	20	2.0	133.8	147.2
12	75	60	2.0	149.4	190.5
13	75	40	1.5	148	166.5
14	75	40	1.5	155	162.7
15	75	40	1.5	152.5	159.8

R_a values of a stack of 4, ¼" thick and 1" thick single composite

Sample number	Pressure (ksi)	Traverse speed (in/min)	AFR (lb/min)	Stack of 4, 1/4" thick composites				1" thick single composite			
				Surface roughness, R_a (μin)				Surface roughness, R_a (μin)			
				d=1/8 in	d=3/8"	d=5/8"	d=7/8"	d=1/8 in	d=3/8"	d=5/8"	d=7/8"
1	80	30	2.0	137.4	213.8	225.8	285.0	148.9	184.7	278.3	410.2
2	80	40	2.0	139.2	261.4	224.4	316.8	151.8	207.0	297.5	409.6
3	80	50	2.0	147.5	219.3	283.6	402.3	158.0	183.4	260.0	403.0
4	70	30	1.5	151.0	263.0	295.8	354.6	163.8	200.8	280.7	326.5
5	70	40	1.5	158.7	253.9	280.5	396.8	175.5	272.3	387.9	440.3
6	70	50	1.5	160.9	221.2	364.0	470.7	162.5	237.8	346.3	430.5
7	60	30	1.0	174.4	284.9	430.8	436.5	177.4	265.2	364.5	488.2
8	60	40	1.0	175.5	318.5	Out of range of		195.6	278.6	Out of range of	
9	60	50	1.0	204.1	333.9	measurement		258.9	414.9	measurement	

Experiments are conducted for the verification of predicted second order model equations for surface roughness choosing the levels of the process variables within experimental design. Actual values of Ra for the samples and predicted values are shown in this appendix.

Experimental data for model verification at an abrasive flow rate of 1.0 lb/min

Run	Pressure (ksi)	Traverse speed (in/min)	Abrasive size	**Experimental R_a (µin)**			**Predicted R_a (µin)**		
				d=1/4 in	d=1/2 in	d=3/4 in	d=1/4 in	d=1/2 in	d=3/4 in
1	60	30	60	198.5	233.9	330.8	192.3	254.3	284.9
2	60	50	60	215.8	297	380.5	210.7	290.8	331.7
3	70	40	60	196.2	255.6	350.6	203.4	269.1	347.6
4	80	30	60	174.1	229	286.5	181.1	235.7	286.7
5	80	50	60	210.8	259	417.9	216.2	278.1	398.7

Experimental data for model verification at an abrasive flow rate of 1.5 lb/min

Run	Pressure (ksi)	Traverse speed (in/min)	Abrasive size	**Experimental R_a (µin)**			**Predicted R_a (µin)**		
				d=1/4 in	d=1/2 in	d=3/4 in	d=1/4 in	d=1/2 in	d=3/4 in
1	60	30	60	161.8	211	287.1	181.3	241.3	334.1
2	60	50	60	211.4	279.2	407.1	213.3	288.0	440.3
3	70	40	60	180.9	237.1	335.4	181.9	240.8	358.9
4	80	30	60	143.5	209.1	269.4	155.6	213.5	285.1
5	80	50	60	164.1	242.5	339.1	188.5	248.8	395.9

Experimental data for model verification at an abrasive flow rate of 2.0 lb/min

Run	Pressure (ksi)	Traverse speed (in/min)	Abrasive size	**Experimental R_a (µin)**			**Predicted R_a (µin)**		
				d=1/4 in	d=1/2 in	d=3/4 in	d=1/4 in	d=1/2 in	d=3/4 in
1	60	30	60	167.4	226.5	282.1	158.1	224.2	274.6
2	60	50	60	195.6	254.9	430.7	187.6	249.5	317.8
3	70	40	60	170.1	224.6	319	159.4	229.1	301.0
4	80	30	60	147	222.7	278.4	143.0	204.2	273.4
5	80	50	60	181.8	237.1	372.6	167.3	239.1	337.2

Experimental data for model verification with 80 HPX Barton garnet

Run	Pressure (ksi)	Traverse speed (in/min)	AFR (lb/min)	**Experimental R_a (µin)**			**Predicted R_a (µin)**		
				d=1/4 in	d=1/2 in	d=3/4 in	d=1/4 in	d=1/2 in	d=3/4 in
1	60	30	1.5	180.7	216.2	313.4	178.8	215.8	290.4
2	60	50	1.5	209.3	268.8	395.6	227.7	280.6	420.0
3	70	40	1.5	168.5	231.2	262.8	180.4	224.5	335.4
4	80	30	1.5	157.6	231.2	282.6	155.9	195.6	276.3
5	80	50	1.5	176.1	249.9	332	190.6	234.8	377.2

Experimental data for model verification at a depth of 1/8” from the top surface

Run	Pressure (ksi)	Traverse speed (in/min)	AFR (lb/min)	**Experimental R_a (µin)**		**Predicted R_a (µin)**
				t=1"	t=1/4"	
1	60	30	1.5	163.2	150.5	160.9
2	60	50	1.5	202.1	163.4	172.1
3	70	40	1.5	163.5	150.1	155.9
4	80	30	1.5	155	139.8	143.4
5	80	50	1.5	160	143.2	151.8

Experimental data for model verification of stack of four ¼” thick composites and 1” thick solid composite

Sample number	Pressure (ksi)	Traverse speed (in/min)	AFR (lb/min)	Surface roughness at d=1/8 in, R_a (µin)		
				Four 1/4" thick stack	1" thick composite	Predicted
1	80	30	2.0	137.4	148.9	149.1
2	80	40	2.0	139.2	151.8	155.1
3	80	50	2.0	147.5	158.0	164.0
4	70	30	1.5	151.0	163.8	147.0
5	70	40	1.5	158.7	175.5	156.2
6	70	50	1.5	160.9	162.5	168.3
7	60	30	1.0	174.4	177.4	175.6
8	60	40	1.0	175.5	195.6	188.0
9	60	50	1.0	204.1	258.9	203.3

In the experimental setup for analyzing the Barton garnet disintegration in the cutting head, abrasive was collected in a container under a combination of 3 pressures and 3 abrasive flow rates. At each AFR, the experiment was repeated three times for accuracy. After drying of abrasive slurry, sieving was performed. Particle size distribution for each trial of the experiment is shown in this appendix.

Disintegration of 80 HPX Barton garnet at pressure of 60 ksi

Screen number	Particle size distribution in percent by weight								
	AFR= 2.0 lb/min			AFR = 1.5 lb/min			AFR = 1.0 lb/min		
40	0	0	0.11	0	0	0.1	0	0	0
50	0.8	1.85	1.1	1.54	1.41	1.49	1.58	1.04	1.46
60	4.69	8.36	6.38	7.56	6.76	7.14	9.1	7.29	8.53
70	8.45	9.85	8.91	9.94	8.18	9.27	10.49	11.71	12.19
80	11.67	8.36	13.42	13.16	15.61	14.49	14.65	12.76	14.63
100	12.21	7.43	13.09	12.46	13.86	11.72	11.68	13.28	13.17
>100	30.13	64.12	56.98	55.04	54.03	53.83	52.47	53.9	50.48

Disintegration of 80 HPX Barton garnet at pressure of 75 ksi

Screen number	Particle size distribution in percent by weight								
	AFR= 2 lb/min			AFR = 1.5 lb/min			AFR = 1 lb/min		
40	0	0.2	0.23	0.12	0.23	0.11	0	0	0
50	0.71	0.62	0.82	0.63	0.83	0.7	0.99	0.53	0.78
60	4.09	4.04	4.82	4.06	4.75	4.25	5.82	5.03	5.23
70	6.74	6.11	6.82	7.24	7.61	7.55	9.98	8.48	9.68
80	8.69	12.33	11.29	12.7	14.26	12.98	13.31	13.26	11.5
100	11.04	12.53	11.88	13.85	13.43	15.11	14.97	14.05	12.56
>100	68.6	64.45	64.23	61.11	58.73	59.5	55.07	58.09	60.2

Disintegration of 80 HPX Barton garnet at pressure of 90 ksi

Screen number	Particle size distribution in percent by weight								
	AFR= 2.0 lb/min			AFR = 1.5 lb/min			AFR = 1.0 lb/min		
40	0.34	0.36	0.19	0.11	0.25	0.32	0	0	0
50	0.56	0.54	0.76	0.69	0.88	0.53	0.66	0.53	0.78
60	3.85	3.26	4.18	4.87	4.67	3.87	5.63	4.58	5.49
70	8.27	6.17	6.47	9.51	7.95	6.68	7.29	9.16	9.42
80	10.09	10.62	11.98	13.45	10.73	11.96	14.42	11.59	12.04
100	14.05	12.44	12.55	14.73	11.23	14.87	14.26	12.93	12.82
>100	63.6	66.57	63.5	56.49	64.39	61.96	57.54	60.91	59.42

BIBLIOGRAPHY

Alberdi, A., Suarez, A., Artaza, T., Palafox, G.A. and Ridgway, K., "Composite Cutting with Abrasive Waterjet," *Procedia Engineering*, 63, 2013, pp. 421-429.

Osman, A.H., Mabrouki, T., Thery, B. and Buisine, D., "Experimental analysis of high speed air-waterjet flow in an abrasive waterjet mixing tube," *Flow Measurement and Instrumentation*, 15, 2004, pp. 37-48.

Akkurt, A., Kulecki, M.K., Seker, U. and Ercan, F., "Effect of feed rate on surface roughness in abrasive waterjet cutting applications," *Journal of Material Processing Technology*, 147, 2004, pp. 389-396.

Azmir, A.K. and Ahsan, M.A., "A study of abrasive waterjet machining process on glass/epoxy composite laminate," *Journal of Material Processing Technology*, 209, 2009, pp. 6168-6173.

Akkurt, A., "Surface properties of the cut face obtained by different cutting methods from AISI 304 stainless steel materials," *Indian Journal of Engineering & Material Sciences*, Vol 16, 2009, pp. 373-384.

Srinivas, S. and Babu, N.R., "Role of garnet and silicon carbide abrasives in abrasive waterjet cutting of aluminum-silicon carbide particulate metal matrix composites," *International Journal of Applied Research in Mechanical Engineering*, Vol 1, Issue 1, 2011, pp. 109-122.

Jegaraj , J.J and Babu, N.R., "A strategy for efficient and quality cutting of materials with abrasive waterjets considering the variation in orifice and focusing nozzle diameter," *International Journal of Machine Tools and Manufacture*, 45, 2005, pp. 1443-1450.

Jegaraj , J.J and Babu, N.R., "A soft computing approach for the controlling the quality of cut with abrasive water jet cutting system experiencing orifice and focusing tube wear," *Journal of Materials Processing Technology*, 185, 2007, pp. 217-227.

Kang, C., Liu, H. and Yang, M., "Verification of turbulent correlation and impact study of high pressure abrasive waterjet," *Jet Forces and Cut Surfaces, Paper C3, WJTA - IMCA Conference and Expo*, September 9-11, 2013, Houstan, Texas.

Cebeci, Y. and Aslan, N., "Application of Box - Behenken design and response surface surface methodology for modelling of some turkish coals," *Fuel* 86, 2007, pp. 90-97.

Babu, M.K. and Chetty, O.V., "A study on the use of single mesh size abrasives in abrasive waterjet machining," *International Journal of Advanced Manufacturing Technology*, 29, 2006, pp. 532-540.

Folkes, J., "Waterjet - An innovative tool for manufacturing," *Journal of Material Processing Technology*, 209, 2009, pp. 6181-6189.

Fowler, G., Shipway, P.H. and Pashby, I.R., "Abrasive waterjet controlled depth milling of Ti6Al4V alloy- an investigation of the role of jet-workpiece traverse speed and abrasive grit size on the characteristics of the milled material," *Journal of Materials Processing Technology*, 161, 2005b, pp. 407-414.

Fowler, G., Shipway, P.H. and Pashby, I.R., "A technical note on grit embedment following Abrasive waterjet milling of a titanium alloy," *Journal of Material Processing Technology,*161, 2005a, pp. 356-368.

Liu, H., Wang, J., Kelson, N. and Brown, R.J., "A study of abrasive waterjet characteristics by CFD simulation," *Journal of Material Processing Technology*, 153-154, 2004, pp. 488-493.

Khan, A.A. and Haque, M.M., "Performance of different abrasive materials during abrasive waterjet machining of glass," *Journal of Material Processing Technology*, 191, 2007, pp. 404-407.

Hashish, M., "Trimming of CFRP aircraft components," *Abrasive Jet Applications, Paper A3, WJTA-IMCA Conference and Expo*, September 9-11, *2013*, Houstan, Texas.

Miles, P. and Henning, A., "Rz: A better measurement of Abrasive waterjet cut surface finishes," *WJTA - IMCA Conference and Expo*, September 2013, Houston, Texas.

Valicek, J., Drzik, M., Hloch, S., Ohlidal, M., Miloslav, L., Gombar, M., Radvanska, A., Hlavacek, P. and Palenikova, K., "Experimental analysis of irregularities of metallic surfaces generated by abrasive waterjet," *International Journal of Machine Tools and Manufacture*, 47, 2007, pp. 1786-1790.

Anand, U. and Katz, J., "Prevention of nozzle wear in abrasive water suspension jets using porous lubricated nozzles,"*ASME Journal of Tribology*, Vol. 125, January 2003, pp. 168-180.

Krajcarz, D., "Comparison Metal Waterjet Cutting with Laser and Plasma Cutting," *24th DAAM International Symposium on Intelligent Manufacturing and Automation*, 2013, *Procedia Engineering*, 69, 2014, pp. 838-843.

Gent, M., Menendez, M.,Torno, S., Torano, J. and Schenk, A., "Experimental evaluation of the physical properties required of abrasives for optimizing waterjet cutting of ductile materials," *Wear*, 284-285, 2012, pp. 43-51.

Galecki, G. and Mazurkiewicz, M., "Hydro Abrsive cutting head-Energy tranfer efficiency," *Proceedings of the Fourth U.S. Waterjet Conference*, 1987, Berkeley, California, pp. 172-177.

Kok, M., Kanca, E. and Eyercioglu, O., "Prediction of surface roughness in abrasive waterjet machining of particle reinforced MMCs using genetic expression programming," *International Joournal of Advanced Manufacturing Technology*, 55, 2011, pp. 955-968.

Perec, A., "Abrasive grain breakage process during the high pressure waterjet formation." *WJTA-IMCA Conference and Expo*, September 19-21, 2011, Houston, Texas.

Summers, D. A., "Waterjetting Technology," *E&FN Spon*, London, England, 1995

Kovacevic, R., Wang, L. and Wang, Y.M., "Identification of abrasive waterjet nozzle based on parametric spectrum estimation of accoustic signal," *Proceedings of the institution of mechanical engineers*, Vol 208, 1994, pp. 173-181.

Arola, D. and Ramulu, M., "A study of kerf characteristics in abrasive waterjet machining of graphite/epoxy composite," *Journal of material and technology*, Vol 118, Issue 2, 1996, pp. 256-265.

Arola, D. and Ramulu, M., "Mechanism of material removal in abrasive waterjet machining of common aerospace materials," *Proceedings of the seventh American waterjet conference*, 1993, Seattle, pp. 43-64.

Srinivasu, D.S. and Axnite, D.A., "Surface integrity analysis of plain waterjet milled advanced engineering composite materials," *Procedia,CIRP* 13, 2014, pp. 371-376.

Vorburger, T.V., Renegar, T.B., Zheng, A.X., Song, J.F., Soons, J.A. and Silver, R.M., "Surface roughness and step height calibrations- Measurement conditions and Sources of Uncertainty," *National Institute of Standards and Technology*, Gaithersburg

Thery, A.H. and Osman, B., "Velocity doppler investigations of the flow in abrasive waterjet using a fabry-petrot interferometer," *5th Pacific Rim International Conference on Waterjet Technology*, 1998, New Delhi.

Aich, U., Banerjee, S., Bandyopadhyay, A. and Das, P.K., "Abrasive waterjet Cutting of Borosilicate Glass," *3rd Inernational conference on Materials Processing and Charcaterization*, *ICMPC* 2014, *Procedia Materials Science, 6*, pp. 775-785.

Wang, R. and Wang, M., "A two-fluid model of abrasive waterjet," *Journal of Material Processing Technology*, 210, 2010, pp. 190-196.

Box George, E. P. and Draper, N. R., "Empirical Model Building and Response Surfaces," *John Wiley and Sons*, New York, 1987, pp. 477.

Galecki, G., Mazurkiewicz, M. and Jordan, R., "Abrasive disintegration effect during jet ejection," *International Water Jet Symposium*, September 1987, Beijing, China, pp. 4.71-4.77.

Korat, M. M. and Acharya, G. D., "A review on current research and development in abrasive waterjet machining," *Int. Journal of Engineering Research and Applications*, Vol. 4, Issue 1, January 2014, pp. 423-432.

NIST/SEMATECH, "e-Handbook of statistical methods- Box-Behnken response surface design," *http://www.itl.nist.gov/div898/handbook*, 5.3.3.6, August 25, 2015.

Mesh size to Particle Size Conversion Table, Retrieved 2015, September 10, from *http://www.sigmaaldrich.com/chemistry/stockroom-reagents/learning-center/technical-library/particle-size-conversion.html*

Geology, Garnet physical and chemical properties, Retrieved 2016, April 20, from *http://geology.com/minerals/garnet.shtml*

VITA

Prabhakar Bala was born in Andhra Pradesh, India. He completed his school education in Santhi Vidya Nikethan, Raghavapuram, India. He received his Bachelor's degree in Mechanical Engineering from Acharya Nagarjuna University, Guntur in May, 2013. He joined Missouri University of Science & Technology (formerly university of Missouri-Rolla) in Spring 2015. He received his Master's degree in Manufacturing Engineering from Missouri University of Science & Technology in July 2016. His areas of interest include abrasive waterjet cutting, statistical techniques, quality engineering, continuous improvement methods and manufacturing equipment automation.